# SEMMELWEIS EGYETEM DOKTORI ISKOLA

## Ph.D. értekezések

## 3384.

**IDAN CARMI**

## Humán molekuláris genetika és géndiagnosztika

## című program

Programvezető: Dr. Wiener Zoltán, egyetemi tanár

Témavezető: Dr. Wiener Zoltán, egyetemi tanár

# Studies on the heterogeneity and function of molecules critical in colorectal cancer progression

**Ph.D. Thesis**


## Idan Carmi

Molecular Medicine Doctoral Division

Doctoral College of Semmelweis University



Supervisor: Zoltán Wiener, D.Sc

Official Reviewers: Gerda Gabriella Wachtl, Ph.D

Krisztina Vellainé Takács, Ph.D

Head of the Complex Examination Committee: Péter Igaz, MD, D.Sc

Members of the Complex Examination Committee: Krisztián Tárnok, Ph.D

Gábor Barna, Ph.D

# Table of Contents

# List of abbreviations

| Abbreviation | Word |
|---|---|
| 5-FU | 5-Fluorouracil |
| 5-HIAA | 5-hydroxyindoleacetic acid |
| 5-HT | 5-Hydroxytryptamine |
| 5-HTP | 5-hydroxytryptophan |
| AADC | L-amino acid decarboxylase |
| AKT | Ak strain transforming |
| ANOVA | Analysis of Variance |
| APC | Adenomatous Polyposis Coli |
| ASCs | adult stem cells |
| AXIN1 | axis inhibition protein 1 |
| AXIN2 | axis inhibition protein 2 |
| BAX | Bcl-2-Associated X protein |
| BRAF | viral-RAF murine sarcoma viral oncogene homolog B |
| BSA | bovine serum albumin |
| CAF | Cancer associated fibroblast |
| cAMP | cyclic adenosine monophsate |
| CCL | chemokine (C-C motif) ligand |
| CCND1 | Cyclin D1 |
| CD133 | Cluster of Differentiation 133 |
| CD44 | Cluster of Differentiation 44 |
| CDX2 | Caudal-type homeobox transcription factor 2 |
| c-FOS | cellular-FBJ murine osteosarcoma viral oncogene homolog |
| CIMP | CpG island hypermethylation |
| CIN | chromosomal instability |
| c-JUN | cellular-Jun |
| CK1α | casein kinase 1α |
| CMS | Consensus Molecular Subtype |
| CRC | Colorectal Cancer |
| CXCL | chemokine (C-X-C motif) ligand |

| | |
|---|---|
| DAG | Diacylglycerol |
| DAPI | 4',6-diamidino-2-phenylindole |
| DAPT | N-[N-(3,5-difluorophenacetyl)-L-alanyl]-S-phenylglycine t-butyl ester |
| DBZ | Dibenzazepine |
| DLL | Delta-like ligands |
| DMEM | Dulbecco's Modified Eagle Medium |
| DMSO | Dimethyl sulfoxide |
| DVL | Disheveled |
| EC | Enterochromaffin |
| ECM | Extracellular matrix |
| EDTA | ethylenediaminetetraacetic acid |
| EGF | Epidermal Growth Factor |
| EGFR | Epidermal Growth Factor Receptor |
| EHS | Engelbreth-Holm-Swarm |
| EMT | epithelial-to-mesenchymal transition |
| ERK1/2 | extracellular signal regulated kinase 1/2 |
| EVs | Extracellular Vesicles |
| FACS | Fluorescence-activated cell sorting |
| FBS | Fetal Bovine Serum |
| FGFR | Fibroblast Growth Factor Receptor |
| FRMD6 | FERM domain-containing protein 6 |
| FZD | Frizzled |
| GDP | guanosine diphosphate |
| GEF | guanine nucleotide exchange factor |
| GPCR | G-protein coupled receptor |
| Grb2 | growth factor receptor bound protein 2 |
| GSK3ß | Glycogen synthase kinase 3-ß |
| GTP | guanosine triphosphate |
| HEPES | 4-(2-hydroxyethyl)-1-piperazineethanesulfonic acid |
| HTR2B | 5-Hydroxytryptamine receptor 2B |
| IL | Interleukin |

| | |
|---|---|
| IP3 | inositol trisphosphate |
| JAK | Janus kinase |
| KI67 | Antigen Kiel 67 |
| K-RAS | Kirsten RAS |
| LEF | Lymphoid Enhancer Binding Factor |
| LOX | Lysyl oxidase |
| LRP5/6 | LDL receptor-related protein 5/6 |
| LUM | Lumican |
| MAO-A | monoamine oxidase A |
| MAPK | mitogen-activated protein kinase |
| MDM2 | murine double minute 2 |
| MDSC | myeloid-derived suppressor cells |
| MEK | mitogen activated protein kinase kinase |
| MEM | Minimum Essential Medium |
| MHPs | microvesicular hyperplastic polyps |
| MLH1 | MutL protein homolog 1 |
| MMP | Matrix Metalloproteinase |
| MSI | microsatellite instability |
| mTOR | mammalian target of rapamycin |
| mTORC1 | mTOR-complex 1 |
| MYC | myelocytomatosis |
| NF-κB | Nuclear Factor kappa-light-chain-enhancer of activated B cells |
| NK | Natural Killer |
| noAA | amino acid-free |
| noGl | carbohydrate-free |
| N-RAS | Neuroblastoma RAS |
| OD | optical density |
| p110α/PIK3C A | phosphatidylinositol 4,5-bisphosphate 3-kinase catalytic subunit alpha |
| PBS | Phosphate buffer solution |
| PDAC | Pancreatic Ductal Adenocarcinoma |
| PDK1 | Pyruvate dehydrogenase kinase 1 |

| | |
|---|---|
| PDOs | Patient-derived organoids |
| pEMT | partial epithelial-to-mesenchymal transition |
| PFA | Paraformaldehyde |
| PI3K | Phosphoinositide 3-kinase |
| PIP2 | phosphatidylinositol 4,5-bisphosphate |
| PIP3 | phosphatidylinositol 3,4,5-trisphosphate |
| PKA | Protein Kinase A |
| PKC | Protein Kinase C |
| PLC | Phospholipase-C |
| P-S6 | phosphorylation of the ribosomal protein S6 |
| PTEN | phosphatase and tensin homolog |
| PTK7 | Protein Tyrosine Kinase 7 |
| PUMA | p53 upregulated modulator of apoptosis |
| qPCR | quantitative-polymerase chain reaction |
| RAF | rapidly accelerated fibrosarcoma |
| RAS | rat sarcoma virus protein |
| ROCK | Rho-associated protein kinase |
| SERT | Serotonin transporter |
| SH2 | src homology domain 2 |
| SLC6A4 | Solute carrier family 6 member 4 |
| SMAD | Sma- and Mad- related protein |
| SNAIL | Snail Family Transcriptional Repressor 1 |
| SOS | son of seven-less |
| SSLs | sessile serrated lesions |
| SSRIs | selective serotonin reuptake inhibitors |
| ß-TrCP | ß-Transducin repeat-containing protein |
| STAT3 | Signal transducer and activator of transcription 3 |
| TAM | tumor-associated macrophage |
| TBS-T | Tris-buffered saline with 0.1% Tween-20 |
| TCF | T-cell factor |
| TGFBR1 | Transforming growth factor-ß reeptor type 1 |
| TGFBR2 | Transforming growth factor-ß reeptor type 2 |

| | |
|---|---|
| TGF-ß | Transforming growth factor-ß |
| TME | Tumor microenvironment |
| TNM | Tumor, Node, and Metastasis |
| TPH1 | Tryptophan hydroxylase 1 |
| Treg | Regulatory T |
| TSAs | traditional serrated adenomas |
| TWIST | Twist-related protein 1 |
| VEGF | Vascular endothelial growth factor |
| VIM | Vimentin |
| Wnt | Wingless/Integrated |
| ZEB1 | Zinc Finger E-box binding homeobox 1 |
| α-SMA | α-smooth muscle actin |

# 1. Introduction

## 1.1 Epidemiology

Colorectal Cancer (CRC) remains a major global health burden, ranking as the third most frequently diagnosed malignancy and the second leading cause of cancer-related mortality worldwide (1). Its incidence demonstrates considerable geographical variation, with the highest rates observed in developed regions, which is largely attributed to lifestyle, dietary factors, and screening practices (2). Although CRC primarily affects older populations, an alarming increase in incidence has been documented among younger adults, underscoring potential shifts in risk factor exposure and the need for updated preventive strategies. Early disease stages are frequently asymptomatic, and clinical presentation often occurs only once the tumor has advanced, contributing to late-stage diagnosis and poorer survival outcomes. In countries with organized screening programs, such as fecal occult blood testing and colonoscopy, both incidence and mortality have declined, highlighting the crucial role of early detection (3). However, in regions with limited screening availability, the majority of patients still present with advanced disease, where prognosis is significantly worse. In Hungary, CRC remains of particular concern, with the world's highest age-standardized incidence rate and the second highest mortality, reflecting both genetic susceptibility and healthcare system challenges (4, 5). Understanding the interplay between epidemiological trends, molecular pathogenesis, and health policy is therefore essential to improving outcomes and guiding effective public health interventions.

## 1.2 Signaling pathways of CRC

### 1.2.1 Wnt/ß-catenin Pathway

The Wnt (Wingless/Integrated) /ß-catenin signaling cascade represents one of the most crucial pathways in colorectal tumorigenesis, particularly in the initiation stage of the adenoma-carcinoma sequence (6). Under physiological conditions, Wnt ligands bind to Frizzled (FZD) and LRP5/6 (LDL receptor-related protein) coreceptors, leading to the recruitment of Disheveled (DVL) proteins that inhibit the ß-catenin destruction complex, which is composed of APC (Adenomatous Polyposis coli), AXIN1 (axis inhibition protein 1), CK1α (casein kinase 1α), and GSK3ß (Glycogen synthase kinase 3-ß). When

this complex is inactivated, cytoplasmic ß-catenin is stabilized and accumulates, subsequently translocating to the nucleus where it interacts with TCF (T-cell factor) /LEF (Lymphoid Enhancer Binding Factor) transcription factors to activate downstream genes such as MYC (myelocytomatosis), CCND1 (Cyclin D1), and AXIN2 (Axis inhibition protein 2) (Fig 1). In the absence of Wnt ligand, ß-catenin is constitutively phosphorylated by CK1α and GSK3ß, targeted for ubiquitination by ß-TrCP (ß-Transducin repeat-containing protein), and degraded in the proteasome, thereby preventing uncontrolled gene expression. Most sporadic CRC cases harbor truncating mutations in APC, leading to constitutive activation of the Wnt/ß-catenin pathway independent of ligand stimulation. This aberrant signaling promotes proliferation, survival, epithelial-to-mesenchymal transition (EMT), and metastatic competence. Moreover, dysregulated Wnt signaling contributes to stemness features of cancer stem cells, sustaining tumor heterogeneity and chemoresistance. Therefore, the Wnt/ß-catenin axis is considered a hallmark pathway in colorectal carcinogenesis, providing both diagnostic and therapeutic potential(7).

### 1.2.2 EGFR/RAS/RAF/MAPK Pathway

The EGFR/RAS/RAF/MAPK signaling cascade plays a pivotal role in regulating cell proliferation, survival, and differentiation, and its dysregulation is a well-established driver of CRC progression. Physiologically, binding of EGF (Epidermal growth factor) or other ligands to EGFR (Epidermal growth factor receptor) promotes receptor dimerization and autophosphorylation on tyrosine residues, creating docking sites for SH2 (src homology domain 2)-domain-containing adaptor proteins such as Grb2 (growth factor receptor bound protein 2) (8). This, in turn, recruits SOS (son of seven-less), which functions as a guanine nucleotide exchange factor (GEF), facilitating the conversion of RAS (rat sarcoma virus protein) – GDP (guanosine diphosphate) to RAS-GTP (guanosine triphosphate) and thereby activating RAS. Activated RAS initiates a phosphorylation cascade through RAF (rapidly accelerated fibrosarcoma), MEK (mitogen activated protein kinase kinase), and ERK1/2 (extracellular signal regulated kinase), culminating in nuclear translocation of ERK where transcription factors such as c-FOS (cellular – FBJ murine osteosarcoma viral oncogene homolog), and c-JUN (cellular-Jun) are activated to promote genes driving proliferation and survival (Fig 1). Pathologically, mutations in K-RAS (Kirsten RAS), N-RAS (Neuroblastoma RAS), or BRAF (viral-RAF murine sarcoma viral oncogene homolog B) can render this pathway constitutively active,

bypassing upstream EGFR control (9). These mutations not only enhance pro-proliferative and anti-apoptotic signals but also contribute to angiogenesis, invasion, and metastasis. Clinically, K-RAS/N-RAS and BRAF mutation status serves as a predictive biomarker for resistance to anti-EGFR monoclonal antibodies such as cetuximab and panitumumab (10). Thus, the EGFR/RAS/RAF/MAPK (Mitogen-Activated Protein Kinase) pathway exemplifies a central oncogenic signaling hub in CRC with both prognostic and therapeutic implications.

### 1.2.3 PI3K/AKT/mTOR Pathway

The PI3K (Phosphoinositide 3-kinase)/AKT (Ak strain transforming)/mTOR (mammalian target of rapamycin) pathway represents another major signaling axis downstream of EGFR activation that regulates metabolism, survival, and angiogenesis in both normal and malignant colorectal epithelial cells (11). Upon ligand binding to receptor tyrosine kinases, the PI3K catalytic subunit p110α/PIK3CA (phosphatidylinositol 4,5-bisphosphate 3-kinase catalytic subunit alpha), often through its interaction with SH2-domain-containing adaptor proteins, phosphorylates PIP2 (phosphatidylinositol 4,5-bisphosphate) into PIP3 (phosphatidylinositol 3,4,5-trisphosphate) at the plasma membrane (12). This recruits and activates AKT through phosphorylation by PDK1 (Pyruvate dehydrogenase kinase 1), which subsequently phosphorylates a wide array of downstream targets regulating apoptosis, cell cycle progression, and glucose metabolism. AKT also activates mTORC1 (mTOR-complex 1), a master regulator of protein synthesis and cell growth, thereby sustaining anabolic metabolism and angiogenesis in tumor cells (Fig 1). In CRC, activating mutations in PIK3CA or inactivation of the tumor suppressor PTEN (phosphatase and tensin homolog) frequently lead to constitutive signaling through this pathway. Furthermore, crosstalk between PI3K/AKT and MAPK pathways can amplify tumor progression and complicate targeted therapy (13). Consequently, the PI3K/AKT/mTOR pathway remains a critical therapeutic target under investigation in CRC, with multiple inhibitors currently in clinical trials.

### 1.2.4 TGF-ß/SMAD Pathway

The TGF-ß (Transforming growth factor-ß) /SMAD (Sma- and Mad-related protein) signaling pathway exerts a paradoxical role in CRC, functioning as a tumor suppressor in

early stages but promoting invasion and metastasis in advanced disease. Under physiological conditions, binding of TGF-ß to its type II serine/threonine kinase receptor (TGFBR2) recruits and phosphorylates type I receptor (TGFBR1), which subsequently phosphorylates receptor-regulated SMADs (R-SMADs: SMAD2/3) (14). These form complexes with co-SMAD (SMAD4) and translocate to the nucleus to regulate transcription of genes involved in cell cycle arrest and apoptosis (Fig 1). In CRC, frequent mutations in TGFBR2 or loss of SMAD4 disrupt this suppressive function, thereby allowing unrestrained proliferation (14, 15). Intriguingly, in late-stage CRC, persistent TGF-ß signaling promotes EMT, extracellular matrix remodeling, and immunosuppression, thereby facilitating metastatic dissemination and poor prognosis. The dual role of TGF-ß underscores its context-dependent function, shifting from tumor suppression to oncogenic driver depending on genetic background and tumor stage (16). Given this complexity, therapeutic targeting of TGF-ß signaling remains challenging, as inhibition may prevent metastasis but also risk eliminating its early suppressive functions.

### 1.2.5 p53 Pathway

The p53 tumor suppressor pathway is central to maintaining genomic stability and orchestrating the cellular response to stress, with its inactivation being a late but critical event in CRC progression. Under normal conditions, p53 is tightly regulated by MDM2 (murine double minute 2)-mediated ubiquitination and degradation, but upon DNA damage or oncogenic stress, post-translational modifications stabilize p53, allowing it to activate transcription of genes involved in apoptosis BAX (Bcl-2-Associated X protein), PUMA (p53 upregulated modulator of apoptosis)), cell cycle arrest (p21), and DNA repair (17). In CRC, TP53 mutations occur in more than 50% of cases, often resulting in loss of tumor suppressor function and, in some cases, gain-of-function mutations that actively promote tumorigenesis. The loss of functional p53 leads to impaired apoptosis, tolerance of DNA damage, chromosomal instability, and accumulation of oncogenic mutations. Furthermore, p53 dysfunction allows cancer cells to evade senescence and enhances resistance to chemotherapeutic agents that rely on intact apoptotic signaling (18). Importantly, p53 interacts with other oncogenic pathways such as Wnt/ß-catenin and PI3K/AKT, further compounding its role in CRC progression. Thus, p53 represents not only a key molecular hallmark of advanced colorectal cancer but also a challenging

therapeutic target, as direct reactivation strategies have shown limited clinical success (19).

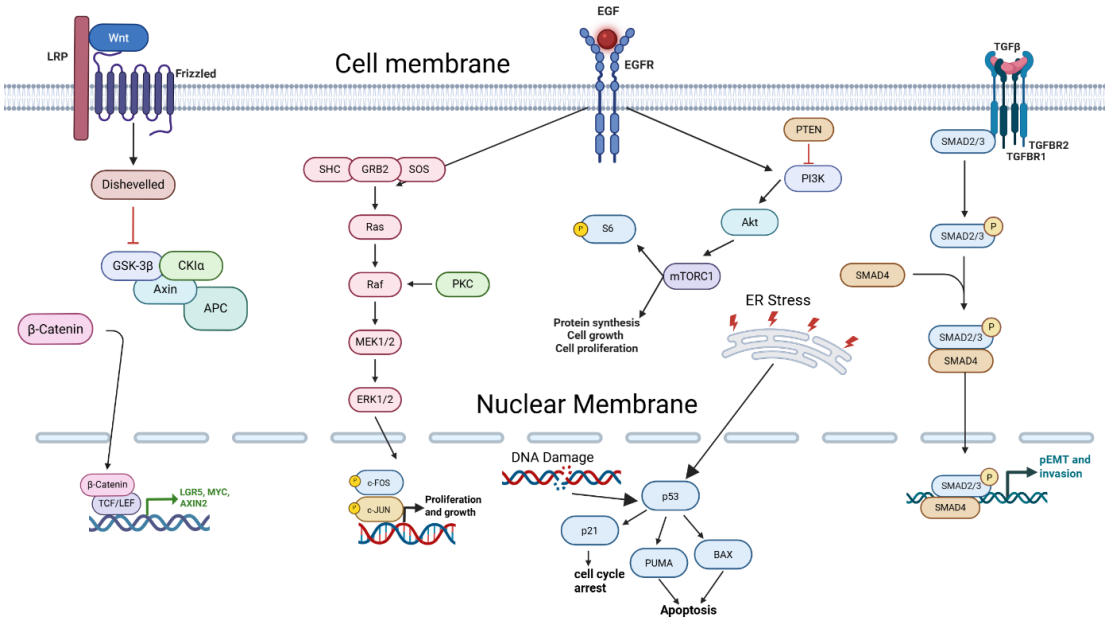


**Figure 1. Schematic overview of the key signaling pathways involved in colorectal cancer.** Canonical oncogenic pathways (Wnt/ß-catenin, EGFR/MAPK, PI3K/AKT/mTOR, TGF-ß/SMAD, and p53) interact dynamically to regulate proliferation, survival, and invasion (unpublished own figure made by Biorender).

## 1.3 Colon Polyp Morphology and Histology

Colorectal polyps represent precursor lesions for the majority of colorectal cancers, making their morphology and histology critical to understanding malignant transformation. Morphologically, polyps are classified according to the Paris endoscopic classification into pedunculated, sessile, flat, depressed, or excavated types, each with varying clinical significance (20, 21). Pedunculated lesions typically exhibit a stalk with a bulbous head, while sessile polyps are broad-based, lying in the same plane as the mucosal surface, a feature that can complicate endoscopic detection. From a histological perspective, the WHO 5$^{th}$ edition classification of digestive system tumors recognizes colorectal polyps as either non-neoplastic (e.g., hyperplastic polyps) or neoplastic, with the latter comprising adenomatous and serrated categories (22). Adenomas are further classified as tubular, tubulovillous, or villous, with a higher proportion of villous architecture correlating with increased malignant potential. Serrated polyps, including sessile serrated lesions (SSLs), traditional serrated adenomas (TSAs), and microvesicular hyperplastic polyps (MHPs), are now established as key precursors within the serrated

neoplasia pathway, reflecting a major refinement from earlier WHO classifications. Importantly, the degree of epithelial dysplasia, stratified into low- and high-grade according to WHO criteria, remains a pivotal determinant of progression risk and guides clinical management. Thus, integration of morphological and histological classification, as defined by international consensus, is essential for risk stratification and surveillance strategies in colorectal cancer prevention.

## 1.4 Tumorigenesis

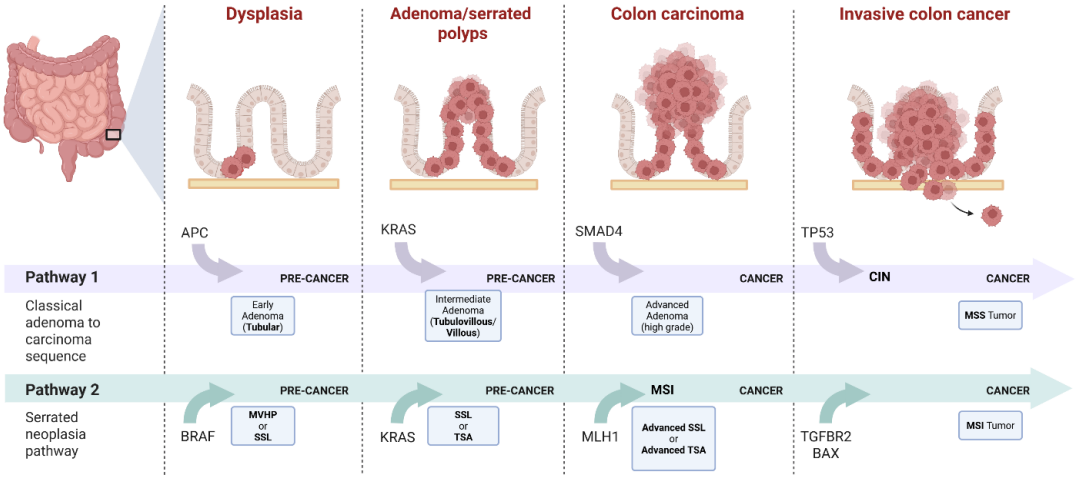


**Figure 2. Morphological and molecular pathways of colorectal tumorigenesis.** The conventional adenoma-carcinoma sequence (pathway 1) typically arises from tubular or villous adenomas through sequential mutations in APC, KRAS, SMAD4, and TP53, leading to chromosomal instability (CIN) and invasive carcinoma. In contrast, the serrated pathway (pathway 2) develops from microvesicular hyperplastic polyps (MVHP), sessile serrated lesions (SSLs), or traditional serrated adenomas (TSAs) characterized by activating BRAF mutations, CpG island methylator phenotype (CIMP), MLH1 silencing resulting microsatellite instability (MSI), followed by mutations in TGFBR2 and BAX. Both pathways ultimately converge on invasive colorectal carcinoma, illustrating the interplay between polyp morphology, histology, and genetic progression in colorectal cancer development (unpublished own figure made by Biorender).

CRC arises through a stepwise accumulation of genetic and epigenetic alterations that progressively transform normal epithelium into adenomatous or serrated polyps, and eventually invasive carcinoma (Fig 2). This biological continuum closely parallels the morphological and histological features of precursor polyps, highlighting the tight interplay between polyp phenotype and molecular pathogenesis.

### 1.4.1 The classical adenoma-carcinoma sequence

The most established route of colorectal tumorigenesis follows the adenoma-carcinoma sequence, first conceptualized by Fearon and Vogelstein (23). In this model, neoplastic

progression is typically initiated in conventional adenomas (tubular, tubulovillous, or villous) through biallelic inactivation of APC. Loss of APC function leads to constitutive activation of the Wnt/ß-catenin pathway, enabling uncontrolled proliferation and expansion of aberrant crypt foci into early adenomas. Subsequent activating mutations in KRAS enhance proliferative signaling via the MAPK cascade, driving growth of intermediate adenomas (24). Progression to advanced adenomas is then facilitated by inactivation of TGF-ß pathway components (SMAD4, TGFBR2), which removes growth-inhibitory signals and permits dysplastic expansion (25). Another critical transition to invasive carcinoma is marked by TP53 loss, which abolishes genome surveillance, fosters chromosomal instability (CIN), and accelerates clonal evolution (Fig 2). Histologically, this progression corresponds to the increasing architechural complexity and dysplasia seen in adenomas, particularly those with villous features or high-grade dysplasia.

### 1.4.2 The serrated pathway

An alternative but equally significant route of CRC development is the serrated neoplasia pathway, which accounts for a substantial proportion of cancers arising from MHPs, SSLs and TSAs (26). Morphologically, SSLs are frequently flat or sessile, posing diagnostic challenges during colonoscopy. At the molecular level, serrated pathway lesions are often characterized by activating mutations in BRAF (and less freqeuently KRAS), coupled with widespread CpG island hypermethylation (CIMP) (27). In sporadic cases, CIMP frequently leads to epigenetic silencing of the mismatch repair gene e.g. MLH1 (MutL protein homolog 1), resulting in microsatellite instability (MSI). MSI tumors exhibit mutations in genes such as TGFBR2 and BAX, driving malignant progression (28) (Fig 2). Unlike the conventional pathway, serrated lesions can progress to carcinoma without passing through an overt villous adenoma stage, underscoring the importance of histological recognition of serrated precursors.

Together, these pathways illustrate that colorectal tumorigenesis is not a uniform process, but rather a set of parallel evolutionary routes defined by the interplay of precursor morphology, histological subtype, and underlying genetic alterations. Conventional adenomas generally progress via the CIN-driven adenoma-carcinoma sequence, while serrated lesions give rise to cancers through MSI and/or CIMP mechanisms. Importantly, the degree of epithelial dysplasia, low versus high grade, remains a pivotal histological

determinant of malignant potential, regardless of morphological subtype. Thus, integrating polyp morphology and histology with molecular progression models provides a comprehensive framework for risk stratification, surveillance, and precision prevention strategies in CRC.

## 1.5 Tumoral Heterogeneity

CRC is not a uniform disease entity but rather a mosaic of diverse cellular populations shaped by genetic, epigenetic, and microenvironmental factors. Tumoral heterogeneity operates at multiple levels: inter-tumoral, and intra-tumoral; each contributing to disease behavior, therapeutic response, and clinical outcomes. High-resolution technologies such as single-cell sequencing, spatial transcriptomics, and organoid models have begun to unravel the full spectrum of CRC heterogeneity (29). These approaches reveal that subclonal diversity is not a static phenomenon but evolves dynamically during progression, therapy, and recurrence.

### 1.5.1 Inter-tumoral heterogeneity

At the macroscopic and histological levels, CRC demonstrates considerable variability in precursor lesions and evolutionary trajectories. As outlined previously, adenomatous polyps (tubular, tubulovillous, villous) typically follow the classical adenoma-carcinoma sequence, whereas serrated lesions progress via the serrated pathway characterized by CIMP and MSI. These morphological and molecular distinctions not only define divergent routes of tumorigenesis but also manifest in distinct clinical phenotypes, with serrated pathway cancers often arising in the proximal colon and showing differential prognosis and therapy responsiveness.

### 1.5.2 Intra-tumoral heterogeneity

Within a single tumor, spatial and temporal diversity among cancer cell populations is a defining hallmark (30). Clonal diversification arises through the accumulation of somatic mutations, copy number alterations, and epigenetic reprogramming, often facilitated by CIN and MSI. This results in subclones with distinct proliferative, metabolic, and invasive properties coexisting within the same lesion. An example for this heterogeneity is the presence of cancer stem cells that are major drivers of tumor growth. Several molecules, such as CD44, PTK7 or CD133 have been suggested as markers of this aggressive tumor

cell population fueling tumor growth. Over time, selective pressures from endogenous factors (e.g., defective mismatch repair, hypoxia, altered signaling dynamics) and exogenous exposures (e.g, diet, alcohol, microbiome-derived metabolites) further sculpt the clonal architecture, favoring the expansion of fitter subpopulations (31-33). This Darwinian selection underlies tumor evolution and progression.

In summary, tumoral heterogeneity in CRC is a multidimensional phenomenon encompassing inter-tumoral diversity between morphological and molecular subtypes, intra-tumoral clonal evolution, and microenvironmental variability. Together, these layers of heterogeneity complicate disease management but also provide opportunities for biomarker discovery and personalized therapy development.

## 1.6 CRC Classifiers

The substantial morphological, histological, and molecular diversity of CRC has necessitated the development of refined classification systems that capture the complexity of its pathogenesis. While early frameworks focused on morphology (e.g., Paris endoscopic classification) and histology (e.g., WHO classification into adenomatous and serrated polyps), and subsequent models described distinct signaling pathways of tumorigenesis (CIN, MSI, and CIMP), more recent efforts have aimed to integrate these features into molecularly defined subtypes. These classifiers not only reflect the underlying biology but also hold promise for risk stratification, prognosis, and guiding personalized therapeutic strategies.

### 1.6.1 Consensus Molecular Subtype (CMS) Classification

In 2015, the Colorectal Cancer Subtyping Consortium integrated 18 independent transcriptomic datasets to establish the Consensus Molecular Subtypes (CMS), a widely recognized molecular taxonomy of CRC (34). Four robust subtypes were defined, covering ~87% of cases, with ~13% exhibiting mixed features (Fig 3). The CMS framework captures not only the genetic and epigenetic underpinnings of CRC but also tumor microenvironmental influences such as immune infiltration and stromal composition, thus linking intrinsic tumor biology with extrinsic factors of tumor heterogeneity. Interestingly, although some mutations occur at an uneven frequency among CMS subgroups, none of the groups can be connected to specific genetic events,

highlighting the role of epigenetic and microenvironmental factors in modifying cancer cell behavior.

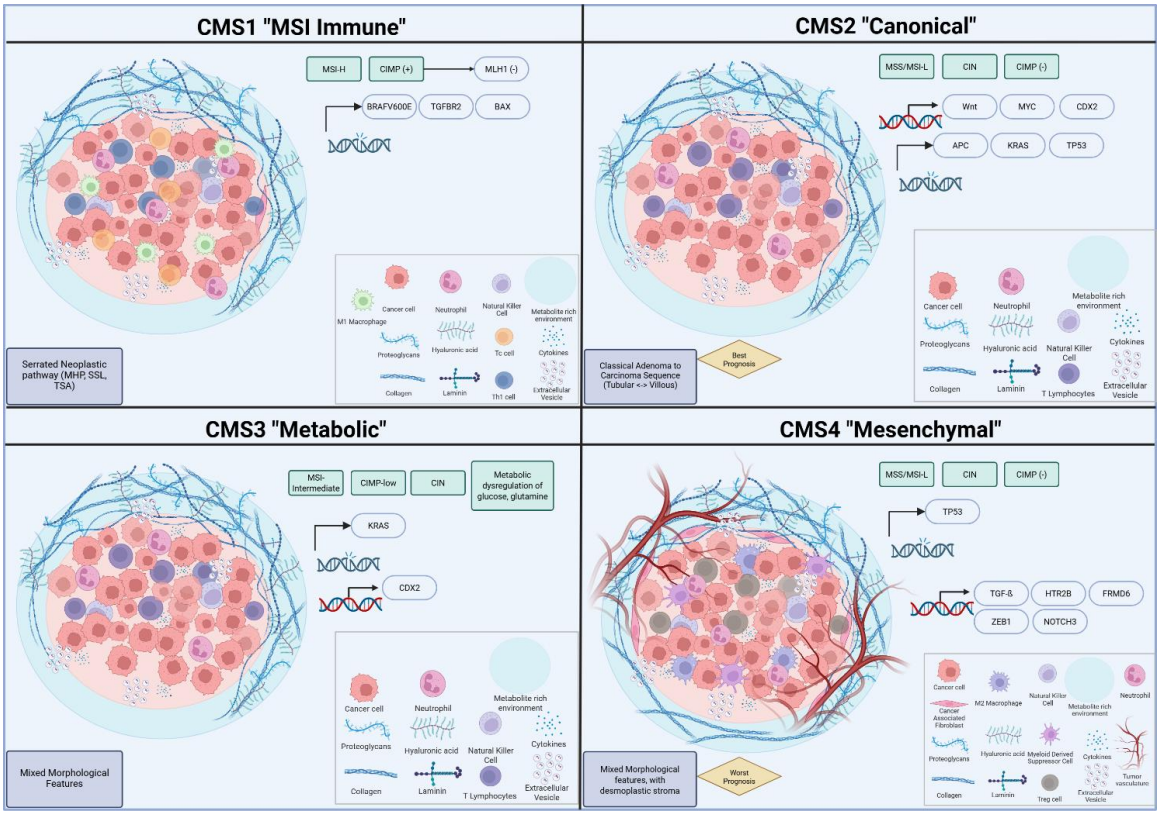


**Figure 3. Consensus Molecular Subtypes (CMS) of colorectal cancer: integrating Genomic, morphological and microenvironmental traits.** The CMS1-CMS4 represent distinct biological and clinical entities in colorectal cancer. CMS1 ("MSI Immune") tumors arise from serrated lesions, exhibit BRAF mutation, CIMP-high phenotype, and strong immune activation. CMS2 ("Canonical") follows the classical adenoma-carcinoma sequence with APC/KRAS/TP53 mutations and active Wnt/MYC signaling, showing the best prognosis. CMS3 ("Metabolic") is defined by KRAS mutation, deregulated metabolism, and intermediate molecular instability. CMS4 ("Mesenchymal") features TP53 mutation, TGF-ß driven stromal activation, EMT, and poor prognosis. The CMS framework captures both intrinsic tumor biology and microenvironmental influences shaping colorectal cancer progression (unpublished own figure made by Biorender).

#### *1.6.1.1 CMS1*

Characterized by high microsatellite instability, CIMP positivity, and strong immune activation. It exhibits low CIN but frequent BRAF mutations, along with MLH1 silencing and TGFBR2 mutations. Morphologically, these tumors often arise from SSLs in the proximal colon. The immune-enriched microenvironment underpins favorable early prognosis, yet patients may have poor outcomes following relapse (35). Immune checkpoint inhibitors may function in this subgroup.

#### *1.6.1.2 CMS2*

The most prevalent subtype, defined by epithelial differentiation, high CIN, and activation of WNT and MYC signaling, reflecting the classical adenoma-carcinoma sequence. It typically follows an APC, KRAS, TP53 mutational trajectory. Morphologically, CMS2 is commonly associated with tubular adenocarcinomas (36). Patients with CMS2 generally have the best overall survival.

#### *1.6.1.3 CMS3*

Distinguished by deregulated cellular metabolism, including glutamine, glucose, and fatty acid pathways (37). It displays intermediate MSI, low-CIMP, frequent KRAS mutations, and CIN. Morphologically, CMS3 tumors show features overlapping both serrated and conventional adenomas, reflecting their hybrid biological profile (36, 38). Prognostically, CMS3 has limited therapeutic responsiveness, particularly to anti-EGFR therapies (when KRAS is mutated), and overall poorer outcomes compared to CMS2 especially in metastatic disease setting (38, 39).

#### *1.6.1.4 CMS4*

CMS4, often denoted the mesenchymal subtype, accounts for approximately 23% of colorectal cancers and is characterized by pronounced stromal activation, angiogenesis, and TGF-ß pathway signaling. Tumors in this category frequently exhibit EMT features, accompanied by dense infiltration of cancer-associated fibroblasts (CAFs) and a pro-inflammatory milieu (40).

Functionally, CMS4 tumors harbor early TP53 mutations, yet despite sharing genomic instability with CMS2, their dominant mesenchymal phenotype confers a high metastatic propensity and resistance to standard therapies, culminating in the worst overall prognosis among CMS subtypes (41). Recent spatial and expression analyses underscore that CMS4 tumors are not homogenous but rather comprise distinct epithelial subpopulations overlaying a fibrotic tumor microenvironment (TME), highlighting the interplay between cancer cell-intrinsic traits and the microenvironment (36).

Although CMS classification has become a benchmark in research, its transcriptomic requirements limit routine clinical applicability. To address this, simplified immunohistochemistry-based classifiers have been developed, using markers such as

CDX2 (Caudal-type homeobox transcription factor 2) for CMS2/3 and HTR2B (5-Hydroxytryptamine receptor 2B), FRMD6 (FERM domain-containing protein 6), ZEB1 (Zinc Finger E-box binding homeobox 1) for CMS4, providing a pragmatic bridge between molecular classification and pathology practice (42).

### 1.6.2 Alternative Classifiers

While CMS remains the most widely cited integrative classifier, several alternative systems complement or refine its framework. MSI, CIN, and CIMP remain cornerstone molecular stratifiers. MSI testing is now standard in clinical practice due to its prognostic and predictive relevance, particularly in identifying candidates for immune checkpoint inhibitor therapy. CIN and CIMP, while less commonly used in daily practice, are central to understanding the biological basis of CRC heterogeneity.

#### *1.6.2.1 Immunoscore*

Developed as a prognostic tool, the Immunoscore quantifies CD3+ and CD8+ T-cell infiltration in the tumor core and invasive margin (43). Graded from 0 (absent) to 4 (high infiltration in both compartments), this score has demonstrated superior prognostic power compared to conventional AJCC TNM staging. It exemplifies the shift from tumor-intrinsic to immune microenvironment-based classifiers, underscoring the importance of host-tumor interactions in CRC outcomes.

#### *1.6.2.2 Colorectal Cancer Intrinsic Subtypes (CRIS)*

Proposed by Isella et al., the CRIS system focuses on cancer cell-intrinsic transcriptomic features, filtering out stromal contributions by leveraging patient-derived xenograft models (44). Five CRIS subtypes (A-E) were identified. CRIS-A and CRIS-B are MSI-enriched, inflammatory, or poorly differentiated, with BRAF/KRAS mutations and EMT/TGF-ß activation. CRIS-C, CRIS-D, and CRIS-E are MSS/CIN-enriched, with signatures of EGFR, MYC, WNT, FGFR (Fibroblast Growth Factor Receptor), and stemness. This classification shows strong alignment with CMS (e.g, CRIS-C/D/E with CMS2, CRIS-B with CMS4), but offer greater specificity for predicting therapeutic responses such as anti-EGFR sensitivity (CRIS-C) or prognosis (CRIS-B poor outcome).

#### *1.6.2.3 IMF Classification (Intrinsic Epithelium-MSI-Fibrosis)*

A cutting-edge refinement of CRC molecular taxonomy is the IMF classification, introduced by Joanito et al. in Nature Genetics (2022), which integrates three layered dimensions: intrinsic epithelial state (I), microsatellite instability status (M), and presence of fibrosis (F) (45). Through single-cell and bulk transcriptomic analyses, two intrinsic epithelial subtypes iCMS2 and iCMS3 were delinated. Notably, iCMS3 includes both MSI-high cancer and a substantial proportion of MSS tumors whose transcriptional and regulatory profiles resemble MSI tumors more than other MSS counterparts.

By overlaying epithelial subtype, MSI status, and fibrosis, the IMF framework defines five major CRC classes, including fibrotic versus non-fibrotic subdivisions, which together recapitulate approximately 90% of cases. Importantly, fibrotic CMS4 tumors can stem from either iCMS2 or iCMS3 epithelium, with the iCMS3_MSS_fibrotic subgroup exhibiting particularly poor relapse-free and overall survival (45). This refined stratification moves beyond bulk CMS to better resolve inter- and intra-tumoral heterogeneity, highlighting how epithelial cellular programs, genomic instability, and microenvironmental fibrosis converge to define tumor behavior.

## 1.7 Tumor Microenvironment (TME)

The TME plays a central role in the pathogenesis and progression of colorectal cancer (CRC), functioning not as a passive scaffold but as a dynamic ecosystem of stromal, immune, and vascular components interacting with neoplastic epithelial cells (46). Building upon the framework of tumoral heterogeneity and molecular classifiers (CMS and IMF), each molecular subtype of CRC reflects not only intrinsic genomic and epigenetic alterations, but also the selective pressures and reciprocal interactions imposed by its surrounding microenvironment. Notably, CMS4 (“mesenchymal”) tumors exemplify this paradigm, where stromal activation, extracellular matrix (ECM) remodeling, and an abundant fibro-inflammatory milieu shape tumor morphology and drive aggressive clinical behavior.

The TME is composed of multiple interconnected elements, including the ECM, CAFs, immune infiltrates, and a spectrum of soluble mediators such as growth factors, cytokines and chemokines. Furthermore, metabolic adaptations in glucose, amino acid, and fatty acid utilization extend beyond cancer cell-intrinsic traits to involve reciprocal nutrient

exchange with stromal and immune populations. Together, these factors form a co-evolving ecosystem, driving tumor progression, immune evasion, metastasis, and therapeutic resistance.

### 1.7.1 Extracellular Matrix

The ECM provides both a structural scaffold and a dynamic signaling platform for tumor and stromal cells. ECM remodeling is a hallmark of CRC progression, encompassing deposition, degradation, and cross-linking of collagens, proteoglycans, and glycoproteins (47). These modifications alter tissue stiffness, cell adhesion, and mechanotransduction, directly influencing epithelial plasticity and metastatic dissemination. In CRC, progressive accumulation of fibrillar collagens (e.g., collagen I) and enhanced activity of matrix metalloproteinases (MMP-2, MMP-9) promote invasion, while loss of basement membrane components such as collagen IV facilitates stromal infiltration (48). Increased ECM stiffness through enzymatic crosslinking (e.g, LOX (Lysyl oxidase)-mediated) fosters EMT, cytoskeletal reorganization, and invadopodia formation, thereby linking structural alterations to signaling cascades such as Wnt/ß-catenin and TGF-ß (49).

#### *1.7.1.1 Collagen*

Collagens, particularly types I, III, and V, are enriched in the CRC interstitial matrix and correlate with tumor stage and invasion depth. Type I collagen deposition stiffens the ECM, enhancing integrin-mediated signaling and promoting EMT through transcription factors such as SNAIL (Snail Family Transcriptional Repressor 1) and TWIST (Twist-related protein 1) (50, 51). Conversely, basement membrane-specific collagen IV is often reduced in invasive CRC, marking the loss of polarity and barrier function (48). Collagen remodeling enzymes (LOX, MMPs) act as critical regulators of these dynamics and have emerged as therapeutic targets to mitigate stromal-driven invasion.

### 1.7.2 Cancer-Associated Fibroblasts

CAFs are the dominant stromal cell type within CRC, particularly enriched in CMS4 tumors, where they constitute a hallmark of the mesenchymal signature. Arising primarily from resident fibroblasts under the influence of TGF-ß and interleukin(IL)-6, CAFs adopt a spindle-like morphology and express mesenchymal markers such as vimentin and α-smooth muscle actin (α-SMA) (52). Functionally, CAFs remodel the ECM, secrete growth factors (e.g., HGF, TGF-ß, IL-6), and exchange extracellular vesicles with tumor

cells (53-55). These actions collectively reinforce proliferative signaling, stabilize ß-catenin, promote EMT, and foster angiogenesis (56). Moreover, CAF-derived IL-6 activates the JAK(Janus kinase)/ STAT3(Signal transducer and activator of transcription 3) axis in tumor cells, enhancing migration and metastatic competency, while reciprocal TGF-ß signaling establishes a self sustaining fibroblast-epithelium feedback loop (53, 57).

### 1.7.3 Metabolites (Glucose, Amino Acids, Fatty Acids)

Metabolic reprogramming in CRC extends beyond cancer cells to involve metabolic symbiosis within the TME. For glucose metabolism, aerobic glycolysis (Warburg effect) drives lactate accumulation, acidifying the microenvironment and suppressing cytotoxic T-cell function (58). CAFs can undergo glycolytic reprogramming themselves exporting lactate and pyruvate to fuel oxidative phosphorylation in cancer cells ("reverse Warburg effect") (58). For amino acid metabolism, glutamine metabolism in particular supports nucleotide biosynthesis and redox balance, but also shapes immune evasion by depleting nutrients required for T-cell activation (59). Altered lipid metabolism, including enhanced fatty acid oxidation and uptake of exogenous fatty acids, supports metastatic seeding and increases likelihood of peroxidation due to oxidative stress activating an inflammatory response in colonic epithelial cells therefore promoting tumor progression (60). Stromal adipocytes and CAFs contribute to this lipid pool, reinforcing tumor-stroma metabolic coupling.

### 1.7.4 Tumoral Immune Cells

The immune landscape of CRC is highly variable across subtypes. CMS1 tumors exhibit dense immune infiltration with M1 macrophages, cytotoxic T cells and Th1 polarization but are counterbalanced by immune checkpoint upregulation and an immunosuppressive myeloid component (61, 62). CMS4 tumors harbor an immune-excluded phenotype, characterized by myeloid-derived suppressor cells (MDSCs), tumor-associated macrophages (TAMs), especially M2 macrophages, and regulatory T (Treg) cells, all within a fibrotic ECM barrier that restricts effector lymphocyte infiltration (63). Neutrophils and mast cells contribute to angiogenesis and immunosuppression, while NK (Natural Killer) cells are often functionally impaired, especially with fibroblast accumulation (46, 64). Importantly, the prognostic value of the immune infiltrate has been

formalized via the Immunoscore, demonstrating that the type, density, and location of immune cells within the tumor predict outcomes more robustly than TNM (Tumor, Node, and Metastasis) staging (65).

## 1.8 Serotonin signaling

Serotonin (5-hydroxytryptamine, 5-HT) is classically recognized as a neurotransmitter in the central nervous system, yet the majority (~90%) of systemic serotonin is synthesized peripherally by enterochromaffin (EC) cells in the gastrointestinal tract (66). Within the CRC microenvironment, serotonin functions not only as a neuromodulator but also as a paracrine and endocrine regulator that influences epithelial proliferation, stromal activation, angiogenesis, and immune cell polarization (67, 68). Increasing evidence highlights that serotonin signaling intersects with oncogenic pathways and stromal crosstalk, particularly in CMS4 tumors, where HTR2B expression is enriched (69). Thus, understanding serotonin metabolism and receptor-specific functions is central to elucidating its contribution to CRC progression and therapeutic vulnerabilities.

### 1.8.1 Serotonin metabolism

Serotonin is synthesized from the essential amino acid tryptophan through a two-step enzymatic process. Tryptophan hydroxylase 1 (TPH1), expressed primarily in EC cells, catalyzes the conversion of tryptophan to 5-hydroxytryptophan (5-HTP), followed by decarboxylation by aromatic L-amino acid decarboxylase (AADC) to yield serotonin (70). Once released into the extracellular space, serotonin can be actively taken up by cells via the serotonin transporter (SERT, SLC6A4 (Solute Carrier family 6 member 4)), regulating its local availability.

Degradation occurs primarily through monoamine oxidase A (MAO-A), generating 5-hydroxyindoleacetic acid (5-HIAA), a metabolite often used clinically as a biomarker of serotonin turnover (71). Pharmacological inhibition of SERT by selective serotonin reuptake inhibitors (SSRIs), clinically given to patients with depression, anxiety, insomnia and/or chronic pain, has been shown to attenuate CRC growth in preclinical models and epidemiological data from family clusters with high CRC presentation (72, 73).

### 1.8.2 Serotonin receptors

Serotonin exerts its pleiotropic effects through a diverse family of 15 known receptors, broadly divided into seven classes (5-HT1 to 5-HT7) (74). With the exception of 5-HT3 receptors, which are ligand-gated ion channels, all the others are GPCRs (Fig 4). In CRC, differential receptor expressions shape distinct aspects of tumor biology. 5-HT1D enhances invasive capacity by modulating the Axin1/ß-catenin/MMP7 axis (75). 5-HT3 has been implicated in the modulation of cell proliferation and chemotherapy-induced emesis (76, 77). 5-HT2 family members (including HTR2B) integrate serotonin signaling with classical oncogenic cascades such as MAPK, PI3K/AKT/mTOR, and NF-κB (Nuclear Factor kappa-light-chain-enhancer of activated B cells) (78). The selective receptor distribution across tumor cells, immune populations, and stromal compartments provides a mechanistic explanation for serotonin's role as both a mitogenic and immunomodulatory factor in CRC.

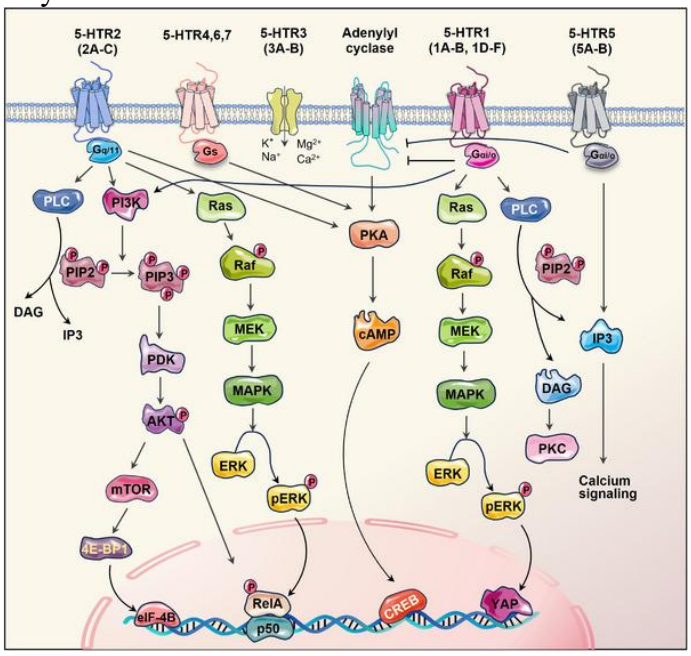


**Figure 4. Overview of Serotonin receptors and their respective major pathways.** Except for the ionotropic 5-HTR3 receptor, all 5-HT receptor subtypes are metabotropic receptors that activate four major interconnected pathways: PI3K/AKT/mTOR, PLC/DAG/PKC, AC/PKA/cAMP, and RAS/RAF/MEK/ERK1/2. These cascades converge on key regulatory nodes controlling proliferation, survival, and transcriptional activity in colorectal cancer cells. (Figure taken from: (79))

#### *1.8.2.1 HTR2B*

HTR2B, a member of the 5-HT2 receptor subfamily, is a GPCR coupled to Gq/11 proteins (78). Upon activation, it stimulates phospholipase C (PLC) to generate diacylglycerol (DAG) and inositol trisphosphate (IP3), which in turn mobilize intracellular calcium and

activate protein kinase C (PKC). Beyond this canonical signaling, HTR2B can activate oncogenic PI3K/AKT/mTOR and RAS/RAF/MEK/ERK1/2 pathways, promoting CRC proliferation and survival (80, 81). In CMS4 tumors, HTR2B is markedly upregulated, aligning with the mesenchymal, stromal-rich phenotype of this subtype. Functionally, HTR2B signaling extends beyond tumor cells to influence the tumor microenvironment. For example, serotonin acting via HTR2B on macrophages biases polarization towards the M2 phenotype, thereby suppressing MMP-12 expression and permitting angiogenesis (82). This suggests that HTR2B is a key mediator of serotonin's immunomodulatory and pro-angiogenic roles in CRC.

Interestingly, evidence from other cancers (e.g., breast) indicates that serotonin receptor signaling can modulate metabolic reprogramming, enhancing glycolysis through pyruvate kinase M2 upregulation and stimulating mitochondrial biogenesis via cAMP (cyclic adenosine monophosphate)/PKA (Protein Kinase A) (82). Whether these metabolic functions of HTR2B extend to CRC remains under investigation, but they represent a promising area for future exploration. Given its multifaceted role in tumor growth, immune modulation, and angiogenesis, HTR2B may serve as a biomarker for CMS4 tumors and as a potential therapeutic target. The responsiveness of CRC to SSRIs and the availability of serotonin receptor antagonists further underscore the translational potential of targeting HTR2B-mediated signaling in colorectal cancer.

## 1.9 Notch Signaling

The Notch-Delta pathway is an evolutionarily conserved signaling cascade that plays a pivotal role in maintaining intestinal epithelial homeostasis by regulating stem cell renewal, lineage commitment, and differentiation (83). In the context of CRC, aberrant activation of Notch signaling fosters malignant transformation by sustaining undifferentiated progenitor populations and suppressing secretory lineages, thereby contributing to tumor heterogeneity (84). Crosstalk between Notch and other oncogenic pathways such as Wnt/ß-catenin, PI3K/AKT, and TGF-ß further amplifies its role in driving proliferation, EMT, and therapeutic resistance (85). Within the TME, stromal cells and immune elements provide Delta-like (DLL) and Jagged ligands that reinforce Notch signaling in cancer cells, establishing a reciprocal axis of tumor-stroma communication (86, 87).

Notch signaling contributes to several hallmarks of CRC, including sustained proliferation, evasion of differentiation, and angiogenesis. Notch-driven EMT programs are mediated through transcription factors such as SNAIL, linking pathways activation to invasive and metastatic phenotypes (85). Furthermore, elevated Notch signaling has been correlated with CMS4 tumors, which are enriched for stromal activation and mesenchymal features, underscoring its relevance to both molecular and morphological classifiers of CRC (88).

### 1.9.1 Notch3

Among the Notch receptors, Notch3 has emerged as a particularly relevant player in CRC progression. Unlike Notch1, which is broadly required for intestinal crypt maintenance, Notch3 appears to be more selectively associated with EMT induction, angiogenesis, ECM remodeling, and immunosuppression (89, 90). Upregulation of Notch3 has been reported in advanced CRC stages, correlating with poor prognosis, chemoresistance, and association with the mesenchymal CMS4 subtype (91). Mechanistically, PI3K/AKT signaling has crosstalk with Notch3, reinforcing the pro-invasive TME (92).

## 1.10 Organoid technology

Cell culturing has long been pivotal in unraveling molecular mechanisms of cancer biology and has provided important clinical insights. The advent of three-dimensional (3D) culture systems marked a transformative step, enabling the generation of cultures that not only retain molecular and structural features of native tissues but also preserve intra- and inter-tumoral heterogeneity (93). Organoid technology has emerged as a particularly powerful approach, allowing cells to self-organize into tissue-like structures composed of differentiated, organ-specific cell types arranged in near-native architectures. Organoids can be derived from embryonic stem cells, induced pluripotent stem cells, or neonatal/adult stem cells (ASCs). Of these, patient-derived ASC organoids (PDO) are especially valuable for modeling CRC, as their growth in defined media supplemented with niche factors allows faithful recapitulation of signaling pathways that maintain epithelial homeostasis (94, 95).

A key technical consideration in organoid culture is the avoidance of direct contact between cells and the rigid plastic surface of culture plates, commonly preventing 3D tissue reconstruction. This is typically overcome by embedding cells in a supportive

scaffold, most commonly Matrigel, a protein-rich extracellular matrix (ECM) hydrogel produced from Engelbreth-Holm-Swarm (EHS) mouse sarcoma (96). Matrigel contains critical ECM components such as laminin, collagen IV, entactin, and heparan sulfate, providing both structural support and ECM signaling cues (97). The landmark work of Toshiro Sato and colleagues in 2009 demonstrated that intestinal ASCs embedded in Matrigel self-organize into crypt-villus structures without the requirement for mesenchymal stroma (98). This discovery laid the foundation for extending organoid technology to CRC, where patient-derived tumor organoids retain histological and molecular features of their parental tumors.

The translational applications of CRC organoids are rapidly expanding. Organoid biobanking enables high-throughput drug screening and the development of precision oncology approaches, where therapeutic responses can be predicted ex vivo using patient-specific cultures (93, 99). Moreover, organoids provide a powerful preclinical tool to uncover mechanisms of drug resistance, identify novel drug combinations, and explore tumor-microenvironment interactions when cocultured with stromal or immune cells (100). These features position organoids as a central platform in efforts to personalize CRC therapy.

# 2. Objectives

CMS provides an essential framework for prognostic and therapeutic stratification in CRC. Among the signaling pathways implicated in CRC progression, serotonin and its receptor HTR2B have gained recognition for their prognostic and therapeutic potential as a marker of the CMS4 subtype, with context-dependent effects that appear to vary with tumor stage. In parallel, molecules characterizing the aggressive CRC subpopulation, such as CD44 (Cluster of Differentiation 44), CD133 (Cluster of Differentiation 133), and PTK7 (Protein Tyrosine Kinase 7) have been associated with proliferative potential (101). Recent evidence also highlights the emerging role of Notch3 in CRC progression and its interplay with tumor heterogeneity and invasion. However, the expression heterogeneity of these molecules and its functional role in CRC tumorigenesis have not been fully clarified yet.

Thus, this thesis aims to elucidate the contributions of CD44, CD133, PTK7, HTR2B, and Notch3 to CRC progression, with a particular emphasis on their roles in tumor heterogeneity, subtype dynamics, proliferation and invasion. This aim is addressed through the following key questions:

1. What are the expression patterns of cancer stem cell markers (CD44, CD133, and PTK7), markers of CMS2/3 (CDX2) and CMS4 (FRMD6, ZEB1, HTR2B) in CRC?
2. To what extent do CMS2/3 and CMS4 markers overlap within the same organoids?
3. How do alterations in the TME affect intratumoral heterogeneity and behavior, focusing on HTR2B?
4. What is the functional role of the HTR2B receptor in CRC progression?
5. Is there a relationship between HTR2B and Notch signaling?

# 3. Methods

A graphical summary of the applied methods is shown in Fig 5.

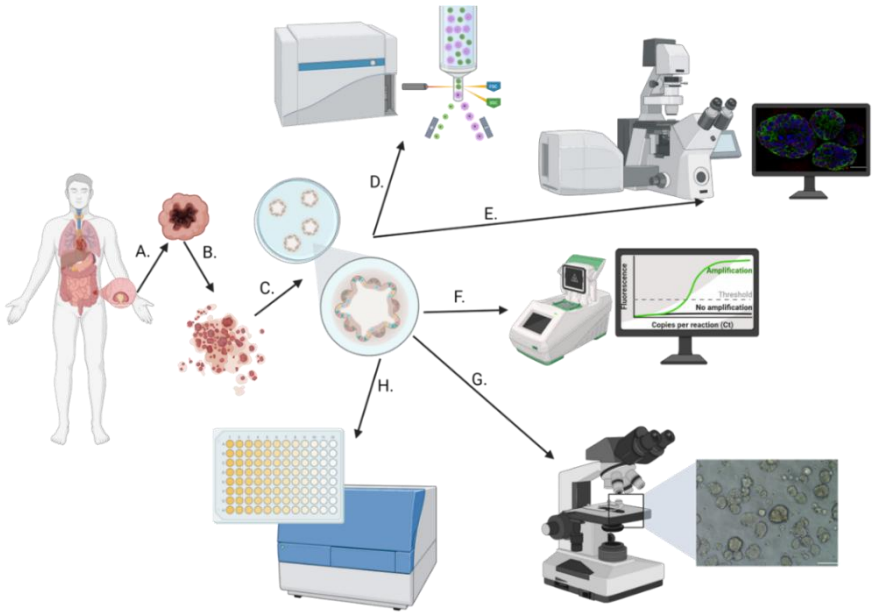


**Figure 5. Methods overview**. **A)** Surgical biopsy from primary CRC tumor. **B)** Chemical and physical dissociation of tumor. **C)** Growing tumor dissociated CRC epithelial cells in ECM to create PDOs. **D)** Flow cytometry measurements and fluorescently activated cell sorting for reculturing of CRC cell subgroups. **E)** Confocal microscopy analysis and Z-stack formation from CRC PDOs. **F)** qRT-PCR analysis for gene expression in CRC PDOs. **G)** Light microscopic qualitative and quantitative evaluation of CRC PDOs. **H)** Serotonin ELISA and luminescent viability assays of CRC PDOs (unpublished own figure made by Biorender).

## 3.1 Cell Cultures

### 3.1.1 Human CRC PDO Cultures

PDOs were used as the experimental model system. Tumor samples were obtained from surgical resections, with informed consent from patients and approval from the Medical Research Council of Hungary (No 51323-4/2015/EKU, TUKEB). The establishment and baseline characterization of the CRC organoid lines employed in this study have been previously described by our research group (101-103). For this thesis, numerical codes identified organoid lines (e.g., Organoid 1-4, Table 1 in Appendix). Tumor biopsies were processed to isolate epithelial cells by a combination of chemical and mechanical dissociation. Cells were embedded in growth factor-reduced Matrigel (Corning) and plated as 20 µL droplets in 24-well plates. After polymerization at 37°C for 20 minutes, droplets were overlaid with complete CRC culture medium. The CRC medium consisted of advanced DMEM/F12 (Gibco) supplemented with 500 nM A83-01 (Merck; TGF-ß

receptor inhibitor), 10 µM SB202190 monohydrochloride (Merck; p38 MAPK inhibitor), 50 ng/mL recombinant EGF (Peprotech, UK), 10 mM Nicotinamide (Merck), 1 mM N-acetyl-L-cysteine (Merck), 10 mM Glutamine (Gibco), B27 supplement (Gibco), 10 mM HEPES (4-(2-hydroxyethyl)-1-piperazineethanesulfonic acid) (Merck), and 10 µM Y-27632 (Rho-associated protein kinase [ROCK] inhibitor; Selleckchem) to prevent anoikis. Organoid cultures were passaged every 5 to 7 days. Briefly, cultures were dissociated by incubation with TrypLE Express (Thermo Fisher) until partial fragmentation of the organoids was achieved. Fragments were washed in Phosphate-Buffer Solution (PBS) and re-seeded in fresh Matrigel, before overlaying with CRC medium as described above. For functional studies, organoid cultures were subjected to the following treatments: HTR2B inhibition via 10 µM RS-127445 (Selleckchem) or 10 µM SB-204741 (MedChemExpress), serotonin stimulation via 10 µM serotonin (Merck), HTR2B agonist 10 µM α-methylserotonin maleate (Merck), or 5-Fluorouracil (5-FU, 1 or 10 µM, MedChemExpress).

**Table 1. Data of patient derived organoids (101, 104)**

| Sample | Gender | Age | Tumor | Differentiation grading | Stage | TP53 wild type | EGF dependency |
|---|---|---|---|---|---|---|---|
| CRC1 | F | 63 | colon adenocarcinoma | Grade 2 | T3N0M0 | no | yes |
| CRC2 | M | 74 | colon adenocarcinoma | Grade 2 | T3N0M0 | no | yes |
| CRC3 | M | 75 | colon adenocarcinoma | Grade 2 | T3N2aM0 | no | yes |
| CRC4 | M | 74 | colon adenocarcinoma | Grade 2 | T3N1M0 | yes | yes |

#### *3.1.1.1 Culturing Collagen-Based PDOs*

While Matrigel was used as the standard extracellular matrix for CRC PDO culture, selected experiments were performed in collagen-I to better mimic an invasive tumor phenotype. Either individual cells or developed organoids isolated from collagen-I matrix or Matrigel were inoculated in this collagen-I hydrogel without mechanical disruption. A collagen-I based hydrogel was prepared fresh and in a defined order to maintain gel integrity. The mixture contained 10% Minimum Essential Medium (MEM; Gibco), 60% distilled water, 30% collagen-I (Corning) and a pH of 7.2 was established with 1M NaOH.

The sequence of addition was critical, as improper mixing led to premature polymerization and loss of the desired matrix properties.

### 3.1.2 Fibroblast culturing and coculturing with PDOs in Matrigel

Human colon fibroblasts (CCD-18Co, ATCC-1459) were used for coculture experiments. Cells were maintained in Dulbecco's Modified Eagle Medium (DMEM; Gibco, Thermo Fisher) containing 4.5 g/L glucose, supplemented with 10% fetal bovine serum (FBS), 1% penicillin/streptomycin, and 1% L-glutamine. Fibroblasts were passaged using TrypLE Express (Thermo Fisher) for 20 minutes at 37°C to dissociate adherent cells from the culture surface. Prior to coculture, fibroblasts were harvested and counted using a Bürker chamber. In parallel, PDO cells were dissociated and similarly counted. Fibroblasts and CRC cells were then mixed at a ratio of 20,000:10,000 cells (2:1 ratio) before placing them in 24-well plates or 8-well chamber slides via 20 µL Matrigel droplets as co-cultures. After polymerization at 37°C for 15 minutes, standard CRC culture medium was added. For each coculture experiment, parallel monocultures of PDO CRCs in Matrigel were established as controls.

## 3.2 Flow Cytometry and Cell Sorting

For flow cytometric analysis, organoid cultures grown in collagen were dissociated into single-cell suspensions using Collagenase II (Merck), followed by TrypLE Express (Thermo Fisher); otherwise, when grown in Matrigel, they were directly dissociated using TrypLE Express. Cells were collected by centrifugation and resuspended in FACS (fluorescence-activated cell sorting) buffer, consisting of phosphate-buffered solution (PBS) supplemented with 2 mM EDTA (ethylenediaminetetraacetic acid), 10 mM HEPES, and 1% bovine serum albumin (BSA). For detection of intracellular antigens, cells were fixed with 4% paraformaldehyde (PFA) in PBS for 20 minutes, then permeabilized using 0.1% saponin in PBS, followed by inoculation of cells with antibodies in 0.1% saponin solution. Otherwise, cells were incubated with primary antibodies in FACS buffer for 20 minutes at room temperature, followed by washing and subsequent incubation with fluorophore-conjugated secondary antibodies also in FACS buffer for an additional 20 minutes under the same conditions (Table 2 in Appendix). Stained cells were washed and resuspended in fresh FACS buffer prior to measurement. Flow cytometric analysis was performed using a Cytoflex cytometer (Beckman Coulter).

For analytical experiments, 5,000-10,000 events were recorded per sample. For preparative experiments, subpopulations of interest were sorted into Qiazol lysis buffer (Qiagen) for RNA isolation or in DMEM with 10% FBS, 1% penicillin/streptomycin, 25 mM HEPES and glutamine for further culturing by FACS using a Sony SH800S cell sorter (Sony Biotechnology). Sorted cells were centrifuged at 300g for 10 minutes at 4°C, embedded in either Matrigel (Corning) or collagen-I, and replated as 20 µL droplets in 24-well plates or 8 well chamber slides for downstream culturing and functional assays. Equal cell numbers were used across experimental conditions to ensure proportional and unbiased comparisons between groups.

## 3.3 Immunostaining

### 3.3.1 Immunocytochemistry

Patient-derived organoids were cultured in 8-well chamber slides (BD Biosciences) and fixed in 4% paraformaldehyde (PFA) for 20 minutes at room temperature, followed by two washes in PBS. Samples were permeabilized and blocked using a whole-mount blocking buffer consisting of 5% FBS, 1% BSA, and 0.3% Triton-X-100 in PBS for 1 hour at room temperature. Organoids were subsequently incubated overnight at 4°C with primary antibodies diluted in blocking buffer (Table 2 in Appendix). After three washes in washing buffer, samples were incubated with fluorophore-conjugated secondary antibodies for 2 hours at room temperature in the dark, followed by three more washes in washing buffer. Nuclei were counterstained with DAPI (4',6-diamidino-2-phenylindole) using ProLong Diamond Antifade Mountant (Thermo Fisher). Confocal imaging was performed using a Leica TCS SP8 laser scanning confocal microscope. Image acquisition settings were kept constant across experimental conditions to enable quantitative comparison. Images were processed and analyzed using Fiji (ImageJ), and quantification of fluorescence intensity and cell populations was performed manually unless otherwise specified.

### 3.3.2 Immunohistochemistry

Samples that were already fixed in PFA and embedded in paraffin were first deparaffinized and rehydrated. Then, sections were boiled using Tris-EDTA high-pH buffer (0.05% Tween-20, 1 mM EDTA solution, and 10 mM Tris base in distilled water with pH of 9) for 15 minutes and then cooled to room temperature for 20 minutes.

Following a wash, sections were blocked via Tris-buffered saline with 0.1% Tween-20 (TBS-T) and 1% BSA, and primary antibodies were inoculated overnight at 4°C, and secondary antibodies were later inoculated for 2 hours at room temperature (all in TBS-T based blocking buffer) (Table 2 in Appendix). Covering of samples was conducted with ProLong Diamond antifade mountant containing DAPI (Thermo Fisher Scientific).

**Table 2. Antibodies used in experiments (101, 104)**

| Antibody | Manufacturer | Host | Clone/Cat No |
|---|---|---|---|
| anti-goat IgG Alexa 568 | Invitrogen | Donkey | A11057 |
| anti-mouse IgG Alexa 488 | Invitrogen | Donkey | A21202 |
| anti-mouse IgG Alexa 568 | Invitrogen | Donkey | A10037 |
| anti-rabbit IgG Alexa 488 | Invitrogen | Donkey | A21206 |
| anti-rabbit IgG Alexa 568 | Invitrogen | Goat | A11011 |
| anti-rabbit IgG Alexa 750 | Invitrogen | Goat | A21039 |
| anti-rat IgG Alexa 488 | Invitrogen | Donkey | A21208 |
| anti-rat IgG Alexa 568 | Invitrogen | Goat | A11077 |
| E-cadherin | BD Transduction Laboratories | Mouse | 610182 |
| human active caspase-3 | R&D Systems | Rabbit | AF835 |
| human CD133 | Miltenyi Biotec | Mouse | 130-090-851 |
| human CD44 | abcam | Rabbit | Ab157107 |
| human CD44 PE | BD Pharmingen | Mouse | 555479 |
| human CDX2 | R&D Systems | Mouse | MAB3665 |
| human EpCAM PE | BD Biosciences | Mouse | 347198 |
| human FRMD6 | Novus | Rabbit | NBP3-05019 |
| human HTR2B (AB #1, IC) | Merck | Rabbit | HPA012867 |
| human HTR2B (AB #2) | Novus | Rabbit | NLS1187 |
| human HTR2B (AB #3, APC Conjugated) | R&D Systems | Rabbit | FAB11297A |
| human KI67 | eBioscience | Mouse | 14-5699-82 |
| human KI67 | abcam | Rabbit | ab16667 |
| human Lumican | abcam | Rabbit | ab168348 |
| human Lumican | R&D Systems | Goat | AF2846 |
| human Notch3 Alexa Fluor-488 | R&D Systems | Mouse | FAB1559G |
| human Phospho-S6 | Cell Signaling | Rabbit | #2211 |
| human PTK7 | Miltenyi Biotec | Mouse | 130-091-578 |
| human PTK7-APC | Miltenyi Biotec | Mouse | 130-099-660 |
| human Vimentin | R&D Systems | Rat | MAB2105 |
| human ZEB1 | Sigma | Rabbit | HPA027524 |

## 3.4 ELISA

After 48 hours of growing PDOs or fibroblasts (serum-free), their conditioned medium was collected, the cellular debris was centrifuged for removal at 300g for 5 minutes, and

with accordance to the manufacturer's protocol (serotonin ELISA kit, Abnova, Taoyuan City, Taiwan) serotonin detection was performed. As a control, Matrigel droplets devoid of organoids were used. Optical Density (OD) values were measured via HiPo MPP-96 Microplate Photometer (Biosan, Riga, Latvia).

## 3.5 RNA Isolation and Expression Analysis

RNA isolation was conducted using miRNEasy Micro Kit (Qiagen). The source of RNA either came directly from cells grown in Matrigel or collagen or after cell sorting. Firstly, cells were immersed in Qiazol lysis buffer (Qiagen), then continued with the manufacturer's protocol resulting with RNA in 14 µL RNAse-free water. With a NanoDrop instrument (Thermo Fisher) RNA concentration was determined. From 300 ng RNA in 20 µL final volume, cDNA was synthesized via the Sensi-FAST cDNA Synthesis Kit (Bioline, Meridian Bioscience, London, UK). qPCR (quantitative-polymerase chain reaction) was conducted with SensiFAST Sybr No-Rox Kit (Bioline) through a BioRad CFX384 Touch real-time PCR instrument (Hercules, CA, USA) with 384 well plate and 5 µL per well, using SybrGreen for annealing at 60 ºC. Evaluation of the results was performed with: relative expression level = $2^{-(\Delta Ct}$), where ΔCt = Ct (gene of interest)—Ct (housekeeping gene). Primer used in qPCR reactions are listed in Table 3 in the Appendix.

**Table 3. RNA Primers used in the experiments (101, 104)**

| Gene | Primer 1 | Primer 2 |
|---|---|---|
| AXIN2 | CTGGCTATGTCTTTGCACCA | CTTCACACTGCGATGCATTT |
| CD133 | GCCTCTGGTGGGGTATTTCT | TACCTGGTGATTTGCCACAA |
| CD44 | GGCTTTCAATAGCACCTTGC | GTTGTTTGCTGCACAGATGG |
| DDC | TGAGAAAGCTGGAGAAGGGG | TCGGATGAGTAAGCCACCAG |
| DLL1 | CTACTGCAGCTCTTCACCCT | AGGTGCAGGAGAAGTCGTTC |
| DLL3 | CTACCACCGGATGCCTTGTC | GTCCATCTGCACATGTCACC |
| DLL4 | GCGAGAAGAAAGTGGACAGG | GAGCCCATTCTCCAGGTCAT |
| GAPDH | GGGTGTGAACCATGAGAAGT | CAGTGATGGCATGGACTGTG |
| HPRT1 | TGAGGATTTGGAAAGGGTGT | TCCCCTGTTGACTGGTCATT |
| HTR2B | TCTGGCTGTTTCACTGGAGA | ATAGAACAAGTGGGAGGGGC |
| JAG1 | CAGAGGCAGCTGTAAGGAGA | CTAACTGGCACGTTTTCCCA |
| JAG2 | GTGTAATTTGCTCCACGGGG | CCAGTTGGTCTCACAGTTGC |
| LGR5 | AGTGCTGTGCATTTGGAGTG | AGGGCTTTCAGGTCTTCCTC |
| LUM | CCTGGTTGAGCTGGATCTGT | GTAGGATAATGGCCCCAGGA |
| MAOA | AATGTGACCTCTGAGCCTCA | AGGTCCATTATCCGTTCGCT |
| MUC2 | ATCCTCAAAAGCAGCGTGTT | CCCCCTCTTTGGTACACTCC |
| NOTCH1 | GCCAACATCCAGGACAACAT | GCGTGTGAGTTGATGAGGTC |

| | | |
|---|---|---|
| NOTCH3 | ATGGATGTCAATGTGCGTGG | CAAAGCAGTCTCGCCAGTAC |
| OLFM4 | CAGAGTGGAACGCTTGGAAT | CCTTGATCAGCTCGAAGTCC |
| PTK7 | GCAGTGGCTCTTTGAGGATG | AGGTGAAGTGTGGCTTCCAG |
| SLC18A2 | CTGTTCCTTCCGACTGTCCC | GCAGAATCCCGCAAATATGG |
| SLC6A4 | TTCTTCTCTCTTGGTCCGGG | ACCGAGCACTGTGAAGATGA |
| SNAI1 | GATGCACATCCGAAGCCACA | TGACATCTGAGTGGGTCTGG |
| TPH1 | CTCTTAGGTCATGTCCCGCT | AGCCAGCACCAAAGACTCTT |
| TWIST1 | CTGAGCAACAGCGAGGAAG | ACAGCCCGCAGACTTCTTG |
| VIM | GGTACTCGCATTCTCCACCT | CTCAATGTCAAGGGCCATCT |
| ZEB1 | GCTGACTGTGAAGGTGTACC | ACATCCTGCTTCATCTGCCT |

## 3.6 Viability Assays

Per well, in 6 µL 3D Matrigel or collagen-I 5000 PDO derived single cells were plated, cultured for 3 days in CRC medium, and then changed to treatment conditions. The treatment conditions consisted of either CRC medium, glucose-free, or amino-acid free medium with or without either serotonin, HTR2B agonist (α-methylserotonin), HTR2B inhibitor 1 (RS-127445), HTR2B inhibitor 2 (SB-204741), or Notch inhibitors (γ-secretase inhibitors, DAPT (N-[N-(3,5-difluorophenacetyl)-L-alanyl]-S-phenylglycine t-butyl ester) and DBZ (Dibenzazepine), 10 µM, MedChemExpress) or a combination of some of the above agents were applied for 3 days. In a few experiments, the HTR2B inhibitor was given an hour before adding serotonin or agonist. Then, viability of the PDOs was evaluated with CellTiterGlo 3D Cell Viability Assay (Promega) based on the manufacturer's instructions, and followed by photometric evaluation of the plate with a Fluoroskan FL (Thermo Fisher Scientific) instrument. The vehicle control was DMSO (dimethyl sulfoxide) and 5 µM staurosporine (MedChemExpress) was the positive control (105). Four technical parallels were established, and then the arithmetic mean was taken. In certain experiments, PDO cells were dissociated, incubated with LIVE/DEAD™ Fixable Blue Dead Cell Stain Kit (Thermo Fisher) according to the manufacturer's instructions for 30 minutes, and were subsequently analyzed with a flow-cytometer.

## 3.7 Bioinformatic and Statistical Analysis

For survival analysis, Kaplan-Meier curves with log-rank tests were conducted from GSE17537 and GSE14333 (https://www.ncbi.nlm.nih.gov/geo) data sets. The results were organized, and expression levels were z-score transformed before statistical

evaluation using the statistical software SPSS 29.0.1.0 (IBM, Armonk, New York, USA). To evaluate CMS groups, the GSE39582 data set was used. In the Protein Atlas database (www.proteinatlas.org) the 'quantity' metric was evaluated for immunostaining positivity of biomarkers in tumoral cells in CRC tissue sections. The experimental data were analyzed with either Student's paired or unpaired *t*-tests or ANOVA (Analysis of Variance) with Tukey post hoc test where $*p < 0.05$, $**p < 0.01$, and $***p < 0.005$ significance levels were applied. For statistical evaluation and graphical representation of results the softwares SPSS 29.0.1.0, Microsoft Excel (Redmond, WA, USA), and GraphPad (Boston, MA, USA) were utilized. For charts, mean with standard deviation, and median with $25^{th}$ and $75^{th}$ percentiles for box plots are shown. Unless stated otherwise, data are representative of three or four PDO lines where each dot corresponds to one organoid line in all figures (n=3 or 4, where n=3, data was collected from PDO lines #1-3). Quantification of whole-mount immunostaining was summarized based on 5-6 images per condition per PDO line with 2-5 organoids per image.

# 4. Results

## 4.1 Heterogeneity of CRC stem cell markers

To investigate intra-tumoral heterogeneity in colorectal cancer, we examined the expression of previously described markers of aggressive tumor cell populations with high colony-forming ability, namely CD44, CD133, PTK7, using CRC PDOs (106-108). RNA expression analysis revealed that all three markers were present across all organoid lines, though expression levels varied among patients. Importantly, the transcript levels of CD44, CD133, and PTK7 were considered higher than those of the mesenchymal marker ZEB1 used as a control in these experiments (Fig. 6).

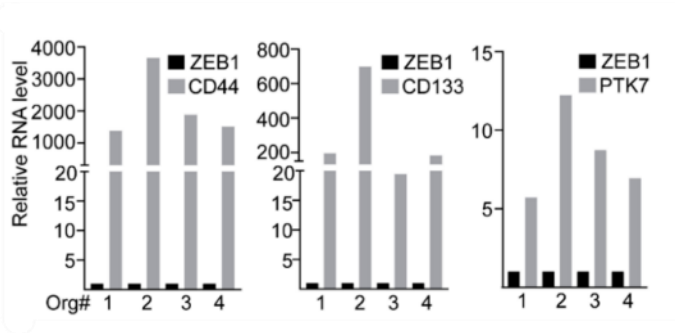


**Figure 6. Heterogeneous RNA expression of CD44, CD133, and PTK7 in CRC PDO lines #1, 2, 3, and #4**. Normalization of the RNA values to HPRT1 as housekeeping was first conducted before normalizing to ZEB1 which was used as a 'standard' relative 1. (the author's own figure: (101)).

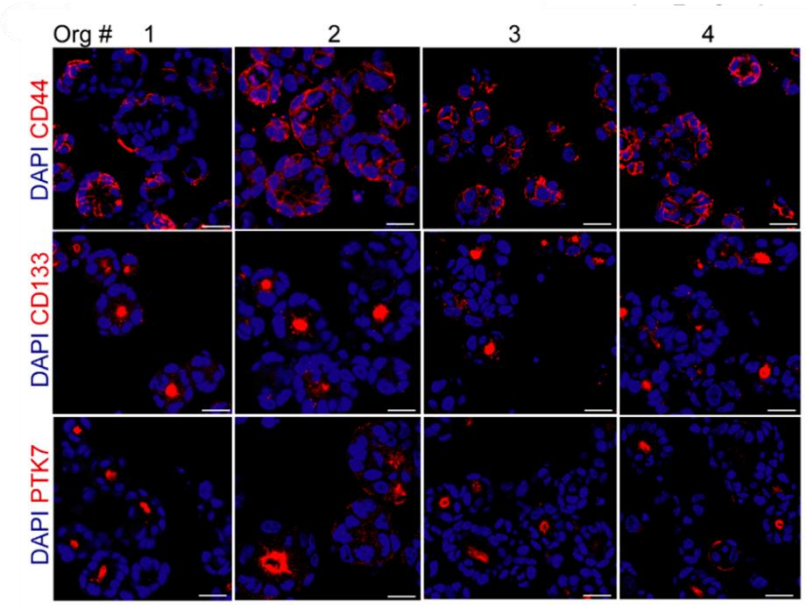


**Figure 7. Heterogenous protein expression of CD44, CD133, and PTK7 in CRC PDOs**. Whole-mount immunostaining for CD44, CD133, and PTK7. Scale bars: 50 µm. (the author's own figure: (101)).

Immunostaining further demonstrated distinct localization patterns: while CD133 and PTK7 were enriched at the apical surface of certain CRC cells, CD44 displayed no such polarized distribution (Fig. 7). Notably, both intra-organoid and inter-organoid heterogeneity was observed in marker expression, indicating that cellular subpopulations with differing levels of CD44, CD133, and PTK7 coexisted within the same patient-derived cultures. Despite this heterogeneity, all three markers were consistently detected in each of the four organoid lines analyzed.

## 4.2 Correlation between the level of CRC stem cell markers and cell proliferation

To investigate the functional relevance of heterogeneity for CD44, CD133, and PTK7 level, we sorted patient-derived organoid cells based on the highest and lowest expression of these markers (Fig. 8A). As anticipated, the sorted populations displayed distinct expression levels immediately after sorting. Functional assays revealed that while PTK7-high and PTK7-low cells exhibited comparable colony-forming capacity, both CD44-high and CD133-high cells generated a significantly greater number of organoids compared to their CD44-low and CD133-low counterparts (Fig. 8B).

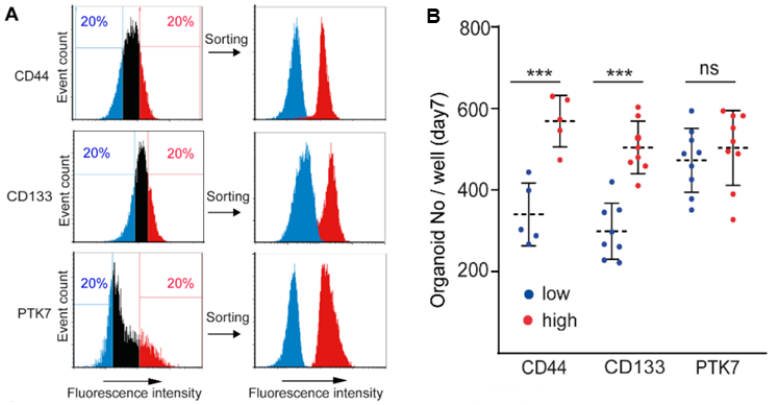


**Figure 8. Organoids can be sorted into high and low populations for CD44, CD133, and PTK7. A**) Flow cytometry-based sorting strategy showing expression levels of CD44, CD133, and PTK7 in the isolated subpopulations. **B**) Quantification of organoid formation from cells sorted according to high or low marker expression, assessed on day 7 (based on 1-2 independent sorting experiments using organoid lines #1-#4). Statistical analysis was performed using the Mann-Whitney U test. ***$p < 0.005$. (the author's own figure: (101)).

In addition, organoids derived from CD44-high and CD133-high cells displayed larger diameters (Fig. 9) and a higher proportion of KI67+ (Antigen Kiel 67) proliferating cells relative to those derived from low-expressing populations (Fig. 10), whereas no such

differences were observed for PTK7-sorted cells (Fig. 9,10). Importantly, the proportion of active caspase-3+ apoptotic cells did not differ across any of the subpopulations (data not shown). Taken together, these findings indicate that CD44 and CD133, but not PTK7, identify CRC cells with elevated proliferative potential.

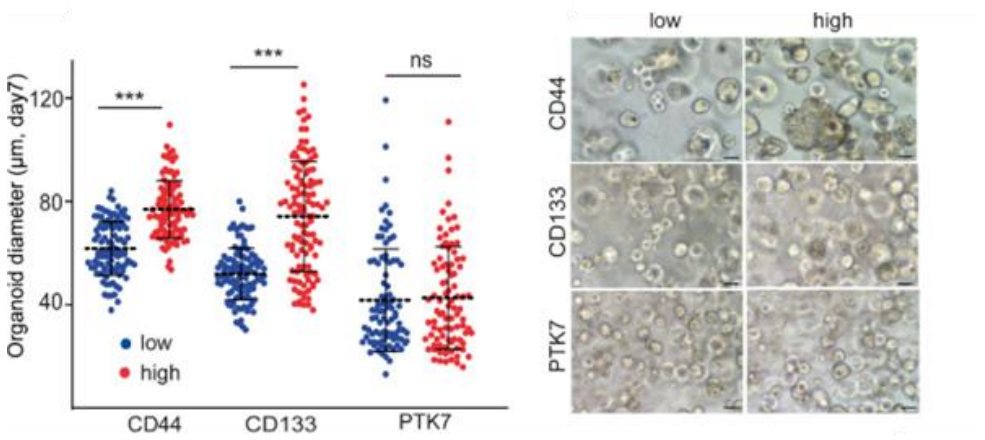


**Figure 9. CD44-high and CD133-high cell-derived organoids are bigger than organoids expressing low amounts of these markers**. Quantification of the organoid diameter 7 days after seeding the sorted cells into Matrigel (left panel) and the representative light microscopy images (right panel) are shown. Scale bars: 25µm. Statistical analysis was performed using the Mann-Whitney U test. ***p <0.005. (the author's own figure: (101)).

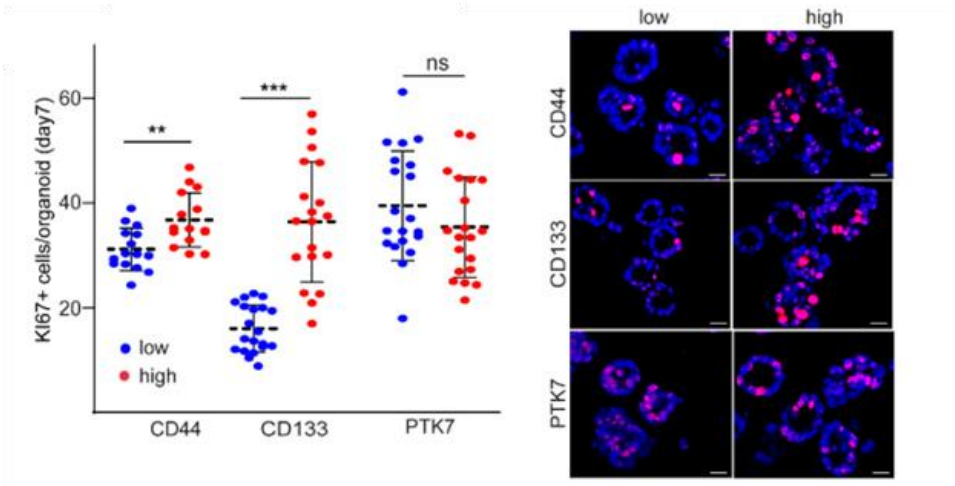


**Figure 10. CD44-high and CD133-high organoids have increase proliferative capacity compared to organoids expressing low levels of these markers**. Quantification of the percentage of KI67+ proliferating cells in the organoids (left panel) and representative confocal microscopic images (right panel). Scale bars: 25 µm. Mann-Whitney U test was used. ** $p < 0.01$, and *** $p < 0.005$. (the author's own figure: (101)).

## 4.3 Heterogeneity of CMS markers in CRC PDOs

Markers associated with the CMS4 subgroup of CRC, including ZEB1, FRMD6, and HTR2B, have been proposed to carry prognostic significance. In public datasets, high

expression of these markers predicted poorer survival outcomes, while elevated expression of the CMS2/3 marker CDX2 correlated with improved survival (Fig. 11).

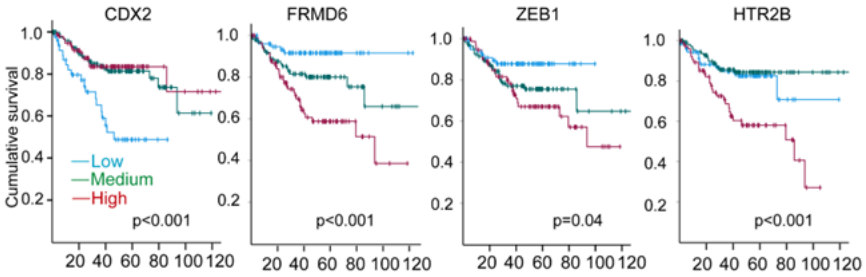


**Figure 11. Expression profiles of CMS2/3 (CDX2) and CMS4 (ZEB1, FRMD6, HTR2B) markers**. Kaplan-Meier survival curves for CDX2, FRM6, ZEB1, and HTR2B. Expression groups were defined based on z-score normalization: low (<—0.5 SD), medium (—0.5 SD to 0.5 SD), and high (< 0.5 SD). Corresponding p-values were calculated using the log-rank test. Analysis of GSE17537 and GSE14333 (https://www.ncbi.nlm.nih.gov/geo) data sets. (the author's own figure: (104)).

Consistent with this, CDX2 was more highly expressed in CMS2/3 tumors whereas ZEB1, FRMD6, and HTR2B showed elevated levels in CMS4 tumors compared to other CMS groups and normal colon samples (Fig. 12).

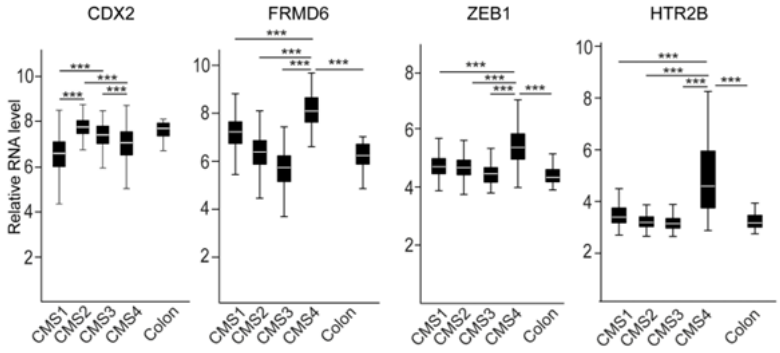


**Figure 12. RNA Expression patterns of CMS2/3 (CDX2) and CMS4 (ZEB1, FRMD6, HTR2B) markers**. Normalized RNA expression levels of the indicated genes across CMS subgroups and normal colon tissue samples (data from the GSE39582). (the author's own figure: (104)).

Analysis of the Human Protein Atlas (www.proteinatlas.org) further supported these observations. FRMD6 displayed uniform positivity across tumor sections, ZEB1 produced variable results depending on the antibody used, and both CDX2 and HTR2B exhibited heterogeneous expression patterns within tumor tissues (Fig. 13).

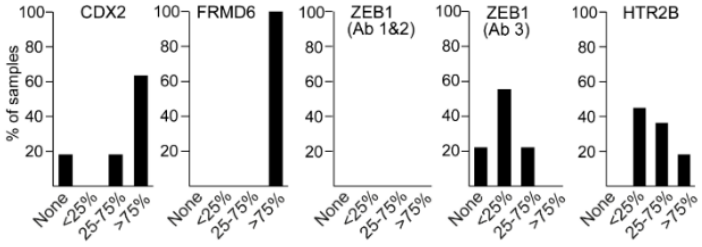


**Figure 13. Expression patterns of CMS2/3 (CDX2) and CMS4 (ZEB1, FRMD6, HTR2B) markers**. Tissue section analysis for the indicated markers based on data from the Human Protein Atlas (proteinatlas.org). Quantitative values were evaluated from 12 samples per antibody (for ZEB1: antibody 1- HPA027524, antibody 2- CAB058686, antibody 3 – CAB079943). The x-axis represents the percentage of positive cells within individual tissue sections, while the y-axis indicates the proportion of samples within each category. (the author's own figure: (104)).

In PDOs, ZEB1 and FRMD6 proteins were undetectable, while CDX2 and HTR2B were consistently expressed across all lines, though with notable heterogeneity (Fig. 14A-B).

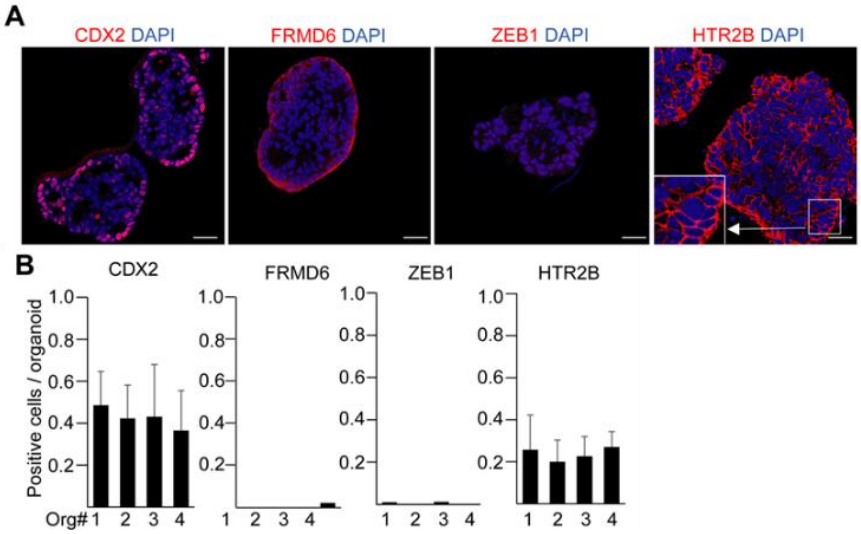


**Figure 14. The CMS4 markers HTR2B exhibits intra-tumoral cellular heterogeneity in colorectal cancer**. **A)** Representative confocal microscopy images and corresponding quantification **B)** of CDX2, FRMD6, ZEB1, and HTR2B expression in PDO lines. Scale bars: 20 µm (A). Quantification was performed on 10-15 organoids per PDO line (B) (the author's own figure: (104)).

Only a subset of tumor cells co-expressed both markers, and a similar partial overlap was observed in CRC tissue sections (Fig. 15A-B). Moreover, $CDX2^+$ and $HTR2B^+$ populations showed only limited overlap with proliferating $KI67^+$ cells (Fig. 15C).

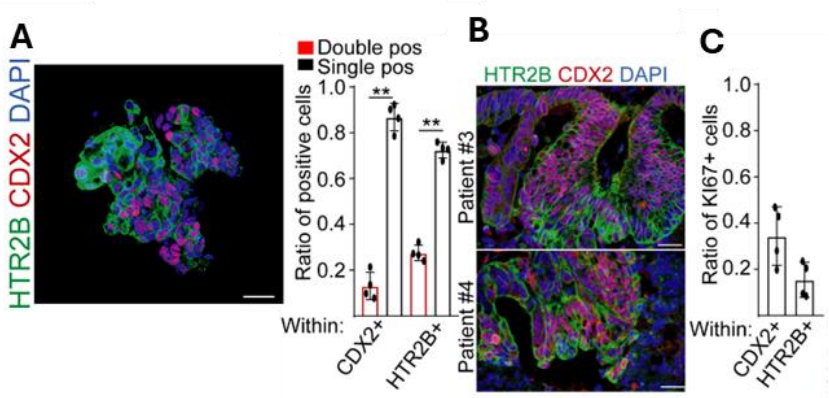


**Figure 15. The CMS4 marker HTR2B demonstrates intra-tumoral cellular heterogeneity in colorectal cancer**. **A)** Ratio of single- and double-positive organoid cells for CDX2 and HTR2B within the CDX2+ or HTR2B+ populations, shown with representative confocal images and quantification. **B)** Immunostaining for CDX2 and HTR2B in colorectal cancer tissue sections. **C)** Ratio of KI67+ proliferating cells within CDX2+ or HTR2B+ PDO cells, based on confocal image analysis. Statistical analysis for A) was performed using Student's t-test (** $p < 0.01$). Scale bars: 20µm (A) and 100µm (B). n = 4 (A,C). (the author's own figure: (104)).

Focusing on HTR2B, we confirmed its expression in CRC organoids using three independent antibodies targeting different domains of the protein (data not shown). Immunohistochemical analysis revealed that HTR2B was absent in mesenchymal stromal cells but present at varying levels on tumor epithelial cells, where it localized predominantly to the plasma membrane (Fig. 16). In summary, CDX2 (CMS2/3 marker) and HTR2B (CMS4 marker) are both expressed within the same CRC samples, though represent distinct cellular subpopulations. This highlights intra-tumoral heterogeneity in CRC and underscores the complementary prognostic value of these markers.

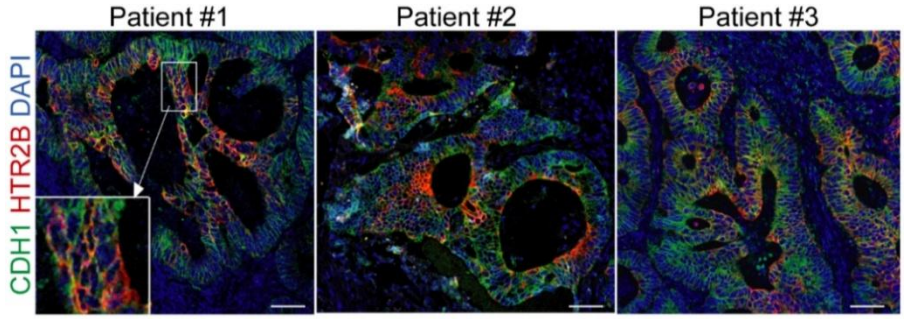


**Figure 16. The CMS4 marker HTR2B displays intra-tumoral cellular heterogeneity in colorectal cancer**. Immunohistochemical staining of tissue sections from three CRC patients for the indicated markers. CDH1 served as an epithelial cell-specific positive control. HTR2B expression shows heterogeneous localization restricted to epithelial cells. Scale bars: 100 µm. (the author's own figure: (104)).

## 4.4 Serotonin Metabolism in CRC

Serotonin signaling has been implicated in several malignancies, including pancreatic ductal adenocarcinoma (PDAC), where tumor cells themselves constitute an important

source of serotonin under stress conditions (109). To assess whether CRC cells or stromal fibroblasts similarly contribute to intratumoral serotonin pools, we examined their capacity for serotonin synthesis under both standard and unfavorable culture conditions (e.g., glucose- or amino acid-deprivation). In contrast to PDAC, neither fibroblasts nor CRC cells produced detectable levels of serotonin under these conditions as measured by ELISA (data not shown). At the transcriptomic level, CRC PDOs demonstrated a marked reduction in tryptophan hydroxylase 1 (TPH1), the rate-limiting enzyme of serotonin biosynthesis, as well as reduced expression of SLC18A2, which mediates serotonin vesicular transport and secretion, compared to normal colon organoids (Fig. 17A). Conversely, CRC PDOs exhibited higher expression of the serotonin reuptake transporter SLC6A4, while no difference was observed in MAO-A, the enzyme responsible for serotonin degradation. These results suggest that although CRC organoids are not a major source of serotonin, they may be capable of metabolizing extracellular serotonin within the tumor microenvironment.

Because serotonin is primarily derived from neuroendocrine cells in the normal intestine, and given that CRC has been proposed to undergo transcriptional plasticity involving the aberrant expression of lineage-inappropriate programs (110), we next examined the overlap between neuroendocrine gene signatures and the CMS4 molecular subtype of CRC. Using a curated neuroendocrine gene program, we detected no overlap with CMS4-defining genes (Fig. 17B). Moreover, when restricting the comparison to tumor-cell-specific CMS4 genes, no enrichment for neuroendocrine signatures was identified. Collectively, these findings indicate that, unlike PDAC, CRC cells and fibroblasts are unlikely to act as significant sources of serotonin. Instead, serotonin within the CRC microenvironment may predominantly originate from the surrounding normal colon epithelium or from systemic sources. These results underscore the tumor-type-specific differences in serotonin metabolism and justify our subsequent focus on receptor-level modulation, particularly HTR2B activation, in CRC PDO systems.

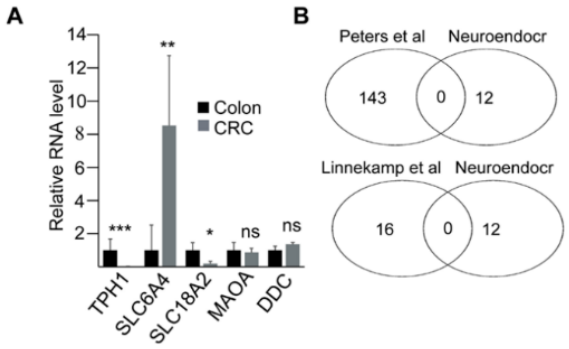


**Figure 17. Reduced expression of the serotonin synthesis pathway in CRC organoids compared to normal colon organoids**. **A)** Relative mRNA expression of the indicated genes determined by RT-qPCR. Values were normalized to housekeeping controls and compared between unpaired normal colon and CRC organoid samples (n = 4 each). Statistical significance was assessed by unpaired t-test (*p < 0.05, **p < 0.01, ***p < 0.005; ns, not significant). **B)** Gene set overlap analysis showing the number of shared and unique genes across the indicated categories. (the author's own figure: (104)).

## 4.5 Synergistic influence of unfavorable conditions and HTR2B stimulation on tumor survival

The mTOR pathway is a central regulator of cell survival and metabolism, and phosphorylation of the ribosomal protein S6 (P-S6), a downstream target of mTORC1, reflects its activation status. To investigate the relevance of mTORC1 signaling to CRC cell survival and growth, we treated patient-derived CRC organoids with the mTORC1 inhibitor rapamycin. Interestingly, inhibition of mTORC1 exerted no significant effect on organoid formation efficiency or organoid size, regardless of whether rapamycin was added immediately or three days after culture initiation (data not shown). This observation suggests that under nutrient-rich conditions, mTORC1 activity is dispensable for CRC PDO colony formation and survival. The efficacy of rapamycin was confirmed by microscopy and flow cytometry, both showing a reduced fraction of P-S6$^+$ cells (data not shown). Notably, there was considerable inter-organoid heterogeneity in the proportion of P-S6$^+$ cells, underscoring the metabolic diversity among patient-derived CRC lines.

Given that HTR2B was previously shown to promote PDAC cell survival under stress (109), we next examined its behavior in CRC organoids under unfavorable metabolic conditions. When CRC organoids were cultured in glucose- or amino acid-free media, we observed a marked reduction in organoid size and KI67$^+$ proliferating cells after two days, coupled with an increased fraction of P-S6$^+$ cells among the surviving population (Fig. 18, 19A).

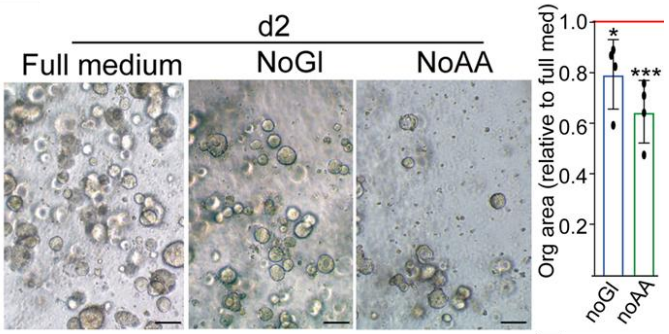


**Figure 18. Nutrient deprivation decreases organoid size.** A) Representative light microscopy images of PDO cultures maintained in control (complete), carbohydrate-free (noGl), and amino acid-free (noAA) media, along with quantification of relative organoid area normalized to the control condition. The horizontal red line represents the control with a relative area of 1. Scale bars: 50 µm. Statistical analysis: paired t-test (*p < 0.05, ***p < 0.005; n = 4). (the author's own figure: (104)).

These findings indicate that, unlike in standard culture conditions, mTORC1 activation becomes crucial for survival under nutrient deprivation. Concomitantly, HTR2B expression was upregulated in glucose- and amino acid-deprived media, suggesting that nutrient stress induces this receptor. Treatment with rapamycin significantly reduced both HTR2B$^{+}$ cell fractions and HTR2B mRNA levels (Fig. 19B-C), demonstrating that HTR2B expression is at least partly regulated by the mTORC1 axis. Similar results were obtained with everolimus, a clinically used mTORC1 inhibitor (Fig. 19D).

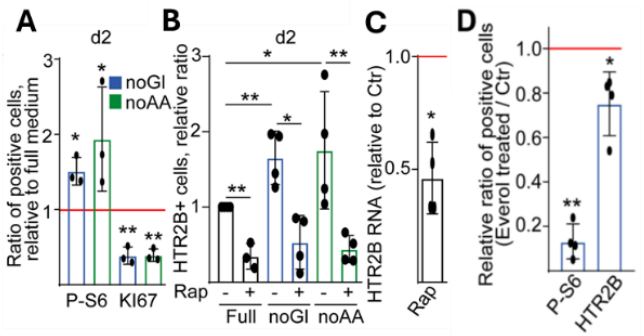


**Figure 19. Nutrient deprivation and mTOR inhibition modulate HTR2B expression and reduce proliferative activity in CRC organoids. A)** Quantification of KI67+ and P-S6+ cell fractions in organoid lines cultured under carbohydrate-free (noGl) or amino acid-free (noAA) conditions relative to complete medium controls (indicated by the horizontal red line). Data were obtained from confocal microscopy analyses. **B)** Assessment of HTR2B+ cell frequency following treatment with the mTOR inhibitor rapamycin under the indicated culture conditions, measured by flow cytometry. **C)** Quantification of HTR2B transcript levels after rapamycin exposure (1 µM for 2 days), determined by RT-qPCR and normalized to housekeeping gene expression. **D)** Proportion of P-S6+ and HTR2B+ cells following treatment with the mTORC1 inhibitor everolimus (1 µM, 2 days). All values were compared to untreated control samples (horizontal red line). Statistical significance was calculated using a paired t-test (*p < 0.05, **p < 0.01); n =4, except for panel A (n = 3). (the author's own figure: (104)).

To determine the functional role of serotonin signaling through HTR2B, we next stimulated CRC PDOs with serotonin or an HTR2B agonist. Under optimal culture conditions, activation of HTR2B did not significantly alter organoid morphology, size or proliferation (Fig. 20A). In contrast, under glucose deprivation, serotonin treatment further decreased organoid survival in a dose-dependent manner, while HTR2B antagonists reversed this effect (Fig. 20B-C, Fig. 21). Interestingly, this effect was specific to glucose-free conditions and not observed in amino acid-free medium, suggesting a metabolic context dependence.

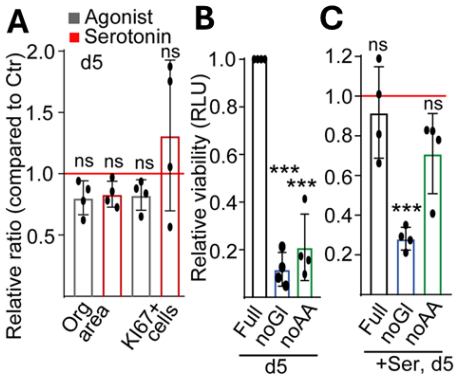


**Figure 20. Nutrient deprivation alters proliferation, viability, and serotonin responsiveness in CRC organoids**. **A)** Changes in organoid size and the proportion of KI67+ proliferating cells in PDO lines cultured in complete medium for 5 days, assessed by light and confocal microscopy. **B)** Effects of various culture conditions on overall cell viability, quantified using the CellTiter-Glo 3D assay. **C)** Impact of serotonin treatment (10 µM) on organoid viability under the indicated culture conditions, compared to untreated controls. Statistical significance was determined using a paired t-test (***p < 0.005; ns, not significant); n=4. (the author's own figure: (104)).

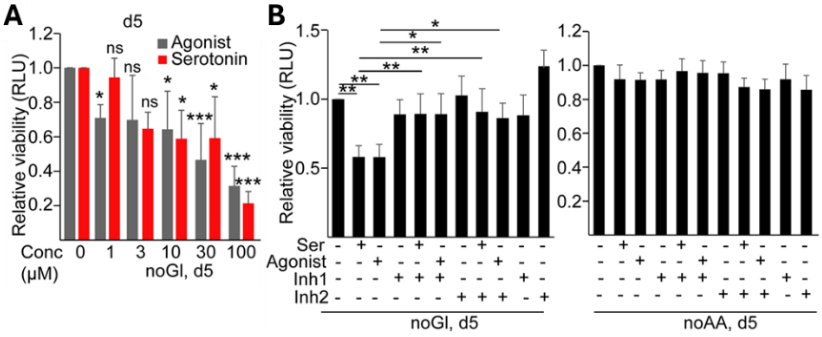


**Figure 21. Serotonin signaling influences CRC organoid viability under nutrient-deprived conditions**. **A)** Concentration-dependent effects of serotonin and its agonist on organoid viability, assessed using the CellTiter-Glo 3D assay. **B)** Viability of orgnaoids cultured in carbohydrate-free (noGl) or amino acid-free (noAA) media in the presence or absence of serotonin (10 µM), the serotonin agonist α-methylserotonin (10 µM), and HTR2B inhibitors (RS-1274451 and SB 204741, both at 1 µM). Statistical significance was evaluated by one-way ANOVA followed by Tukey's post hoc test (*p < 0.05, **p < 0.01, ***p < 0.005; ns, not significant); n = 4. (the author's own figure: (104)).

Further, exposure to the chemotherapeutic 5-fluorouracil (5-FU) at sublethal concentrations ($IC_{50}$) increased the proportion of $HTR2B^+$ cells (Fig. 22A), consistent with a stress-induced upregulation of this receptor. Although HTR2B activation did not influence proliferation in basal conditions, it reduced the proportion of $P\text{-}S6^+$ cells (Fig. 22B), indicating negative feedback on mTORC1 signaling. Notably, serotonin or HTR2B agonists potentiated 5-FU induced cytotoxicity, decreasing cell survival even at drug concentrations that were otherwise sublethal (Fig. 22C).

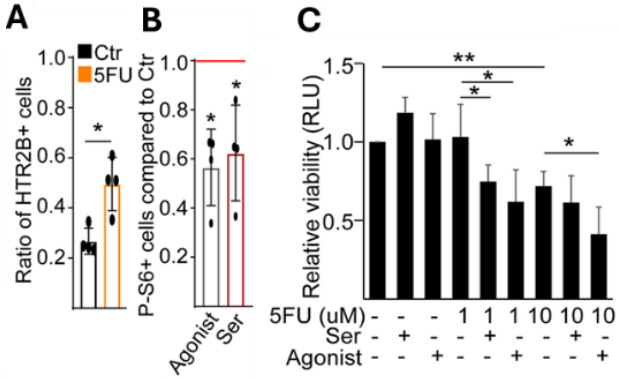


**Figure 22. Serotonin signaling and chemotherapeutic stress influence HTR2B expression, mTOR activity, and viability in CRC organoids. A)** Proportion of HTR2B+ cells following treatment with 5-FU at PDO line-specific IC50 concentrations, as determined in previous studies (105). Organoids were analyzed after 3 days of treatment by flow cytometry. **B)** Relative changes in the proportion of P-S6+ cells in response to serotonin (10 µM) or the HTR2B agonist α-methylserotonin (10 µM), with the control level indicated by the horizontal line (flow cytometry). **C)** Relative cell viability of organoids under the indicated treatment conditions, measured using the CellTiter-Glo 3D assay and normalized to control samples. Statistical analyses were performed using an unpaired t-test (A), paired t-test (B), or one-way ANOVA with Tukey's post hoc test (C) (*$p < 0.05$, **$p < 0.01$); $n = 4$. (the author's own figure: (104)).

Collectively, these findings demonstrate that HTR2B expression in CRC is induced under metabolic and chemotherapeutic stress, likely via mTORC1-dependent mechanisms. While mTORC1 signaling is non-essential for CRC PDO growth under nutrient-rich conditions, it becomes critical during metabolic challenge. Activation of HTR2B under such stress conditions suppresses mTORC1 activity and synergizes with 5-FU treatment, identifying HTR2B as a context-dependent modulator of CRC cell survival and a potential therapeutic target in metabolically compromised tumors.

## 4.6 Fibroblasts modify CRC behavior and HTR2B expression via ECM remodeling

The CMS4 molecular subtype of CRC is characterized by mesenchymal activation, EMT features, and a dense fibroblast-rich stroma, all of which correlate with poor patient outcomes. To investigate how fibroblast-tumor cell interactions influence serotonin receptor expression and EMT dynamics, we established co-culture systems of CRC PDOs with primary fibroblasts (Fig. 23A). Using membrane labeling dyes to trace fibroblasts, we confirmed their close proximity and frequent direct contact with organoid epithelial cells within the co-culture matrix (Fib. 23B), effectively recreating a stromal microenvironment in vitro.

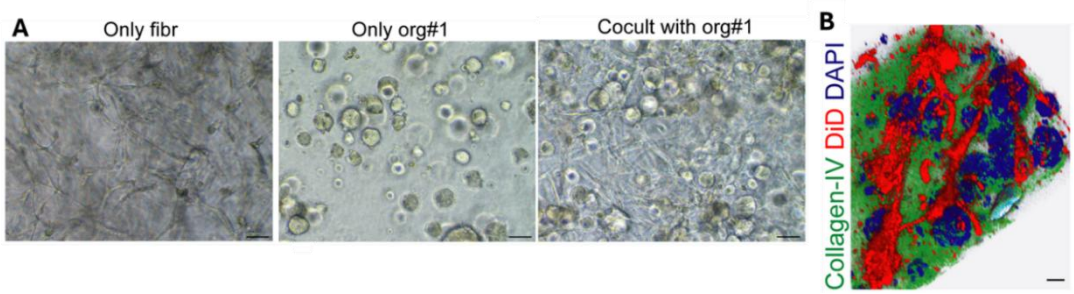


**Figure 23. Co-culture of CRC organoids with fibroblasts. A)** Representative light microscopy images of 3D cultures containing fibroblasts alone (upper left), PDOs alone (upper right), and fibroblast-PDO co-cultures. **B)** Confocal microscopy image of a 3D co-culture showing fibroblasts labeled with the membrane dye DiD prior to co-culturing. Collagen-IV immunostaining was used to visualize the extracellular matrix. The image demonstrates the close spatial association between fibroblasts and organoid structures. Scale bars: 50 µm (A); 20 µm (B). (the author's own figure: (104)).

Molecular analyses of the co-cultures revealed a partial EMT phenotype in CRC cells. Compared to organoid monocultures, a subpopulation of co-cultured tumor cells exhibited reduced expression of the epithelial marker EpCAM, and we observed an increased expression of the mesenchymal-associated proteoglycan lumican (LUM), which has been previously validated as an EMT marker in CRC (Fig. 24-25A) (111, 112). These results indicate that direct fibroblast contact promotes a hybrid epithelial-mesenchymal state rather than a complete EMT transition, consistent with stromal modulation of tumor plasticity seen in CMS4 tumors.

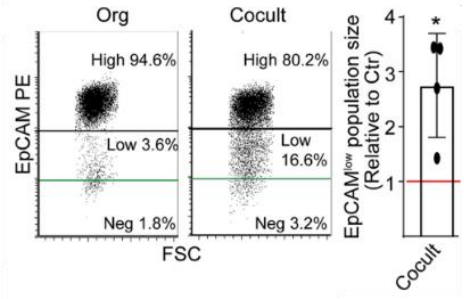


**Figure 24. Co-culture with fibroblasts reduces the expression of epithelial markers in CRC organoids**. Analysis of cell surface EpCAM levels in monocultured organoids and fibroblasts-organoid co-cultures, shown as representative flow cytometry dot plots with corresponding quantification. EpCAM, an epithelial cell surface marker, was used to assess epithelial identity. Isotype control samples (green line) served to define nonspecific background staining. Statistical analysis was performed using a paired t-test (*$p < 0.05$); $n = 4$. (the author's own figure: (104)).

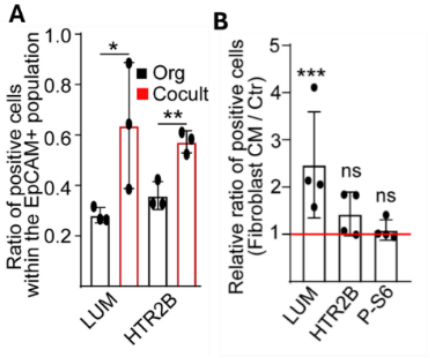


**Figure 25. Fibroblast interaction enhances HTR2B expression and modulates epithelial marker profiles in CRC organoids**. **A)** Relative proportion of LUM+ and HTR2B+ cells within the EpCAM+ epithelial population of PDOs cultured alone or in co-culture with fibroblasts, analyzed by flow cytometry. Fibroblasts were excluded from analysis based on the absence of EpCAM expression. **B)** Changes in the proportion of cells positive for the indicated markers following a 2-day treatment with fibroblast-derived conditioned medium. Conditioned medium was collected from confluent fibroblast cultures maintained in CRC organoid medium for 2 days prior to use. The horizontal red line represents control PDOs. Statistical significance was determined using an unpaired t-test (A) or paired t-test (B) (*$p < 0.05$, **$p < 0.01$, ***$p < 0.005$; ns, not significant); $n = 3$ (A), $n = 4$ (B). (the author's own figure: (104)).

Importantly, within the $EpCAM^+$ CRC population (encompassing both $EpCAM^{low}$ and $EpCAM^{high}$ subsets), we detected a significant increase in $HTR2B^+$ cells in fibroblast co-cultures relative to monocultures (Fig. 25A). This suggests that microenvironmental cues provided by fibroblast proximity, rather than soluble factors alone, induce HTR2B upregulation in CRC cells.

To assess whether fibroblast-secreted molecules alone could reproduce these effects, CRC PDOs were treated with fibroblast-conditioned medium. While conditioned medium modestly altered the proportion of $LUM^+$ cells, it failed to change the frequency of $HTR2B^+$ cells or the percentage of $P\text{-}S6^+$ (mTORC1-active) cells (Fig. 25B). These findings demonstrate that paracrine signaling from fibroblasts is insufficient to drive

HTR2B induction, implying that direct cell-cell or ECM-mediated interactions are required.

Immunofluorescence analysis of CRC tissue sections further supported this finding, as $LUM^{+}/HTR2B^{+}$ double-positive tumor cells were frequently observed adjacent to the mesenchymal compartment in vivo (Fig. 26), reinforcing the physiological relevance of the co-culture observations. Collectively, these results reveal that fibroblast-tumor interactions enhance both partial EMT and HTR2B expression in CRC cells, particularly under conditions mimicking the CMS4 microenvironment. The spatial proximity between fibroblasts and $HTR2B^{+}$ tumor cells suggests a mechanistic link between stromal activation and serotonin receptor signaling within the desmoplastic tumor niche, potentially contributing to the aggressive, therapy-resistant phenotype characteristic of CMS4 tumors.

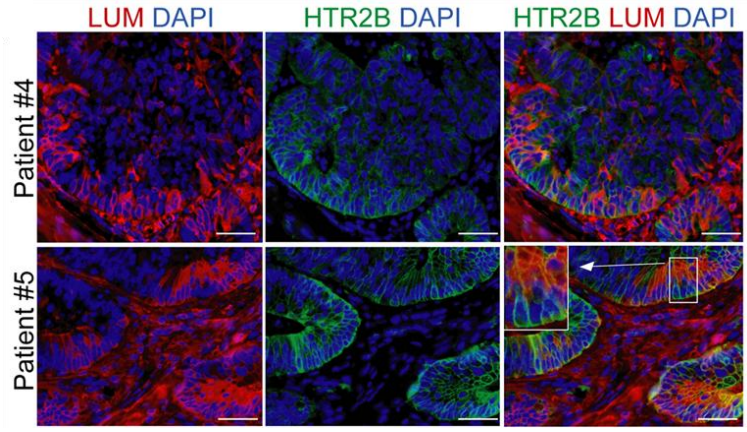


**Figure 26. Expression of fibroblast- and EMT-associated markers in CRC tissue sections.** Immunofluorescent staining of colorectal cancer samples for the indicated markers to assess their localization and expression patterns within the tumor microenvironment. Scale bars: 25 μm. (the author's own figure: (104)).

The tumor microenvironment of CMS4 CRCs is characterized by dense ECM remodeling and high stromal content, largely driven by fibroblast-derived components such as collagen-I. To determine whether ECM composition directly influences serotonin receptor expression and epithelial-mesenchymal plasticity, we examined CRC PDOs cultured in collagen-I matrices. In contrast to Matrigel, which is primarily composed of laminin and collagen-IV and typically provides a non-invasive environment, collagen-I induced a distinct shift in organoid phenotype (Fig. 27A).

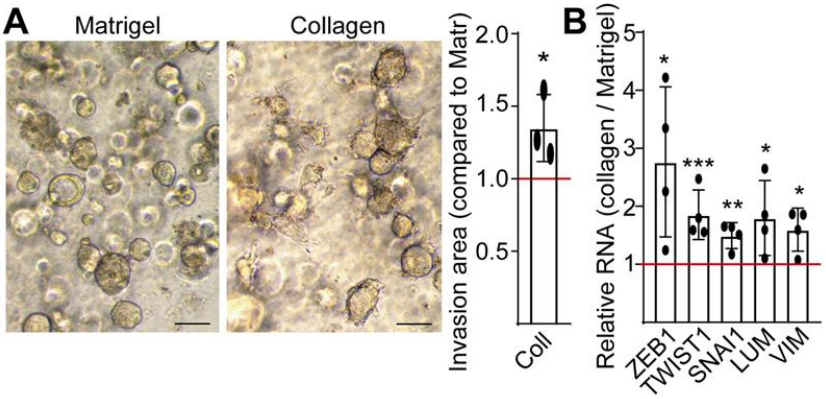


**Figure 27. Morphology and gene expression of CRC PDOs are modified by collagen-I accumulation in the ECM.** A) Representative images showing the morphology of PDOs cultured in Matrigel or collagen-I (left), and quantification of the relative invasion area in collagen-I compared to Matrigel controls (right; horizontal red line indicates the control). Details of invasion area quantification are provided in the Materials and Methods section. B) Relative mRNA expression levels of the indicated genes in PDOs cultured in collagen-I compared to Matrigel, determined by RT-qPCR and normalized to housekeeping genes (red line indicates control). Scale bars: 50 µm. Statistical analysis was performed using a paired t-test (*$p < 0.05$, **$p < 0.01, 0.005$); n =4. (the author's own figure: (104)).

Consistent with previous observations from fibroblast co-cultures, CRC organoids embedded in collagen-I exhibited partial epithelial-to-mesenchymal transition (pEMT), accompanied by enhanced migratory behavior and the formation of a visible invasion zone surrounding the organoids. Transcriptomic analysis revealed a significant upregulation of EMT-associated genes, including those encoding mesenchymal cytoskeletal and adhesion proteins (Fig. 27B). At the protein level, this phenotype was confirmed by increased immunoreactivity for vimentin (VIM) and lumican (LUM) (Fig. 28A), validating the acquisition of pEMT under collagen-rich conditions.

Remarkably, collagen-I also led to a significant expansion of the HTR2B+ CRC cell population, mirroring the effect observed in direct fibroblast co-cultures (Fig. 28A). Spatial analysis of these cultures revealed that $HTR2B^+$ cells were preferentially enriched at the invasive front rather than within the organoid core (Fig. 28B), indicating that HTR2B expression is associated with a migratory, pEMT-like cell state. Taken together, these results demonstrate that collagen-I provides a permissive ECM context that not only promotes partial EMT and invasiveness in CRC cells but also enhances HTR2B expression and function.

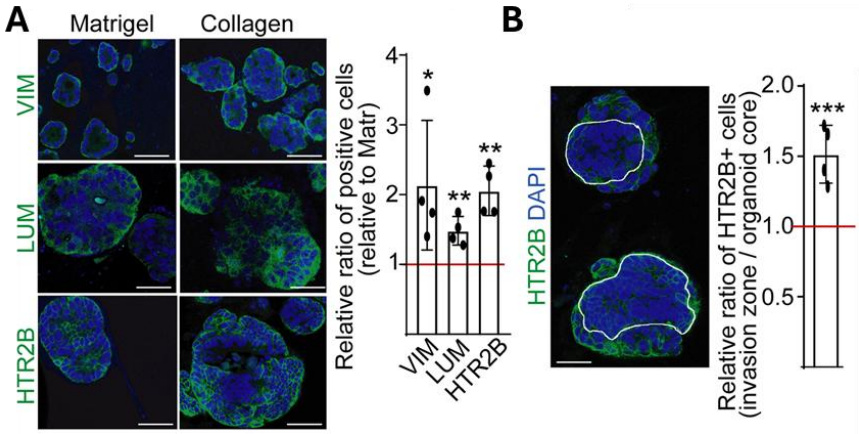


**Figure 28. Collagen-I accumulation causes spatial enrichment of HTR2B-positive cells in PDO CRCs. A)** Representative confocal images and quantification showing the relative proportion of VIM+, LUM+, and HTR2B+ cells in organoids cultured in collagen-I compared to Matrigel. **B)** Localization analysis of HTR2B+ cells within collagen-I cultures, illustrating their enrichment in the invasive front relative to the organoid core. The yellow line indicates the segmentation boundary between the core and the invasion zone. Scale bars: 25 µm. Statistical analysis was performed using paired t-test (*p < 0.05, **p < 0.01, ***p < 0.005); n =4. (the author's own figure: (104)).

## 4.7 HTR2B expression and activity levels impact tumoral invasiveness in a permissive environment

To explore the functional significance of HTR2B activation in a collagen-rich TME, CRC organoids in collagen were treated with serotonin or a specific HTR2B agonist. Both

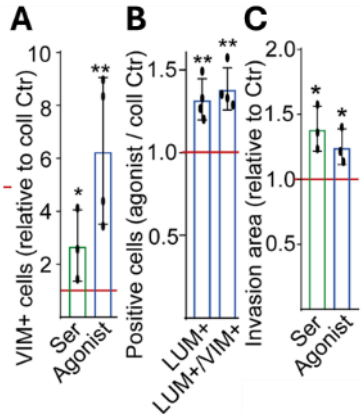


treatments further increased EMT marker expression and expanded the invasion area without reducing cell viability or inducing apoptosis (Fig. 29A-C, 30A-C).

**Figure 29. Activation of HTR2B enhances invasive behavior and promotes mesenchymal marker expression in CRC organoids cultured in collagen-I. A)** Quantification of the proportion of VIM+ cells following treatment with serotonin or an HTR2B agonist (10 µM), based on confocal microscopy analysis. **B)** Effect of HTR2B activation on the ratio of LUM+ and LUM+/VIM+ double-positive cells across different organoid lines. **C)** Relative invasion area of organoids in collagen-I following treatment with the HTR2B agonist. Statistical analysis was performed using paired t-tests (*p < 0.05, p < 0.01); n = 4 (except for panel C, where n = 3). (the author's own figure: (104)).

Moreover, neither serotonin nor the agonist enhanced the cytotoxic effects of 5-FU in collagen matrices (Fig. 30D).

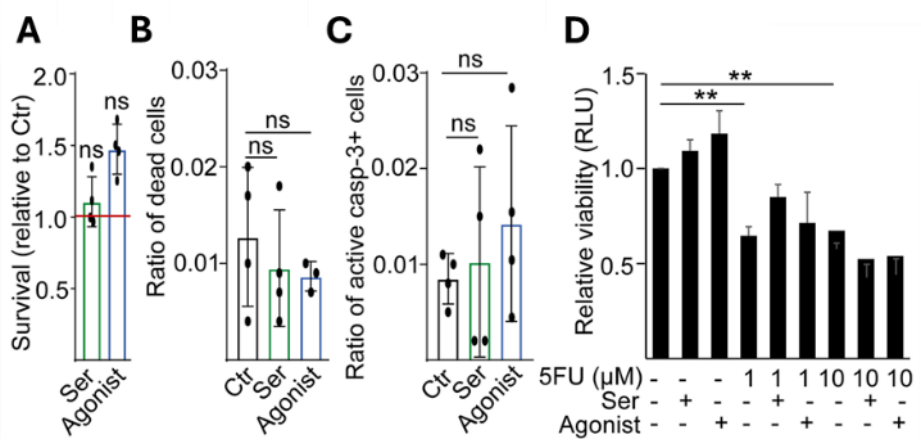


**Figure 30. Influence of HTR2B on cell viability and apoptosis in CRC organoids cultured within collagen-I. A)** Cell viability in collagen-I following treatment with serotonin or an HTR2B agonist, measured using the CellTiterGlo 3D assay. **B)** Quantification of dead cells under the indicated treatment conditions in collagen, determined by flow cytometry using the LIVE/DEAD-TM Fixable Blue Dead Cell Stain Kit. **C)** Proportion of apoptotic cells positive for active caspase-3 in collagen cultures, assessed by flow cytometry. **D)** Comparative analysis of organoid viability across different treatment conditions in collagen-I, based on CellTiterGlo 3D assays. Statistical analyses were performed using paired A) or unpaired (B-C) t-tests, or ANOVA with Tukey's post hoc test (D); *p < 0.05, **p < 0.01, ***p < 0.005. n = 4. (the author's own figure: (104)).

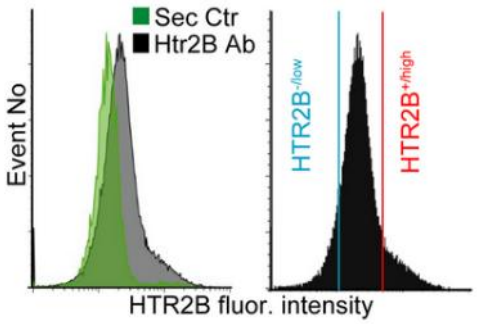


**Figure 31. Flow cytometric identification and isolation of CRC cell populations with differential HTR2B expression**. Representative flow cytometry histograms illustrating $HTR2B^{+/high}$ and $HTR2B^{-/low}$ subpopulations and the corresponding gating and sorting strategy used for downstream analyses. (the author's own figure: (104)).

To further characterize the phenotype and functional properties of $HTR2B^{+}$ CRC cells, we isolated $HTR2B^{+/high}$ and $HTR2B^{-/low}$ populations from PDOs using fluorescence activated cell sorting (FACS) (Fig. 31).

After seven days of culture, organoids originating from HTR2B$^{+/high}$ cells retained a higher proportion of HTR2B$^{+/high}$ cells compared to those derived from HTR2B$^{-/low}$ populations (Fig. 32A), confirming that HTR2B expression levels are stably maintained in CRC PDOs. Morphometric analysis revealed that HTR2B$^{+/high}$ organoids exhibited larger diameters and a higher fraction of proliferating (KI67$^{+}$) cells (Fig. 32 B-C), indicating a more proliferative phenotype.

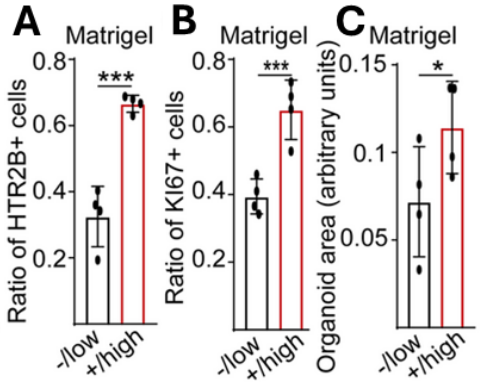


**Figure 32. Organoids derived from HTR2B$^{+/high}$ colorectal cancer cells display enhanced proliferative and growth capacity compared to those from HTR2B$^{-/low}$ cells**. **A)** Proportion of HTR2B+ cells in organoids established from sorted HTR2B$^{+/high}$ and HTR2B$^{-/low}$ PDO populations, analyzed after 7 days of culture in Matrigel using confocal microscopy. **B)** Quantification of KI67+ proliferating cells within the same organoid populations. **C)** Measurement of organoid area derived from the sorted cell fractions, based on light microscopy images analyzed with ImageJ. Unpaired t-tests were applied with *p < 0.05, ***p < 0.005; n = 4. (the author's own figure: (104)).

Gene expression profiling demonstrated a consistent upregulation of EMT-related transcripts in HTR2B$^{+/high}$ organoids (Fig. 33A), accompanied by an increased number of vimentin (VIM)$^{+}$ and lumican (LUM)$^{+}$ cells (Fig. 33B), further supporting the acquisition of a pEMT state. When cultured in collagen-I, HTR2B$^{+/high}$ cells formed larger, more invasive organoids, albeit with a slightly reduced colony-initiating efficiency compared to HTR2B$^{-/low}$ cells (Fig. 33C).

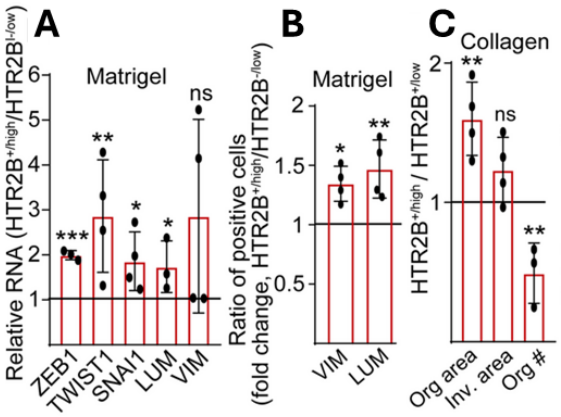

**Figure 33. Organoids derived from HTR2B$^{+/high}$ CRC cells exhibit elevated expression of invasion-associated genes and markers compared to those from HTR2B$^{-/low}$ cells. A)** Relative mRNA expression levels of the indicated genes in organoids derived from HTR2B$^{+/high}$ versus HTR2B$^{-/low}$ populations, assessed by RT-qPCR. **B)** Quantification of VIM+ and LUM+ cells in organoids originating from HTR2B$^{+/high}$ cells compared to those from HTR2B$^{-/low}$ cells, analyzed after 7 days of culture using confocal microscopy (horizontal line indicates HTR2B$^{-/low}$ reference). **C)** Morphological comparison of organoids from the two populations based on light microscopy image analysis. Paired t-tests were applied with *p < 0.05, **p < 0.01, ***p < 0.005, ns: p > 0.05; n = 4. (the author's own figure: (104)).

Upon stimulation with serotonin or a selective HTR2B agonist in collagen, organoids derived from HTR2B$^{+/high}$ cells exhibited further increases in organoid size and invasion area, whereas organoids from HTR2B$^{-/low}$ cells remained unaffected (Fig. 34). These findings indicate that HTR2B$^{+/high}$ CRC cells are more responsive to serotonergic stimulation, leading to enhanced invasion and EMT features in a permissive ECM environment.

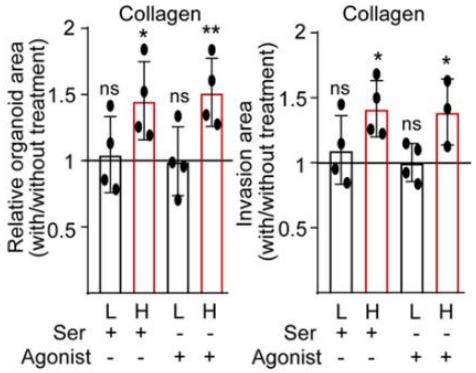


**Figure 34. HTR2B$^{+/high}$ colorectal cancer cell-derived organoids display enhanced invasion in response to serotonin and HTR2B agonist treatment.** Representative light microscopy images and quantification of organoid and invasion areas for HTR2B$^{+/high}$ and HTR2B$^{-/low}$ cell-derived organoids cultured in collagen-I for 7 days, with or without serotonin or HTR2B agonist (10 μM). All measurements were normalized to the respective untreated control. Statistical analysis was performed using paired t-tests (*p < 0.05, **p < 0.01, ns: p > 0.05); n =4. (the author's own figure: (104)).

Given the established link between NOTCH3 signaling and the aggressive CMS4 CRC subtype, we next examined whether HTR2B expression correlates with NOTCH pathway activation. Indeed, HTR2B$^{+/high}$ organoids exhibited elevated expression of NOTCH3 and its downstream target genes MUC2 and OLFM4 (Fig. 35A), while the expression of canonical Wnt target genes (AXIN2 and LGR5) remained unchanged compared to HTR2B$^{-/low}$ samples. Flow cytometric analysis confirmed that HTR2B$^{+/high}$ cells also displayed increased surface NOTCH3 levels (Fig. 35B), suggesting that HTR2B$^{+/high}$ and NOTCH3$^{high}$ CRC cells represent overlapping subpopulations.

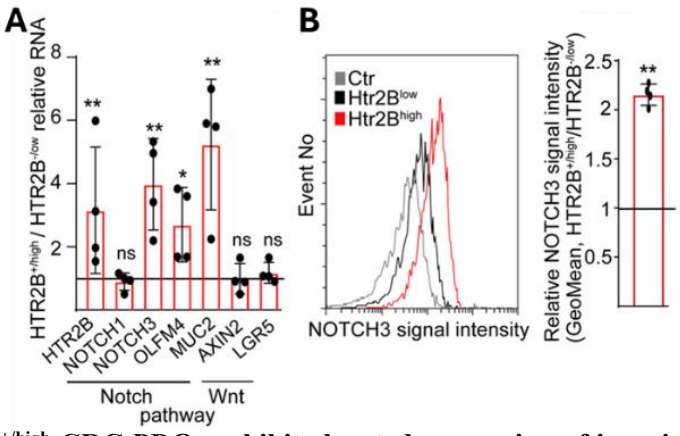


**Figure 35. HTR2B$^{+/high}$ CRC PDOs exhibit elevated expression of invasion- and signaling-related genes compared to HTR2B$^{-/low}$ populations**. A) Relative mRNA levels of the indicated genes in organoids derived from HTR2B$^{+/high}$ versus HTR2B$^{-/low}$ cells, quantified by RT-qPCR. Expression values were normalized to housekeeping genes, with HTR2B$^{-/low}$ organoids set as the reference (horizontal line = 1). B) Flow cytometric analysis of NOTCH3 signal intensity in sorted HTR2B$^{+/high}$ and HTR2B$^{-/low}$ cell populations. Statistical analysis was performed using paired t-tests (*$p < 0.05$, $p < 0.01$, ns: $p > 0.05$); n = 4. (the author's own figure: (104)).

These data identify HTR2B$^{+/high}$ CRC cells as a distinct subpopulation with elevated proliferative capacity, pEMT features in the presence of fibroblast and/or collagen, and NOTCH3 activation, consistent with traits of the CMS4 molecular subtype. The observed co-expression of HTR2B and NOTCH3 supports the hypothesis of functional crosstalk between serotonin and Notch signaling pathways, contributing to tumor cell plasticity and invasiveness in CRC.

Collectively, the ability of serotonin and HTR2B agonists to further potentiate the invasive features suggests a mechanistic link between stromal ECM remodeling, serotonin signaling, and tumor cell plasticity. These findings support the hypothesis that fibroblast-induced collagen deposition contributes to the emergence of HTR2B$^{+}$, migratory CRC subpopulations, particularly in CMS4 tumors where stromal activation and EMT are dominant features.

## 4.8 NOTCH3 cooperates with HTR2B activity to enhance tumoral invasiveness in a permissive microenvironment

Given the observed association between HTR2B expression, EMT activation, and the CMS4 CRC subtype, we next examined whether the Notch signaling pathway, particularly its receptor components NOTCH1 and NOTCH3, may contribute to this phenotype. Analysis of public CRC datasets indicated that both are heterogeneously

expressed, however, NOTCH3, but not NOTCH1, correlated with poor patient survival and was preferentially upregulated in tumors of the CMS4 molecular subtype (Fig. 36 A-C). This pattern was consistent with heterogeneous Notch3 expression observed in patient tumor tissues, suggesting a potential link between Notch3 signaling and the aggressive, mesenchymal-like CRC phenotype.

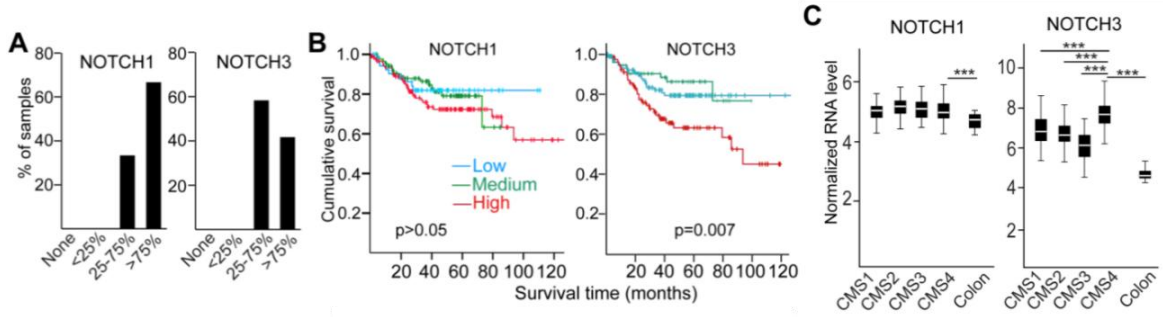


**Figure 36. Differential expression of NOTCH1 and NOTCH3 and their relationship to clinical outcomes in CRC. A)** Immunohistochemical data for NOTCH1 and NOTCH3 expression were retrieved from the Human Protein Atlas and quantitatively evaluated across 12 colorectal cancer samples for each antibody. **B)** Kaplan-Meier survival curves comparing patients with high versus low expression of NOTCH1 or NOTCH3. Statistical significance was determined by log-rank testing, revealing a prognostic association only for NOTCH3. **C)** Comparative analysis of normalized NOTCH1 and NOTCH3 transcript levels among the CMS subtypes of CRC and healthy colonic tissue. Analysis of GSE17537 and GSE14333 (https://www.ncbi.nlm.nih.gov/geo) data sets. (the author's own figure: (104)).

Given the established role of NOTCH signaling in regulating tumor-stroma communication and epithelial plasticity, we next assessed the expression patterns of NOTCH receptors in CRC PDOs. Both NOTCH1 and NOTCH3 were abundantly expressed across multiple PDO lines (Fig. 37A), and their transcript levels remained stable when organoids were transitioned from Matrigel to a collagen-based matrix (Fig. 37B). This observation suggests that NOTCH receptor expression is maintained independently of the surrounding ECM composition.

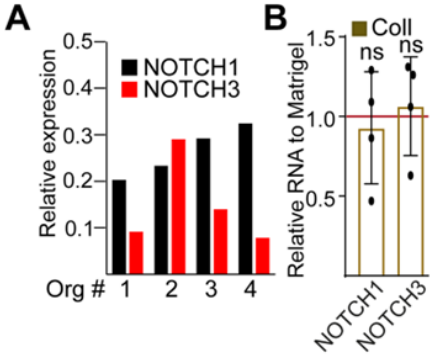


**Figure 37. Expression levels of NOTCH1 and NOTCH3 in CRC PDOs and their response to ECM context. A)** Relative mRNA expression of NOTCH1 and NOTCH3 in four PDO lines, normalized first to housekeeping genes and subsequently to AXIN2, a highly expressed Wnt

pathway target gene. **B)** Comparison of NOTCH1 and NOTCH3 RNA levels in PDOs cultured within collagen-I as opposed to Matrigel ECM, assessed via RT-qPCR. Expression values were normalized to housekeeping controls and expressed relative to Matrigel. Paired t-test results are shown: ns: not significant (n = 3-4). (the author's own figure: (104)).

To further delineate potential sources of NOTCH activation, we examined the expression of canonical NOTCH ligands in both cancer cells and CAFs. While ligands were detectable in both compartments, their expression patterns differed markedly (Fig. 38), indicating that heterotypic interactions between tumor cells and CAFs may contribute to NOTCH pathway activation within the tumor microenvironment.

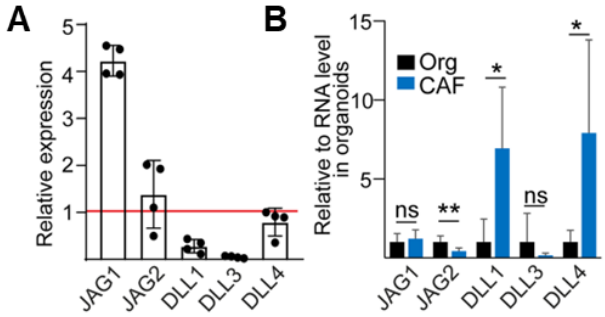


**Figure 38. Differential expression of NOTCH ligands in CRC organoids and CAFs. A)** Relative mRNA expression of selected NOTCH pathway components in CRC PDOs, normalized first to housekeeping genes and subsequently to NOTCH3, to illustrate the proportional expression of NOTCH ligands relative to their receptor. **B)** Comparison of NOTCH ligand transcript levels between CAFs (n = 6) and CRC PDOs (n = 4), assessed by RT-qPCR. Statistical analyses were performed using paired (A) or unpaired (B) t-tests, with significance thresholds indicated as *p < 0.05, **p < 0.01, ns: not significant (n= 3-4). (the author's own figure: (104)).

Consistent with the transcriptomic data, flow cytometric analysis confirmed the presence of NOTCH3 protein at the cell surface of CRC organoid cells (Fig. 39A), validating its potential role as an active signaling receptor. Functionally, inhibition of NOTCH signaling markedly suppressed the increase in invasive capacity that was otherwise induced by serotonin or HTR2B agonist treatment in collagen-I (Fig. 39B).

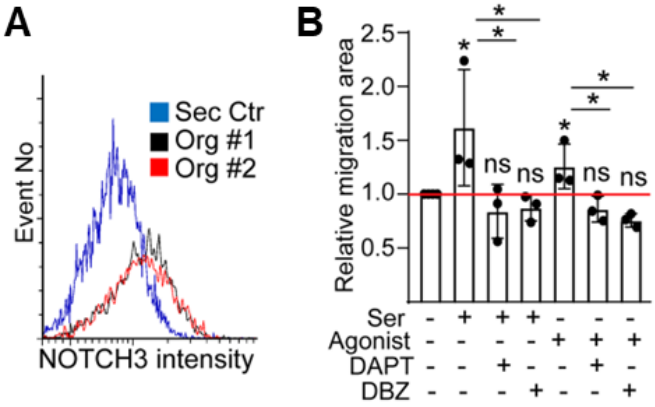


**Figure 39. Surface expression of NOTCH3 and its impact on invasive behavior of CRC. A)** Flow cytometric analysis showing the distribution of NOTCH3 expression on the cell surface in two independent CRC PDO lines. **B)** Quantification of relative invasion area of organoids under

the indicated treatment conditions, expressed as fold change compared to untreated controls. Statistical significance was assessed using paired t-tests, with *p < 0.05 and ns: not significant (n = 3-4). (the author's own figure: (104)).

In conclusion, our results support a model in which NOTCH3 cooperates with HTR2B activity to enhance the invasive behavior of CRC within a permissive microenvironment. We also identify $HTR2B^{+}$/$NOTCH3^{+}$ CRC cells as a clinically relevant subpopulation characterized by high proliferative activity, pEMT, and responsiveness to both serotonergic and NOTCH signaling cues within the collagen enriched tumor microenvironment.

# 5. Discussion

CRC remains one of the most prevalent and lethal malignancies worldwide, with mortality largely driven by metastatic dissemination, chemoresistance, and the complex heterogeneity of the tumor ecosystem. Despite significant progress in early detection and treatment, patient outcomes remain highly variable, reflecting the intricate interplay between cancer cells, the tumor microenvironment, and the molecular programs that govern cellular plasticity. One of the major challenges in CRC biology is to understand how tumor cell subpopulations with distinct phenotypic and molecular signatures cooperate to sustain tumor growth, invasion, and therapy resistance. The present work advances this understanding by dissecting the functional heterogeneity of CRC stem-cell and CMS markers, the metabolic and signaling pathways underpinning serotonin-HTR2B activity, and the stromal factors that shape the malignant phenotype within the ECM.

Using PDOs as a physiologically relevant model, this thesis explored how intra-tumoral heterogeneity, microenvironmental stress, and fibroblast-mediated ECM remodeling collectively regulate tumor behavior. Specifically, we demonstrated that CRC cells exhibit stable heterogeneity for the classical stem cell markers CD44, CD133, and PTK7, that this heterogeneity correlates with proliferative potential, and that CMS4-associated molecules such as HTR2B are dynamically regulated by metabolic stress and ECM context. Furthermore, our data uncovered a mechanistic link between the serotonin receptor HTR2B, mTORC1 signaling, and NOTCH3 receptor, implicating this axis in adaptive tumor behavior and invasion. Together, these findings provide novel insight into how CRC cells integrate environmental cues to maintain plasticity and aggressiveness.

Although all PDO lines expressed these stem cell markers at the transcript and protein levels, their distribution was spatially and quantitatively variable both within and between individual organoids. This pattern recapitulates clinical observations, where CD44 and CD133 expression fluctuate across tumor regions (113, 114), likely reflecting dynamic cell state transitions within the epithelial hierarchy (115).

Importantly, functional assays demonstrated that this heterogeneity carries biological relevance. Organoids derived from $CD44^{high}$ and $CD133^{high}$ subpopulations formed significantly larger colonies and contained more proliferating cells compared to low-expressing counterparts. These findings highlight that both markers define subsets of

tumor cells with enhanced proliferative potential and organoid-initiating capacity. By contrast, PTK7 expression did not correlate with growth advantage, suggesting that its contribution may lie in non-proliferative processes such as cell polarity or Wnt signaling modulation (116). These results support a model in which CD44 and CD133 identify overlapping, yet distinct, CRC cell subsets that sustain tumor expansion.

In the literature, CD44 and CD133 are positioned as functional stemness regulators, CD44 through modulation of cell adhesion, redox balance, EMT (117), and CD133 through the maintenance of asymmetric division and metabolic adaptation (118). The stability of these phenotypes across PDO lines underscores the robustness of stem-like heterogeneity as an intrinsic property of CRC. This cellular diversity provides the substrate for phenotypic plasticity, a trait increasingly recognized as a key determinant of CRC progression and treatment failure.

The CMS subtypes classification offers a framework for understanding CRC heterogeneity at the transcriptomic level, dividing tumors into four subtypes based on distinct biological programs. Among these, CMS2 and CMS3 are characterized by epithelial differentiation and better prognosis, whereas CMS4 encompasses mesenchymal-like tumors associated with poor survival, fibroblast enrichment, and TGF-ß activation. Our data reveal that within individual CRC PDOs, CMS-associated markers, particularly CDX2 (CMS2/3) and HTR2B (CMS4), exhibit pronounced heterogeneity at both the mRNA and protein levels. Notably, these two markers defined largely non-overlapping subpopulations, indicating the coexistence of epithelial and mesenchymal-like cell states within the same tumor. This duality reflects the remarkable plasticity of CRC cells, capable of transiently adopting features from multiple CMS programs. The co-occurrence of $EpCAM^{low}/LUM^{+}$ cells further supports the presence of pEMT, which has been implicated in metastatic competence and drug resistance (119). In agreement with public transcriptomic datasets, we observed that high HTR2B and ZEB1 expression correlated with poor prognosis, emphasizing their clinical relevance as markers of aggressive disease. The persistence of these heterogenous subpopulations within PDOs underscores that CMS4-like traits are maintained autonomously, even in the absence of stromal cells, suggesting intrinsic transcriptional plasticity.

A unique aspect of this work is the exploration of serotonin metabolism and signaling in CRC. While serotonin has long been recognized as a neurotransmitter, its role in epithelial tumor biology is increasingly appreciated. In PDAC, tumor cells themselves are a major source of serotonin, promoting survival under nutrient-limited conditions (109). In contrast, our data demonstrate that CRC cells and fibroblasts produce minimal serotonin, even under conditions of glucose or amino acid deprivation. Instead, CRC PDOs exhibited reduced expression of the serotonin-synthesizing enzyme TPH1 and the vesicular transporter SLC18A2, but higher expression of the serotonin reuptake transporter SLC6A4. These findings suggest that CRC cells are more likely to metabolize or respond to exogenous serotonin rather than synthesize it de novo.

Interestingly, HTR2B, one of the G-protein coupled receptors for serotonin, was highly expressed in CRC PDOs, particularly under unfavorable metabolic conditions. This receptor has been implicated in diverse oncogenic contexts, from promoting angiogenesis to modulating EMT (120). Our results indicate that under metabolic stress, HTR2B and P-S6 (and thus mTOR signaling) increase, while inhibiting mTOR with rapamycin or everolimus decreases HTR2B expression, and activation of HTR2B decreases mTOR signaling, suggesting that HTR2B is functionally coupled to mTOR signaling. In unfavorable conditions such as glucose deprivation or 5-FU treatment, activation of HTR2B with serotonin or a selective agonist led to a paradoxical reduction in cell survival, an effect that could be reversed by pharmacological inhibition of the receptor. This indicates that while HTR2B expression is upregulated in stress conditions, its activation may trigger maladaptive signaling cascades that compromise cell viability, potentially through feedback inhibition of mTORC1. Thus, HTR2B-mTORC1 axis emerges as a potential vulnerability under stress conditions, where targeting either pathway may disrupt tumor cell adaptation and improve chemotherapeutic efficacy.

This link between metabolic stress, serotonin signaling, and mTOR regulation provides a conceptual framework for understanding how CRC cells adapt to fluctuating nutrient availability within the tumor microenvironment. It also highlights that serotonin receptor signaling is not universally tumor-promoting, as is sharply contrasted with PDAC in a nutrient-deprived environment, where it modulates survival or invasion depending on environmental constraints in CRC.

Fibroblasts are key orchestrators of the tumor microenvironment, influencing CRC progression through paracrine signaling, ECM remodeling, and metabolic coupling. Co-culturing CRC PDOs with fibroblasts revealed profound effects on tumor cell phenotype. Fibroblast proximity induced pEMT, evidenced by the downregulation of epithelial EpCAM and the upregulation of the EMT marker lumican (LUM). Notably, fibroblast co-culture expanded the $HTR2B^{+}$ CRC subpopulation, even within the $EpCAM^{+}$ fraction, suggesting that fibroblast-derived cues promote mesenchymal-like states without complete epithelial loss. Immunostaining of CRC tissues confirmed the spatial association of $LUM^{+}/HTR2B^{+}$ tumor cells with stromal regions, reinforcing the in vivo relevance of these findings.

Interestingly, conditioned medium from fibroblasts failed to reproduce these effects, indicating that direct cell-cell contact or ECM deposition, rather than soluble factors, mediates HTR2B induction. Indeed, fibroblasts remodel the ECM through collagen-1 deposition, a stiff ECM component that accumulates during CRC progression and correlates with poor prognosis (121). Our subsequent experiments revealed that culturing PDOs in collagen-I recapitulated the fibroblast-induced pEMT phenotype, leading to upregulation of VIM, LUM, and HTR2B. Thus, ECM composition emerges as a pivotal determinant of HTR2B expression and tumor plasticity, aligning with the concept that biomechanical and structural cues shape cancer cell behavior.

In collagen-I matrices, CRC organoids exhibited increased invasion, particularly within the $HTR2B^{+}$ subpopulation. These cells localized preferentially to the invasion front and retained E-cadherin expression, confirming their pEMT phenotype. Activation of HTR2B with serotonin or a receptor agonist enhanced the expression of EMT markers and expanded the invasion area, without increasing apoptosis or reducing overall viability. These effects were specific to $HTR2B^{high}$ cells, suggesting a feed-forward mechanism in which HTR2B signaling amplifies mesenchymal features in an ECM-permissive context. Important, HTR2B activation did not exacerbate 5-FU-induced cytotoxicity in collagen, underscoring that its primary function in this setting relates to motility rather than survival.

The observation that HTR2B-induced invasion depends on the ECM environment provides a mechanistic explanation for why CMS4 tumors, typically enriched in

fibroblasts and collagen, display high metastatic potential. By integrating ECM-derived mechanical signals with serotonin-HTR2B signaling, CRC cells can transiently adopt invasive phenotypes without full EMT commitment. This hybrid state may enable efficient dissemination while retaining the capacity to revert to an epithelial phenotype during metastatic colonization.

The final part of this study addressed the molecular convergence between serotonin and NOTCH signaling, two pathways independently linked to CRC aggressiveness. Analysis of patient data from the Human Protein Atlas revealed that NOTCH3, but not NOTCH1, correlates with poor survival and is preferentially expressed in CMS4 tumors. Both receptors were expressed across PDO lines, with stable levels in Matrigel and collagen, indicating that their expression is maintained independently of ECM context. NOTCH ligands were detected in both cancer cells and CAFs, suggesting that stromal-tumor interactions contribute to pathway activation, while flow cytometry confirmed surface expression of NOTCH3 in organoid cells. Functionally, inhibition of NOTCH signaling abrogated the HTR2B and serotonin-induced increase in invasion, supporting a cooperative role between these pathways in promoting tumor invasiveness. Collectively, these findings identify $HTR2B^{+}/NOTCH3^{+}$ CRC cells as a functionally distinct, microenvironment-responsive subpopulation driving plasticity and invasive potential within CMS4-like tumors.

# 6. Conclusions

This thesis elucidates how CRC cells dynamically integrate metabolic, mechanical, and paracrine cues to sustain heterogeneity and invasiveness. Through systematic investigation using patient-derived organoids, we have uncovered several key insights. Firstly, CRC stem cell markers (CD44, CD133) define functionally distinct proliferative subpopulations contributing to intra-tumoral heterogeneity. Secondly, CMS4-associated traits such as HTR2B expression and pEMT are maintained intrinsically within CRC cells and are further amplified by stromal and ECM interactions. Thirdly, HTR2B and mTORC1 signaling cooperate to regulate survival and invasion under metabolic stress, highlighting a metabolic-signaling axis of adaptation. Fourthly, fibroblast-derived collagen-I acts as a critical microenvironmental factor promoting pEMT and expansion of the $HTR2B^{+}$ population. Finally, HTR2B and NOTCH3 identify overlapping aggressive CRC cell subsets under the partial control of mTORC1.

Together, these findings position HTR2B at the intersection of metabolic stress response, ECM sensing, and cellular plasticity, providing a unifying mechanistic link between tumor heterogeneity and invasive potential. Future research should explore whether pharmacological modulation of HTR2B or mTORC1 can be leveraged therapeutically to suppress metastasis or sensitize CMS4 tumors to chemotherapy. Integrating single-cell transcriptomics, spatial proteomics, and functional co-culture systems will further refine our understanding of how CRC cells navigate between epithelial and mesenchymal states in response to environmental challenges. Ultimately, this work underscores the power of patient-derived organoids as platforms to unravel complex cell-environment interactions that drive tumor evolution and to identify actionable vulnerabilities within heterogenous cancers.

# 7. Summary

CRC is one of the most prevalent and lethal malignancies worldwide. Despite substantial progress in treatment, patient outcomes remain highly variable due to the pronounced intra-tumoral heterogeneity and the complex tumor-stroma interactions that shape disease progression. Using patient-derived 3D organoids, we studied the heterogeneity of cancer stem cell matkers, the role of serotonin receptor 2B (HTR2B) in tumor behavior, and the influence of fibroblast-mediated extracellular matrix (ECM) remodeling on tumor plasticity and invasion.

We demonstrate that CRC organoids display stable heterogeneity for classical cancer stem cell markers, including CD44, CD133, PTK7. Subpopulations with high CD44 or CD133 expression exhibited enhanced proliferative potential and organoid-forming capacity, confirming that these markers identify hierarchically superior cell subsets within CRC. The expression of CMS markers was also heterogeneous, with epithelial CDX2 and mesenchymal HTR2B marking distinct but partially overlapping cancer cell subpopulations. The coexistence of these states indicates the presence of hybrid epithelial-mesenchymal phenotypes that may underline the plasticity of CRC cells.

Serotonin metabolism was found to play a context-dependent role in CRC. In contrast to pancreatic tumors, CRC cells produced minimal serotonin, but they expressed high levels of HTR2B, particularly under nutrient-limited conditions. Activation of HTR2B decreased cell survival in a glucose-deprived environment, suggesting that receptor signaling interacts with mTORC1 activity in regulating tumor cell adaptation. Inhibiting mTORC1 reduced both HTR2B and NOTCH3 expression, linking metabolic stress to pathways controlling EMT and survival.

Fibroblast co-culture and collagen-rich matrices induced partial epithelial-mesenchymal transition (pEMT), increased HTR2B expression, and promoted tumor cell invasion. $HTR2B^{high}$ cells located at the invasive front of organoids and retained epithelial markers, confirming that HTR2B activity supports invasion through a permissive ECM rather than by complete EMT.

Collectively, our findings reveal that CRC cells integrate metabolic, mechanical, and paracrine cues to maintain phenotypic diversity and invasive potential (Fig. 40). HTR2B

emerges as a key regulator linking stress adaptation, fibroblast-driven ECM remodeling, and tumor invasiveness. Understanding these interconnected mechanisms provides new insight into CRC plasticity and may identify therapeutic opportunities targeting the HTR2B-mTORC1-NOTCH3 axis in aggressive, CMS4-like tumors.

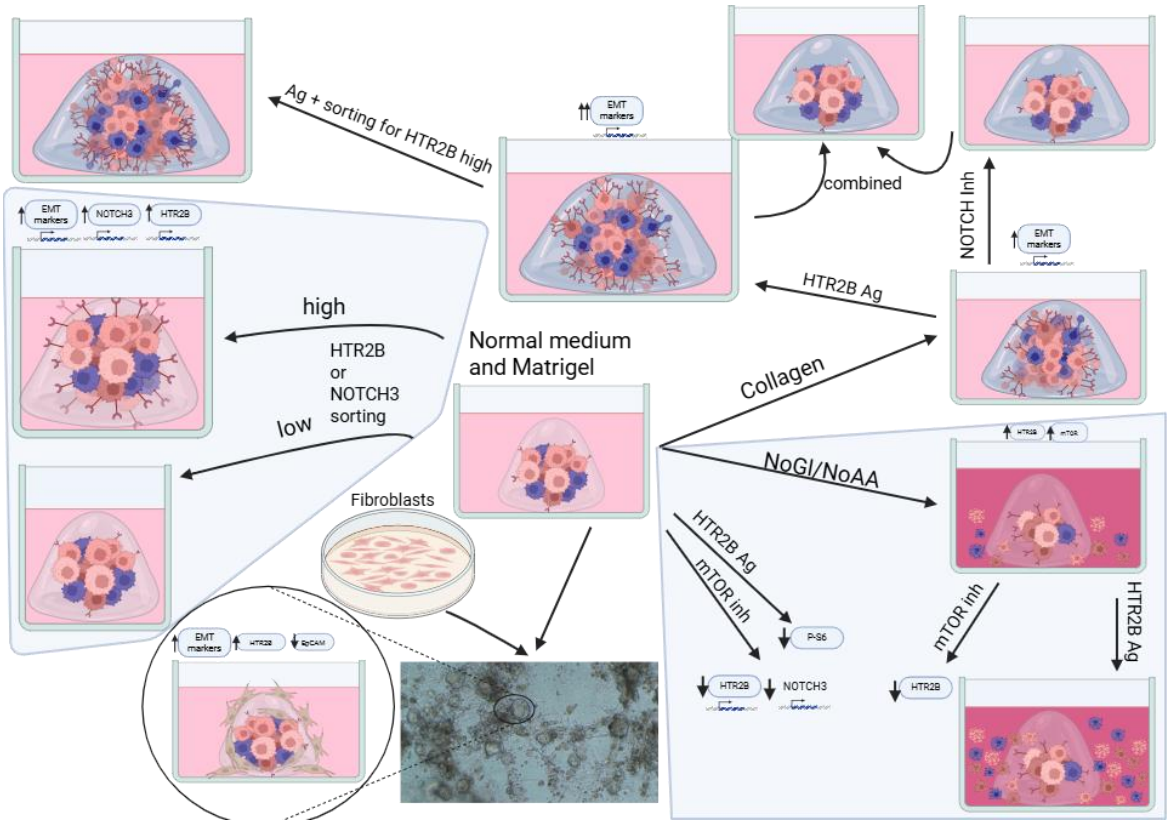


**Figure 40. Graphical summary of the proposed model for HTR2B and NOTCH3 activity in colorectal cancer organoids.** Schematic representation summarizing the main findings of this study. Patient-derived colorectal cancer (CRC) organoids display intratumoral heterogeneity in the expression of HTR2B and NOTCH3 (center). Sorting tumor cells based on high or low HTR2B or NOTCH3 expression results in organoid subpopulations that maintain their respective expression levels in culture (left). Cells with high HTR2B or NOTCH3 expression form larger organoids and display elevated proliferation and pEMT marker expression (upper left). Co-culture with fibroblasts (bottom center) or exposure to collagen I provide permissive extracellular matrix (ECM) conditions and upon activation of HTR2B with serotonin or a specific agonist (upper right and center top) promote pEMT and increase HTR2B+ CRC cells. Nutrient deprivation (absence of glucose or amino acids) increased mTORC and HTR2B (right middle), whereas, inhibition of mTORC1 decreases both HTR2B and NOTCH3 expression and their downstream target genes (bottom right), and HTR2B agonist treatment alone decreased mTORC1 signaling (bottom right), while combined with nutrient deprivation decreased cell viability further (bottom corner right). (unpublished own figure made by Biorender).

# 8. References

1. Bray F, Laversanne M, Sung H, Ferlay J, Siegel RL, Soerjomataram I, Jemal A. Global cancer statistics 2022: GLOBOCAN estimates of incidence and mortality worldwide for 36 cancers in 185 countries. CA: A Cancer Journal for Clinicians. 2024;74(3):229–63.

2. Morgan E, Arnold M, Gini A, Lorenzoni V, Cabasag CJ, Laversanne M, Vignat J, Ferlay J, Murphy N, Bray F. Global burden of colorectal cancer in 2020 and 2040: incidence and mortality estimates from GLOBOCAN. Gut. 2023;72(2):338.

3. Bucchi L, Mancini S, Baldacchini F, Ravaioli A, Giuliani O, Vattiato R, Zamagni F, Giorgi Rossi P, Campari C, Canuti D, Di Felice E, Sassoli de Bianchi P, Ferretti S, Bertozzi N, Biggeri A, Falcini F, Di Felice E, Finarelli AC, Landi P, Naldoni C, Sassoli de Bianchi P, Colamartini A, Borciani E, Fornari F, Gatti G, Pennini F, Seghini P, Dalla Fiora C, Fattibene C, Maradini F, Michiara M, Orsi P, Zurlini C, Mangone L, Paterlini L, Sassatelli R, Carrozzi G, Corradini R, Rossi F, Trande P, Viani S, Bazzani C, Bazzoli F, Cennamo V, Giansante C, Gualandi G, Manfredi M, Mezzetti F, Pasquini A, Caprara L, De Lillo M, Nannini R, Carpanelli MC, De Togni A, Matarese V, Palmonari C, Pasquali D, Zoli G, Dal Re S, Petrini C, Serafini M, Vitali B, Gallinucci M, Imolesi C, Palazzi M, Ricci E, Severi M, Casale C, Giovanardi M, Trombetti D, the Emilia-Romagna Region Workgroup for Colorectal Screening E. How a faecal immunochemical test screening programme changes annual colorectal cancer incidence rates: an Italian intention-to-screen study. British Journal of Cancer. 2022;127(3):541–8.

4. Kenessey I, Nagy P, Polgár C. [The Hungarian situation of cancer epidemiology in the second decade of the 21st century]. Magy Onkol. 2022;66(3):175–84.

5. Kiss Z, Szabó TG, Polgár C, Horváth Z, Nagy P, Fábián I, Kovács V, Surján G, Barcza Z, Kenessey I, Wéber A, Wittmann I, Molnár GA, Gyöngyösi E, Benedek A, Karamousouli E, Abonyi-Tóth Z, Bertókné Tamás R, Fürtős DV, Bogos K, Moldvay J, Gálffy G, Tamási L, Müller V, Krasznai ZT, Ostoros G, Pápai-Székely Z, Maráz A, Branyiczkiné Géczy G, Hilbert L, Tamás Berki Lś, Rokszin G, Vokó Z. Revising cancer incidence in a Central European country: a Hungarian nationwide study between 2011–2019 based on a health insurance fund database. Frontiers in Oncology. 2024;Volume 14 - 2024.

6. He K, Gan WJ. Wnt/β-Catenin Signaling Pathway in the Development and Progression of Colorectal Cancer. Cancer Manag Res. 2023;15:435–48.
7. Chen Y, Chen M, Deng K. Blocking the Wnt/β-catenin signaling pathway to treat colorectal cancer: Strategies to improve current therapies (Review). Int J Oncol. 2023;62(2).
8. Bahar ME, Kim HJ, Kim DR. Targeting the RAS/RAF/MAPK pathway for cancer therapy: from mechanism to clinical studies. Signal Transduction and Targeted Therapy. 2023;8(1):455.
9. Braicu C, Buse M, Busuioc C, Drula R, Gulei D, Raduly L, Rusu A, Irimie A, Atanasov AG, Slaby O, Ionescu C, Berindan-Neagoe I. A Comprehensive Review on MAPK: A Promising Therapeutic Target in Cancer. Cancers (Basel). 2019;11(10).
10. Appleyard JW, Williams CJM, Manca P, Pietrantonio F, Seligmann JF. Targeting the MAP Kinase Pathway in Colorectal Cancer: A Journey in Personalized Medicine. Clin Cancer Res. 2025;31(13):2565–72.
11. Leiphrakpam PD, Are C. PI3K/Akt/mTOR Signaling Pathway as a Target for Colorectal Cancer Treatment. Int J Mol Sci. 2024;25(6).
12. Glaviano A, Foo ASC, Lam HY, Yap KCH, Jacot W, Jones RH, Eng H, Nair MG, Makvandi P, Geoerger B, Kulke MH, Baird RD, Prabhu JS, Carbone D, Pecoraro C, Teh DBL, Sethi G, Cavalieri V, Lin KH, Javidi-Sharifi NR, Toska E, Davids MS, Brown JR, Diana P, Stebbing J, Fruman DA, Kumar AP. PI3K/AKT/mTOR signaling transduction pathway and targeted therapies in cancer. Molecular Cancer. 2023;22(1):138.
13. Mendoza MC, Er EE, Blenis J. The Ras-ERK and PI3K-mTOR pathways: cross-talk and compensation. Trends in Biochemical Sciences. 2011;36(6):320–8.
14. Itatani Y, Kawada K, Sakai Y. Transforming Growth Factor-β Signaling Pathway in Colorectal Cancer and Its Tumor Microenvironment. Int J Mol Sci. 2019;20(23).
15. Fang T, Liang T, Wang Y, Wu H, Liu S, Xie L, Liang J, Wang C, Tan Y. Prognostic role and clinicopathological features of SMAD4 gene mutation in colorectal cancer: a systematic review and meta-analysis. BMC Gastroenterology. 2021;21(1):297.
16. Fasano M, Pirozzi M, Miceli CC, Cocule M, Caraglia M, Boccellino M, Vitale P, De Falco V, Farese S, Zotta A, Ciardiello F, Addeo R. TGF-β Modulated Pathways in

Colorectal Cancer: New Potential Therapeutic Opportunities. International Journal of Molecular Sciences. 2024;25(13):7400.
17. Liebl MC, Hofmann TG. The Role of p53 Signaling in Colorectal Cancer. Cancers (Basel). 2021;13(9).
18. Li XL, Zhou J, Chen ZR, Chng WJ. P53 mutations in colorectal cancer - molecular pathogenesis and pharmacological reactivation. World J Gastroenterol. 2015;21(1):84–93.
19. Yan S, Zhan F, He Y, Zhu Y, Ma Z. p53 in colorectal cancer: from a master player to a privileged therapy target. Journal of Translational Medicine. 2025;23(1):684.
20. Participants in the Paris W. The Paris endoscopic classification of superficial neoplastic lesions: esophagus, stomach, and colon: November 30 to December 1, 2002. Gastrointestinal Endoscopy. 2003;58(6):S3–S43.
21. Johnson G, Helewa R, Moffatt DC, Coneys JG, Park J, Hyun E. Colorectal polyp classification and management of complex polyps for surgeon endoscopists. Can J Surg. 2023;66(5):E491–e8.
22. Nagtegaal ID, Odze RD, Klimstra D, Paradis V, Rugge M, Schirmacher P, Washington KM, Carneiro F, Cree IA. The 2019 WHO classification of tumours of the digestive system. Histopathology. 2020;76(2):182–8.
23. Fearon ER, Vogelstein B. A genetic model for colorectal tumorigenesis. Cell. 1990;61(5):759–67.
24. Smit WL, Spaan CN, Johannes de Boer R, Ramesh P, Martins Garcia T, Meijer BJ, Vermeulen JLM, Lezzerini M, MacInnes AW, Koster J, Medema JP, van den Brink GR, Muncan V, Heijmans J. Driver mutations of the adenoma-carcinoma sequence govern the intestinal epithelial global translational capacity. Proceedings of the National Academy of Sciences. 2020;117(41):25560–70.
25. Nguyen LH, Goel A, Chung DC. Pathways of Colorectal Carcinogenesis. Gastroenterology. 2020;158(2):291–302.
26. Wang J-D, Xu G-S, Hu X-L, Li W-Q, Yao N, Han F-Z, Zhang Y, Qu J. The histologic features, molecular features, detection and management of serrated polyps: a review. Frontiers in Oncology. 2024;Volume 14 - 2024.
27. Yamane L, Scapulatempo-Neto C, Reis RM, Guimarães DP. Serrated pathway in colorectal carcinogenesis. World J Gastroenterol. 2014;20(10):2634–40.

28. De Palma FDE, D'Argenio V, Pol J, Kroemer G, Maiuri MC, Salvatore F. The Molecular Hallmarks of the Serrated Pathway in Colorectal Cancer. Cancers. 2019;11(7):1017.
29. Wang R, Mao Y, Wang W, Zhou X, Wang W, Gao S, Li J, Wen L, Fu W, Tang F. Systematic evaluation of colorectal cancer organoid system by single-cell RNA-Seq analysis. Genome Biology. 2022;23(1):106.
30. Blank A, Roberts DE, Dawson H, Zlobec I, Lugli A. Tumor Heterogeneity in Primary Colorectal Cancer and Corresponding Metastases. Does the Apple Fall Far From the Tree? Frontiers in Medicine. 2018;Volume 5 - 2018.
31. Hale VL, Jeraldo P, Chen J, Mundy M, Yao J, Priya S, Keeney G, Lyke K, Ridlon J, White BA, French AJ, Thibodeau SN, Diener C, Resendis-Antonio O, Gransee J, Dutta T, Petterson X-M, Sung J, Blekhman R, Boardman L, Larson D, Nelson H, Chia N. Distinct microbes, metabolites, and ecologies define the microbiome in deficient and proficient mismatch repair colorectal cancers. Genome Medicine. 2018;10(1):78.
32. Fang A, Ugai T, Gurjao C, Zhong R, Liu Z, Zhang X, Wang P, Nowak J, Wang M, Giannakis M, Ogino S, Zhang X, Giovannucci E. Alcohol and colorectal cancer risk, subclassified by mutational signatures of DNA mismatch repair deficiency. J Natl Cancer Inst. 2024;116(8):1255–63.
33. Suvac A, Ashton J, Bristow RG. Tumour hypoxia in driving genomic instability and tumour evolution. Nat Rev Cancer. 2025;25(3):167–88.
34. Guinney J, Dienstmann R, Wang X, de Reyniès A, Schlicker A, Soneson C, Marisa L, Roepman P, Nyamundanda G, Angelino P, Bot BM, Morris JS, Simon IM, Gerster S, Fessler E, De Sousa E Melo F, Missiaglia E, Ramay H, Barras D, Homicsko K, Maru D, Manyam GC, Broom B, Boige V, Perez-Villamil B, Laderas T, Salazar R, Gray JW, Hanahan D, Tabernero J, Bernards R, Friend SH, Laurent-Puig P, Medema JP, Sadanandam A, Wessels L, Delorenzi M, Kopetz S, Vermeulen L, Tejpar S. The consensus molecular subtypes of colorectal cancer. Nature Medicine. 2015;21(11):1350–6.
35. Valenzuela G, Canepa J, Simonetti C, Solo de Zaldívar L, Marcelain K, González-Montero J. Consensus molecular subtypes of colorectal cancer in clinical practice: A translational approach. World J Clin Oncol. 2021;12(11):1000–8.

36. Valdeolivas A, Amberg B, Giroud N, Richardson M, Gálvez EJC, Badillo S, Julien-Laferrière A, Túrós D, Voith von Voithenberg L, Wells I, Pesti B, Lo AA, Yángüez E, Das Thakur M, Bscheider M, Sultan M, Kumpesa N, Jacobsen B, Bergauer T, Saez-Rodriguez J, Rottenberg S, Schwalie PC, Hahn K. Profiling the heterogeneity of colorectal cancer consensus molecular subtypes using spatial transcriptomics. npj Precision Oncology. 2024;8(1):10.
37. Torang A, Kirov AB, Lammers V, Cameron K, Wouters VM, Jackstadt RF, Lannagan TRM, de Jong JH, Koster J, Sansom O, Medema JP. Enterocyte-like differentiation defines metabolic gene signatures of CMS3 colorectal cancers and provides therapeutic vulnerability. Nature Communications. 2025;16(1):264.
38. Thanki K, Nicholls ME, Gajjar A, Senagore AJ, Qiu S, Szabo C, Hellmich MR, Chao C. Consensus Molecular Subtypes of Colorectal Cancer and their Clinical Implications. Int Biol Biomed J. 2017;3(3):105–11.
39. ten Hoorn S, de Back TR, Sommeijer DW, Vermeulen L. Clinical Value of Consensus Molecular Subtypes in Colorectal Cancer: A Systematic Review and Meta-Analysis. JNCI: Journal of the National Cancer Institute. 2021;114(4):503–16.
40. Dang Q, Zuo L, Hu X, Zhou Z, Chen S, Liu S, Ba Y, Zuo A, Xu H, Weng S, Zhang Y, Luo P, Cheng Q, Liu Z, Han X. Molecular subtypes of colorectal cancer in the era of precision oncotherapy: Current inspirations and future challenges. Cancer Medicine. 2024;13(14):e70041.
41. Mouillet-Richard S, Cazelles A, Sroussi M, Gallois C, Taieb J, Laurent-Puig P. Clinical Challenges of Consensus Molecular Subtype CMS4 Colon Cancer in the Era of Precision Medicine. Clin Cancer Res. 2024;30(11):2351–8.
42. Trinh A, Trumpi K, De Sousa E Melo F, Wang X, de Jong JH, Fessler E, Kuppen PJK, Reimers MS, Swets M, Koopman M, Nagtegaal ID, Jansen M, Hooijer GKJ, Offerhaus GJA, Kranenburg O, Punt CJ, Medema JP, Markowetz F, Vermeulen L. Practical and Robust Identification of Molecular Subtypes in Colorectal Cancer by Immunohistochemistry. Clinical Cancer Research. 2017;23(2):387–98.
43. Galon J, Pagès F, Marincola FM, Angell HK, Thurin M, Lugli A, Zlobec I, Berger A, Bifulco C, Botti G, Tatangelo F, Britten CM, Kreiter S, Chouchane L, Delrio P, Arndt H, Asslaber M, Maio M, Masucci GV, Mihm M, Vidal-Vanaclocha F, Allison JP, Gnjatic S, Hakansson L, Huber C, Singh-Jasuja H, Ottensmeier C, Zwierzina H,

Laghi L, Grizzi F, Ohashi PS, Shaw PA, Clarke BA, Wouters BG, Kawakami Y, Hazama S, Okuno K, Wang E, O'Donnell-Tormey J, Lagorce C, Pawelec G, Nishimura MI, Hawkins R, Lapointe R, Lundqvist A, Khleif SN, Ogino S, Gibbs P, Waring P, Sato N, Torigoe T, Itoh K, Patel PS, Shukla SN, Palmqvist R, Nagtegaal ID, Wang Y, D'Arrigo C, Kopetz S, Sinicrope FA, Trinchieri G, Gajewski TF, Ascierto PA, Fox BA. Cancer classification using the Immunoscore: a worldwide task force. J Transl Med. 2012;10:205.

44. Isella C, Brundu F, Bellomo SE, Galimi F, Zanella E, Porporato R, Petti C, Fiori A, Orzan F, Senetta R, Boccaccio C, Ficarra E, Marchionni L, Trusolino L, Medico E, Bertotti A. Selective analysis of cancer-cell intrinsic transcriptional traits defines novel clinically relevant subtypes of colorectal cancer. Nature Communications. 2017;8(1):15107.

45. Joanito I, Wirapati P, Zhao N, Nawaz Z, Yeo G, Lee F, Eng CLP, Macalinao DC, Kahraman M, Srinivasan H, Lakshmanan V, Verbandt S, Tsantoulis P, Gunn N, Venkatesh PN, Poh ZW, Nahar R, Oh HLJ, Loo JM, Chia S, Cheow LF, Cheruba E, Wong MT, Kua L, Chua C, Nguyen A, Golovan J, Gan A, Lim W-J, Guo YA, Yap CK, Tay B, Hong Y, Chong DQ, Chok A-Y, Park W-Y, Han S, Chang MH, Seow-En I, Fu C, Mathew R, Toh E-L, Hong LZ, Skanderup AJ, DasGupta R, Ong C-AJ, Lim KH, Tan EKW, Koo S-L, Leow WQ, Tejpar S, Prabhakar S, Tan IB. Single-cell and bulk transcriptome sequencing identifies two epithelial tumor cell states and refines the consensus molecular classification of colorectal cancer. Nature Genetics. 2022;54(7):963–75.

46. Li J, Chen D, Shen M. Tumor Microenvironment Shapes Colorectal Cancer Progression, Metastasis, and Treatment Responses. Front Med (Lausanne). 2022;9:869010.

47. Winkler J, Abisoye-Ogunniyan A, Metcalf KJ, Werb Z. Concepts of extracellular matrix remodelling in tumour progression and metastasis. Nature Communications. 2020;11(1):5120.

48. Li ZL, Wang ZJ, Wei GH, Yang Y, Wang XW. Changes in extracellular matrix in different stages of colorectal cancer and their effects on proliferation of cancer cells. World J Gastrointest Oncol. 2020;12(3):267–75.

49. Zhang J, Hu Z, Horta CA, Yang J. Regulation of epithelial-mesenchymal transition by tumor microenvironmental signals and its implication in cancer therapeutics. Semin Cancer Biol. 2023;88:46–66.
50. Yuan Z, Li Y, Zhang S, Wang X, Dou H, Yu X, Zhang Z, Yang S, Xiao M. Extracellular matrix remodeling in tumor progression and immune escape: from mechanisms to treatments. Mol Cancer. 2023;22(1):48.
51. Wei SC, Fattet L, Tsai JH, Guo Y, Pai VH, Majeski HE, Chen AC, Sah RL, Taylor SS, Engler AJ, Yang J. Matrix stiffness drives epithelial-mesenchymal transition and tumour metastasis through a TWIST1-G3BP2 mechanotransduction pathway. Nat Cell Biol. 2015;17(5):678–88.
52. Sánchez-Ramírez D, Mendoza-Rodríguez MG, Alemán OR, Candanedo-González FA, Rodríguez-Sosa M, Montesinos-Montesinos JJ, Salcedo M, Brito-Toledo I, Vaca-Paniagua F, Terrazas LI. Impact of STAT-signaling pathway on cancer-associated fibroblasts in colorectal cancer and its role in immunosuppression. World J Gastrointest Oncol. 2024;16(5):1705–24.
53. Zhong B, Cheng B, Huang X, Xiao Q, Niu Z, Chen Y-f, Yu Q, Wang W, Wu X-J. Colorectal cancer-associated fibroblasts promote metastasis by up-regulating LRG1 through stromal IL-6/STAT3 signaling. Cell Death & Disease. 2021;13(1):16.
54. Tommelein J, Verset L, Boterberg T, Demetter P, Bracke M, De Wever O. Cancer-associated fibroblasts connect metastasis-promoting communication in colorectal cancer. Front Oncol. 2015;5:63.
55. Xie J, Lin X, Deng X, Tang H, Zou Y, Chen W, Xie X. Cancer-associated fibroblast-derived extracellular vesicles: regulators and therapeutic targets in the tumor microenvironment. Cancer Drug Resist. 2025;8:2.
56. Lan X, Li W, Zhao K, Wang J, Li S, Zhao H. Revisiting the role of cancer-associated fibroblasts in tumor microenvironment. Front Immunol. 2025;16:1582532.
57. Zhang Y, Wang S, Lai Q, Fang Y, Wu C, Liu Y, Li Q, Wang X, Gu C, Chen J, Cai J, Li A, Liu S. Cancer-associated fibroblasts-derived exosomal miR-17-5p promotes colorectal cancer aggressive phenotype by initiating a RUNX3/MYC/TGF-β1 positive feedback loop. Cancer Letters. 2020;491:22–35.

58. Zhong X, He X, Wang Y, Hu Z, Huang H, Zhao S, Wei P, Li D. Warburg effect in colorectal cancer: the emerging roles in tumor microenvironment and therapeutic implications. J Hematol Oncol. 2022;15(1):160.
59. Zhu M, Hu Y, Gu Y, Lin X, Jiang X, Gong C, Fang Z. Role of amino acid metabolism in tumor immune microenvironment of colorectal cancer. Am J Cancer Res. 2025;15(1):233–47.
60. Liu W, Dong S, Hao F, Gao Y, Wei Q. Lipid metabolic reprogramming in colorectal cancer: mechanisms and therapeutic strategies. Frontiers in Immunology. 2025;Volume 16 - 2025.
61. Roelands J, Kuppen PJK, Vermeulen L, Maccalli C, Decock J, Wang E, Marincola FM, Bedognetti D, Hendrickx W. Immunogenomic Classification of Colorectal Cancer and Therapeutic Implications. International Journal of Molecular Sciences. 2017;18(10):2229.
62. Karpinski P, Rossowska J, Malgorzata Sasiadek M. Immunological landscape of consensus clusters in colorectal cancer. Oncotarget. 2017;8(62).
63. Zheng Z, Wieder T, Mauerer B, Schäfer L, Kesselring R, Braumüller H. T Cells in Colorectal Cancer: Unravelling the Function of Different T Cell Subsets in the Tumor Microenvironment. Int J Mol Sci. 2023;24(14).
64. Radomska-Leśniewska DM, Białoszewska A, Kamiński P. Angiogenic Properties of NK Cells in Cancer and Other Angiogenesis-Dependent Diseases. Cells. 2021;10(7).
65. Sun G, Dong X, Tang X, Qu H, Zhang H, Zhao E. The prognostic value of immunoscore in patients with colorectal cancer: A systematic review and meta-analysis. Cancer Med. 2019;8(1):182–9.
66. Liu N, Sun S, Wang P, Sun Y, Hu Q, Wang X. The Mechanism of Secretion and Metabolism of Gut-Derived 5-Hydroxytryptamine. Int J Mol Sci. 2021;22(15).
67. Kannen V, Bader M, Sakita JY, Uyemura SA, Squire JA. The Dual Role of Serotonin in Colorectal Cancer. Trends in Endocrinology & Metabolism. 2020;31(8):611–25.
68. Ling T, Dai Z, Wang H, Kien TT, Cui R, Yu T, Chen J. Serotonylation in tumor-associated fibroblasts contributes to the tumor-promoting roles of serotonin in colorectal cancer. Cancer Lett. 2024;600:217150.

69. Lu Y, Gu D, Zhao C, Sun Y, Li W, He L, Wang X, Kou Z, Su J, Guo F. Genomic landscape and expression profile of consensus molecular subtype four of colorectal cancer. Front Immunol. 2023;14:1160052.
70. Moon JH, Oh C-M, Kim H. Serotonin in the regulation of systemic energy metabolism. Journal of Diabetes Investigation. 2022;13(10):1639–45.
71. MOHAMMAD-ZADEH LF, MOSES L, GWALTNEY-BRANT SM. Serotonin: a review. Journal of Veterinary Pharmacology and Therapeutics. 2008;31(3):187–99.
72. Li B, Elsten-Brown J, Li M, Zhu E, Li Z, Chen Y, Kang E, Ma F, Chiang J, Li YR, Zhu Y, Huang J, Fung A, Scarborough Q, Cadd R, Zhou JJ, Chin AI, Pellegrini M, Yang L. Serotonin transporter inhibits antitumor immunity through regulating the intratumoral serotonin axis. Cell. 2025;188(14):3823–42.e21.
73. Zhang N, Sundquist J, Sundquist K, Ji J. Use of Selective Serotonin Reuptake Inhibitors Is Associated with a Lower Risk of Colorectal Cancer among People with Family History. Cancers (Basel). 2022;14(23).
74. Cortes-Altamirano JL, Olmos-Hernandez A, Jaime HB, Carrillo-Mora P, Bandala C, Reyes-Long S, Alfaro-Rodríguez A. Review: 5-HT1, 5-HT2, 5-HT3 and 5-HT7 Receptors and their Role in the Modulation of Pain Response in the Central Nervous System. Curr Neuropharmacol. 2018;16(2):210–21.
75. Sui H, Xu H, Ji Q, Liu X, Zhou L, Song H, Zhou X, Xu Y, Chen Z, Cai J, Ji G, Li Q. 5-hydroxytryptamine receptor (5-HT1DR) promotes colorectal cancer metastasis by regulating Axin1/β-catenin/MMP-7 signaling pathway. Oncotarget. 2015;6(28):25975–87.
76. Tang J, Wang Z, Liu J, Zhou C, Chen J. Downregulation of 5-hydroxytryptamine receptor 3A expression exerts an anticancer activity against cell growth in colorectal carcinoma cells in vitro. Oncol Lett. 2018;16(5):6100–8.
77. Johnston KD, Lu Z, Rudd JA. Looking beyond 5-HT(3) receptors: a review of the wider role of serotonin in the pharmacology of nausea and vomiting. Eur J Pharmacol. 2014;722:13–25.
78. Karmakar S, Lal G. Role of serotonin receptor signaling in cancer cells and anti-tumor immunity. Theranostics. 2021;11(11):5296–312.

79. Chen L, Huang S, Wu X, He W, Song M. Serotonin signalling in cancer: Emerging mechanisms and therapeutic opportunities. Clinical and Translational Medicine. 2024;14(7):e1750.
80. Liu H, Huang Q, Fan Y, Li B, Liu X, Hu C. Dissecting the novel abilities of aripiprazole: The generation of anti-colorectal cancer effects by targeting Gαq via HTR2B. Acta Pharm Sin B. 2023;13(8):3400–13.
81. Lee JY, Park S, Park EJ, Pagire HS, Pagire SH, Choi BW, Park M, Fang S, Ahn JH, Oh CM. Inhibition of HTR2B-mediated serotonin signaling in colorectal cancer suppresses tumor growth through ERK signaling. Biomed Pharmacother. 2024;179:117428.
82. de las Casas-Engel M, Domínguez-Soto A, Sierra-Filardi E, Bragado R, Nieto C, Puig-Kroger A, Samaniego R, Loza M, Corcuera MT, Gómez-Aguado F, Bustos M, Sánchez-Mateos P, Corbí AL. Serotonin Skews Human Macrophage Polarization through HTR2B and HTR7. The Journal of Immunology. 2013;190(5):2301–10.
83. Okamoto R, Tsuchiya K, Nemoto Y, Akiyama J, Nakamura T, Kanai T, Watanabe M. Requirement of Notch activation during regeneration of the intestinal epithelia. American Journal of Physiology-Gastrointestinal and Liver Physiology. 2009;296(1):G23–G35.
84. Brisset M, Mehlen P, Meurette O, Hollande F. Notch receptor/ligand diversity: contribution to colorectal cancer stem cell heterogeneity. Front Cell Dev Biol. 2023;11:1231416.
85. Tyagi A, Sharma AK, Damodaran C. A Review on Notch Signaling and Colorectal Cancer. Cells. 2020;9(6).
86. Goenka A, Khan F, Verma B, Sinha P, Dmello CC, Jogalekar MP, Gangadaran P, Ahn BC. Tumor microenvironment signaling and therapeutics in cancer progression. Cancer Commun (Lond). 2023;43(5):525–61.
87. Peng Y, Li Z, Yang P, Newton IP, Ren H, Zhang L, Wu H, Li Z. Direct contacts with colon cancer cells regulate the differentiation of bone marrow mesenchymal stem cells into tumor associated fibroblasts. Biochemical and Biophysical Research Communications. 2014;451(1):68–73.
88. Green C, Roccia P, Rufini A. Making sense of human colorectal cancer molecular subtypes: mice are stepping in. Cell Death Discovery. 2025;11(1):295.

89. Huang K, Luo W, Fang J, Yu C, Liu G, Yuan X, Liu Y, Wu W. Notch3 signaling promotes colorectal tumor growth by enhancing immunosuppressive cells infiltration in the microenvironment. BMC Cancer. 2023;23(1):55.
90. Tian H, Biehs B, Chiu C, Siebel CW, Wu Y, Costa M, de Sauvage FJ, Klein OD. Opposing activities of Notch and Wnt signaling regulate intestinal stem cells and gut homeostasis. Cell Rep. 2015;11(1):33–42.
91. Xiu M, Wang Y, Li B, Wang X, Xiao F, Chen S, Zhang L, Zhou B, Hua F. The Role of Notch3 Signaling in Cancer Stemness and Chemoresistance: Molecular Mechanisms and Targeting Strategies. Frontiers in Molecular Biosciences. 2021;Volume 8 - 2021.
92. Varga J, Nicolas A, Petrocelli V, Pesic M, Mahmoud A, Michels BE, Etlioglu E, Yepes D, Häupl B, Ziegler PK, Bankov K, Wild PJ, Wanninger S, Medyouf H, Farin HF, Tejpar S, Oellerich T, Ruland J, Siebel CW, Greten FR. AKT-dependent NOTCH3 activation drives tumor progression in a model of mesenchymal colorectal cancer. Journal of Experimental Medicine. 2020;217(10).
93. Zhao Z, Chen X, Dowbaj AM, Sljukic A, Bratlie K, Lin L, Fong ELS, Balachander GM, Chen Z, Soragni A, Huch M, Zeng YA, Wang Q, Yu H. Organoids. Nature Reviews Methods Primers. 2022;2(1):94.
94. Heinzelmann E, Piraino F, Costa M, Roch A, Norkin M, Garnier V, Homicsko K, Brandenberg N. iPSC-derived and Patient-Derived Organoids: Applications and challenges in scalability and reproducibility as pre-clinical models. Curr Res Toxicol. 2024;7:100197.
95. Wang E, Xiang K, Zhang Y, Wang XF. Patient-derived organoids (PDOs) and PDO-derived xenografts (PDOXs): New opportunities in establishing faithful pre-clinical cancer models. J Natl Cancer Cent. 2022;2(4):263–76.
96. Kim S, Min S, Choi YS, Jo S-H, Jung JH, Han K, Kim J, An S, Ji YW, Kim Y-G, Cho S-W. Tissue extracellular matrix hydrogels as alternatives to Matrigel for culturing gastrointestinal organoids. Nature Communications. 2022;13(1):1692.
97. Benton G, Kleinman HK, George J, Arnaoutova I. Multiple uses of basement membrane-like matrix (BME/Matrigel) in vitro and in vivo with cancer cells. International Journal of Cancer. 2011;128(8):1751–7.

98. Sato T, Vries RG, Snippert HJ, van de Wetering M, Barker N, Stange DE, van Es JH, Abo A, Kujala P, Peters PJ, Clevers H. Single Lgr5 stem cells build crypt-villus structures in vitro without a mesenchymal niche. Nature. 2009;459(7244):262–5.
99. van de Wetering M, Francies Hayley E, Francis Joshua M, Bounova G, Iorio F, Pronk A, van Houdt W, van Gorp J, Taylor-Weiner A, Kester L, McLaren-Douglas A, Blokker J, Jaksani S, Bartfeld S, Volckman R, van Sluis P, Li Vivian SW, Seepo S, Sekhar Pedamallu C, Cibulskis K, Carter Scott L, McKenna A, Lawrence Michael S, Lichtenstein L, Stewart C, Koster J, Versteeg R, van Oudenaarden A, Saez-Rodriguez J, Vries Robert GJ, Getz G, Wessels L, Stratton Michael R, McDermott U, Meyerson M, Garnett Mathew J, Clevers H. Prospective Derivation of a Living Organoid Biobank of Colorectal Cancer Patients. Cell. 2015;161(4):933–45.
100. Wu Y, Sha Y, Guo X, Gao L, Huang J, Liu S-B. Organoid models: applications and research advances in colorectal cancer. Frontiers in Oncology. 2025;Volume 15 - 2025.
101. Kelemen A, Carmi I, Seress I, Lőrincz P, Tölgyes T, Dede K, Bursics A, Buzás EI, Wiener Z. CD44 Expression Intensity Marks Colorectal Cancer Cell Subpopulations with Different Extracellular Vesicle Release Capacity. International Journal of Molecular Sciences. 2022;23(4):2180.
102. Kelemen A, Carmi I, Oszvald Á, Lőrincz P, Petővári G, Tölgyes T, Dede K, Bursics A, Buzás EI, Wiener Z. IFITM1 expression determines extracellular vesicle uptake in colorectal cancer. Cellular and Molecular Life Sciences. 2021;78(21):7009–24.
103. Szvicsek Z, Oszvald Á, Szabó L, Sándor GO, Kelemen A, Soós AÁ, Pálóczi K, Harsányi L, Tölgyes T, Dede K, Bursics A, Buzás EI, Zeöld A, Wiener Z. Extracellular vesicle release from intestinal organoids is modulated by Apc mutation and other colorectal cancer progression factors. Cellular and Molecular Life Sciences. 2019;76(12):2463–76.
104. Carmi I, Orosz A, Hajdó S, Zeöld A, Hegedűs T, Kelemen-Győri D, Pozsár J, Tölgyes T, Wiener Z. The aggressive colorectal cancer subtype marker HTR2B has a dual role depending on the tumor microenvironment. Cell Communication and Signaling. 2025;23(1):403.

105. Soós AÁ, Kelemen A, Orosz A, Szvicsek Z, Tölgyes T, Dede K, Bursics A, Wiener Z. High CD142 Level Marks Tumor-Promoting Fibroblasts with Targeting Potential in Colorectal Cancer. International Journal of Molecular Sciences. 2023;24(14):11585.
106. Ziranu P, Pretta A, Aimola V, Cau F, Mariani S, D'Agata AP, Codipietro C, Rizzo D, Dell'Utri V, Sanna G, Moledda G, Cadoni A, Lai E, Puzzoni M, Pusceddu V, Castagnola M, Scartozzi M, Faa G. CD44: A New Prognostic Marker in Colorectal Cancer? Cancers (Basel). 2024;16(8).
107. Sipos F, Műzes G. Interconnection of CD133 Stem Cell Marker with Autophagy and Apoptosis in Colorectal Cancer. International Journal of Molecular Sciences. 2024;25(20):11201.
108. Jin Z, Guo T, Zhang X, Wang X, Liu Y. PTK7: an underestimated contributor to human cancer. Frontiers in Oncology. 2024;14:1448695–.
109. Jiang SH, Li J, Dong FY, Yang JY, Liu DJ, Yang XM, Wang YH, Yang MW, Fu XL, Zhang XX, Li Q, Pang XF, Huo YM, Li J, Zhang JF, Lee HY, Lee SJ, Qin WX, Gu JR, Sun YW, Zhang ZG. Increased Serotonin Signaling Contributes to the Warburg Effect in Pancreatic Tumor Cells Under Metabolic Stress and Promotes Growth of Pancreatic Tumors in Mice. Gastroenterology. 2017;153(1):277–91.e19.
110. Bala P, Rennhack JP, Aitymbayev D, Morris C, Moyer SM, Duronio GN, Doan P, Li Z, Liang X, Hornick JL, Yurgelun MB, Hahn WC, Sethi NS. Aberrant cell state plasticity mediated by developmental reprogramming precedes colorectal cancer initiation. Sci Adv. 2023;9(13):eadf0927.
111. Vellinga TT, den Uil S, Rinkes IHB, Marvin D, Ponsioen B, Alvarez-Varela A, Fatrai S, Scheele C, Zwijnenburg DA, Snippert H, Vermeulen L, Medema JP, Stockmann HB, Koster J, Fijneman RJA, de Rooij J, Kranenburg O. Collagen-rich stroma in aggressive colon tumors induces mesenchymal gene expression and tumor cell invasion. Oncogene. 2016;35(40):5263–71.
112. Thomson S, Petti F, Sujka-Kwok I, Mercado P, Bean J, Monaghan M, Seymour SL, Argast GM, Epstein DM, Haley JD. A systems view of epithelial–mesenchymal transition signaling states. Clinical & Experimental Metastasis. 2011;28(2):137–55.

113. Pradhan T, Padmanabhan K, Prasad M, Chandramohan K, Nair SA. Augmented CD133 expression in distal margin correlates with poor prognosis in colorectal cancer. J Cell Mol Med. 2019;23(6):3984–94.
114. Tang F, Zhu Y, Shen J, Yuan B, He X, Tian Y, Weng L, Sun L. CD44+ cells enhance pro-tumor stroma in the spatial landscape of colorectal cancer leading edge. British Journal of Cancer. 2025;132(8):703–15.
115. Zhang X, Yang L, Lei W, Hou Q, Huang M, Zhou R, Enver T, Wu S. Single-cell sequencing reveals CD133<sup>+</sup>CD44<sup>−</sup>-originating evolution and novel stemness related variants in human colorectal cancer. eBioMedicine. 2022;82.
116. Dessaux C, Ganier L, Guiraud L, Borg J-P. Recent insights into the therapeutic strategies targeting the pseudokinase PTK7 in cancer. Oncogene. 2024;43(26):1973–84.
117. Ando T, Yamasaki J, Saya H, Nagano O. CD44: a key regulator of iron metabolism, redox balance, and therapeutic resistance in cancer stem cells. Stem Cells. 2025;43(6).
118. Moreno-Londoño AP, Robles-Flores M. Functional Roles of CD133: More than Stemness Associated Factor Regulated by the Microenvironment. Stem Cell Reviews and Reports. 2024;20(1):25–51.
119. Pastorino GA, Sheraj I, Huebner K, Ferrero G, Kunze P, Hartmann A, Hampel C, Husnugil HH, Maiuthed A, Gebhart F, Schlattmann F, Gulec Taskiran AE, Oral G, Palmisano R, Pardini B, Naccarati A, Erlenbach-Wuensch K, Banerjee S, Schneider-Stock R. A partial epithelial-mesenchymal transition signature for highly aggressive colorectal cancer cells that survive under nutrient restriction. The Journal of Pathology. 2024;262(3):347–61.
120. Mao L, Xin F, Ren J, Xu S, Huang H, Zha X, Wen X, Gu G, Yang G, Cheng Y, Zhang C, Wang W, Liu X. 5-HT2B-mediated serotonin activation in enterocytes suppresses colitis-associated cancer initiation and promotes cancer progression. Theranostics. 2022;12(8):3928–45.
121. Wu X, Cai J, Zuo Z, Li J. Collagen facilitates the colorectal cancer stemness and metastasis through an integrin/PI3K/AKT/Snail signaling pathway. Biomedicine & Pharmacotherapy. 2019;114:108708.

# 9. Bibliography of the candidate's publications

*Publications used for the dissertation:*

A. Kelemen, **I. Carmi**, I. Seress, P. Lőrincz, T. Tölgyes, K. Dede, A. Bursics, E. I. Buzás, Z. Wiener (2022) CD44 Expression Intensity Marks Colorectal Cancer Cell Subpopulations with Different Extracellular Vesicle Release Capacity. *Int. J. Mol. Sci.* **23**, 2180. **IF: 5.6**

**I. Carmi**, A. Orosz, Sz. Hajdó, A. Zeöld, T. Hegedűs, D. Kelemen-Győri, J. Pozsár, T. Tölgyes, Z. Wiener (2025) The aggressive colorectal cancer subtype marker HTR2B has a dual role depending on the tumor microenvironment. *Cell Commun Signal.* **23**, 403. **IF: 8.9**

*Other Publications:*

**A. Kelemen**, I. Carmi, Á. Oszvald, P. Lőrincz, G. Petővári, T. Tölgyes, K. Dede, A. Bursics, E. I. Buzás, Z. Wiener (2021) IFITM1 expression determines extracellular vesicle uptake in colorectal cancer. *Cell. Mol. Life Sci.* **78**, 7009–7024. **IF: 9.234**

# 10. Acknowledgments

I owe my deepest gratitude to my supervisor, Dr. Zoltán Wiener, for introducing me to the world of scientific research and for guiding me throughout my academic journey. From my earliest days as a student researcher, he encouraged me to think critically, to ask questions fearlessly, and to explore the unknown with curiosity and confidence. His mentorship has been instrumental in shaping my scientific mindset and helping me grow into an independent researcher. I am especially thankful for his constant encouragement to present our results on the global stage, at international conferences such as ESMO and EACR, as well as at local scientific meetings, which greatly contributed to my professional and personal development. I am grateful for his dedication, enthusiasm, and the warm, collaborative atmosphere he fosters within the Molecular Cancer Biology Research Group.

I would like to thank Prof. Dr. Edit Buzás, Director of the Department of Genetics, Cell- and Immunobiology at Semmelweis University, for providing me with the environment and resources that made my research possible, and for supporting my scientific growth during my PhD studies.

My sincere thanks go to Andrea Kelemen, who first guided me through the intricate world of molecular biology and taught me many of the laboratory techniques that later became fundamental to my research. I started my scientific career under her supervision, and I have great respect for her diligence, precision, and tireless work ethic. Working alongside her and contributing to the research that culminated in our CD44 publication was an invaluable experience that helped shape my approach to science.

I would also like to express my appreciation to Szabolcs Hajdó, my colleague and fellow PhD candidate, for the countless discussions, idea exchanges, and collaborations that enriched our projects. I am equally grateful for his help with experiments and teaching assistance; we grew together as scientists and as educators. I am also grateful to Anikó Zeöld for her kindness, patience, and insightful feedback, whether it was during discussions about experimental design or when preparing presentations. I thank Lajkó Eszter and Hargita Hegyesi for the teaching opportunities they provided in the courses *Cell Science* and *Genetics and Genomics*, respectively, which allowed me to gain experience and confidence as an instructor.

I extend my gratitude to all current and former members of the Molecular Cancer Biology Research Group and to the wider community of the Department of Genetics, Cell- and Immunobiology at Semmelweis University. Working in such an intellectually vibrant and supportive environment has been both motivating and rewarding. I also wish to thank all co-authors of my publications, whose collaboration, insight, and dedication made my scientific work and this thesis possible.

I would like to acknowledge the ÚNKP Scholarship Foundation, the MD-PhD Program coordinators, the Semmelweis 250+ Excellence Scholarship, Predoctoral Scholarship organizers, K137554, 2024-1.2.3-HU-RIZONT-2024-00003, and TKP2021-EGA-24 (NRDI Office, Hungary) grants for financial funding, and the organizers of the Molecular Medicine Doctoral Program for their financial and institutional support throughout my doctoral studies.

On a personal note, I want to thank my dear friends and colleagues Anna Streiff and Anat Bendayan for always being there to listen, support, and share both frustrations and

laughter during the most demanding moments of this journey. I am also deeply thankful to Kostas Konstantinou Fantaios, my “brother in books,” who has been by my side since our first days of medical school. We grew together through every challenge, and I am incredibly proud to see him now completing his first year of medical residency in Germany, where I hope to join him soon.

I am profoundly grateful to Dano Vincent and Sahib Bhasin, my two best friends from childhood, with whom I grew up and shared the joys, sorrows, and formative experiences that shaped who I am today. Over more than fifteen years of friendship, we have built an unshakable bond founded on laughter, honesty, and deep understanding. No matter how far life takes us, their friendship continues to ground me, reminding me of where I come from and of the values that truly matter.

I am grateful to Meir and Dela for their newfound friendship and the mutual support we shared in navigating the rigors of this degree. I thank my siblings, Shiraz Carmi and Roy Carmi, for their kindness, encouragement, and unwavering faith in me. I also thank my aunt Yasmin Carmi for her emotional wisdom and for helping me stay grounded and true to myself through periods of change.

I owe profound gratitude to my parents, Yovav and Shelley Carmi, for their constant love, patience, and guidance. They have always wanted what was best for me, even when I didn’t always want to hear it, and challenged me to think deeply about my choices, ensuring that whatever I pursue is something I truly believe in.

To my beloved girlfriend, Julia Abild Cs. Nagy, to whom I owe endless thanks for her unwavering love, tenderness, understanding, and care. She has been my source of calm

and strength, making sure I sleep, eat, and take care of myself, while surrounding me with warmth, affection, and encouragement through every step of my PhD journey.

Finally, I wish to remember my late grandfathers, Emmanuel Carmi and Jack Saul whose passing during my studies left a profound mark on me. Emmanuel implanted in me the seed of critical thinking and a thirst for knowledge that continues to guide my scientific curiosity, and I carry both of their memories with deep love and gratitude.

To all the mentors, colleagues, friends, and family who have shaped this journey, thank you for your guidance, companionship, and faith in me. Your influence has been immeasurable, and this work would not have been possible without you.